Modeling Oscillations in the cAMP-PKA Network Within Budding Yeast

by

Kevin E Gonzales

Department of Mathematics
Duke University

Date: _____

Approved:

_____
David Schaeffer, Advisor

_____
Harold Layton

_____
John Harer

_____
Paul Magwene

Dissertation submitted in partial fulfillment of the requirements for the degree of
Doctor of Philosophy in the Department of Mathematics
in the Graduate School of Duke University
2011

ABSTRACT
(Mathematics)

Modeling Oscillations in the cAMP-PKA Network Within Budding Yeast

by

Kevin E Gonzales

Department of Mathematics
Duke University

Date: _____

Approved:

_____
David Schaeffer, Advisor

_____
Harold Layton

_____
John Harer

_____
Paul Magwene

An abstract of a dissertation submitted in partial fulfillment of the requirements
for
the degree of Doctor of Philosophy in the Department of Mathematics
in the Graduate School of Duke University
2011

Abstract

In our work we develop and analyze an ordinary differential equation model that describes the cyclic adenosine monophosphate (cAMP) – Protein Kinase A (PKA) pathway in budding yeast. In particular our model describes the effect of glucose stimulation on the concentration of cAMP in the short term, and the effect of stress in the long term. We develop this model in order to understand two specific experimental results, reported by Ma et al. (1999) and Garmendia-Torres et al. (2007). In order to describe the surprising results published by Ma et al. (1999) we make a key assumption that three enzymes within the cAMP-PKA network compete with one another for activation by PKA. This assumption sets our model apart from previous models of the cAMP-PKA network.

Our model focuses on two forms of negative feedback that drive oscillations in the concentration of cAMP. Under high or low stress conditions (for example, following glucose stimulation) our model reduces to a single negative feedback loop, resulting in decaying oscillations in the concentration of cAMP towards a unique equilibrium point. Under intermediate stress levels, a second negative feedback loop also exists, resulting in the possible loss of stability through a Hopf bifurcation, which leads to sustained oscillations in the concentration of cAMP. Given the novel prediction that the concentration of cAMP experiences decaying oscillations for a wide range of parameters, our collaborators in biology, Dr. Magwene's Lab, undertook new experiments in which they verified decaying cAMP oscilla-

tions at low stress levels. In an initial experiment they also verify the possibility of sustained oscillations at intermediate stress levels as predicted by our model. Our model of the cAMP-PKA network has both predictive and explanatory power and will serve as a foundation for future mathematical and experimental studies of this key signaling network.

I would like to dedicate this work to my wife Amanda Gonzales and my daughter Sophia Grace Gonzales

Contents

List of Tables

List of Figures

List of Abbreviations and Symbols

Abbreviations

The following proteins and enzymes play a role within the cAMP-PKA network we model. See Figure 1.3 for details.

Bcy1	Bypass of cyclase mutations
cAMP	Cyclic adenosine monophosphate
Cdc25	Cell division cycle 25
Cyr1	Adenylate cyclase
Gpa2	Guanine nucleotide-binding protein alpha-2
Ira	Inhibitory regulator protein
Pde	Phosphodiesterases
PKA	Protein kinase A
Ras	RAt sarcoma
Tpk	Thiamin pyrophosphokinase

Other abbreviations used within the paper.

G-proteins	(Guanine nucleotide binding proteins) A type of protein that can take an active (GTP) or inactive (GDP) form.
GDP	(Guanine di-phosphate) form of a protein. Ras·GDP and Gpa2·GDP are the inactive forms of Ras2 and Gpa2 respectively.
GTP	(Guanine tri-phosphate) form of a protein. Ras·GTP and Gpa2·GTP are the active forms of Ras2 and Gpa2 respectively.

SNP	(single-nucleotide polymorphism) DNA sequence variation occurring when a single nucleotide in the genome differs between members of the same biological species.

Abbreviations referring to Experimental Cases introduced in Section 1.3.1.

wt	wild type
Δ*pde1*	Pde1 knockout case
Δ*pde2*	Pde2 knockout case
Δ*pde1*Δ*pde2*	Pde1 and Pde 2 double knockout case
Δ*pde1*^{ala152}	Pde1 disable case, that is Pde1 phosphorylation mutant

Symbols

Scaled variables and parameters used in our simplified model.

p	case–dependent variable representing the concentration of either Pde1 or Pde2
r	variable representing the concentration of the active form of Ras
x	variable representing the concentration of cAMP
z	variable representing the concentration of Ira1 and Ira2
$*_{ss}$	equilibrium value of variable $*$
A	activation rate of Ras, dependent on the stress
B	inactivation rate of Ras
C	basal activation rate of cAMP
D_0	basal decay rate of cAMP
D	decay rate of cAMP due to Pde1
G	concentration of glucose, scaled to be one when glucose pulse is applied
M	activation/inactivation rate of Pde1

N	activation/inactivation rate of Ira1
Γ_1	the affinity of Ira and Cdc25 for Ras
Γ	the affinity of Pde for cAMP

Variables and parameters used in the full model, note that the same notation is used for several of the variables.

a	variable representing the concentration of adenylate cyclase
c	variable representing the concentration of Cdc25
g	variable representing the concentration of the active form of Gpa2
p_1	variable representing the concentration of Pde1
p_2	variable representing the concentration of Pde2
r	variable representing the concentration of the active form of Ras
x	variable representing the concentration of cAMP
y	variable representing the concentration of active PKA
z	variable representing the concentration of Ira1 and Ira2
C	total concentration of an enzyme
D	linear decay rate
K	reaction coefficient in a binary (or higher order) reaction
P	production term at a rate independent of the concentration of the enzyme being produced
R	reaction coefficient in a catalyzed reaction (that is the Michaelis-Menten rate)
Γ	Michaelis-Menten affinity

.

Acknowledgements

I would like to thank the many people who supported me during my graduate school experience. I am greatly indebted to David G. Schaeffer for his continuing support, encouragement, and patience through my time at Duke. I am also very grateful to Paul Magwene for the opportunity to work in collaboration with him and his lab and for being on my committee. This dissertation would not be possible without them.

I would like to acknowledge both John Harer and Harold Layton for being on my committee. I would also like to thank Lewis Blake, Clark Bray and Jack Bookman for their invaluable guidance in my development as a teacher.

I owe my fellow graduate students at Duke many thanks for their ongoing friendship and help. I would especially like to thank Ömür Kayıkçı for helping me understand much of the necessary biological background needed for this work. I would like to express my appreciation to the Duke Catholic Student Center and the Graduate Christian Fellowship at Duke. The friends that I created in both groups made my years at Duke enjoyable.

I would like to thank my family, especially my brothers for all their encouragement in my time at Duke.

Finally, I also want to express my gratitude and love to my wife Amanda for her understanding and patience in helping me to finish my dissertation. In particular I would like to thank her for all the editing of my work.

This dissertation work was supported by a grant from the Duke Center for Systems Biology, grant NIH P50GM081883-04.

1

Biological Background

In this section we provide the biological background needed to develop and understand our model of the cAMP-PKA network in budding yeast. We start by explaining the importance of studying budding yeast (*Saccharomyces cerevisiae*). Next we examine the budding yeast cell's life cycle and the various developmental decisions a budding yeast cell makes, highlighting the role that the cAMP-PKA network plays in determining the developmental outcome of the budding yeast cell. Then we give a detailed description of the cAMP-PKA network. Finally we give an overview of the two experiments that motivated the development of our model.

1.1 Yeast Cells

Studies of the life cycle of budding yeast (*Saccharomyces cerevisiae*) have revealed a considerable amount about the molecular mechanisms that determine cell specialization and control gene expression in eukaryotes (Herskowitz (1988)). A eukaryote is an organism whose cells contain complex structures within their membrane, most notably a nucleus containing the cell's genetic material, organized as multiple long linear DNA molecules to form chromosomes (Alberts et al. (1998)). Budding yeast cells are particularly interesting eukaryotes since they are single cell organisms. As a single cell organism they are a useful model organism for more complicated eukaryotes. Budding yeast cells are easy to work with and manipulate, allowing predictions about how different genes interact within the cell to be tested.

1.1.1 Yeast Cell's Life Cycle

In this section we give a brief overview of the budding yeast cell's life cycle, described by Herskowitz (1988). Yeast cells are single cell organisms that exist in any of three specialized cell types. Two of these cell types are mating types **a** and α

which are both haploid cells. These two cell types can mate with each other and form the third cell type, that is the $\mathbf{a}/\alpha$ diploid. A haploid cell is a cell that contains only one copy of its chromosome in its nucleus, while a diploid cell contains two identical copies of its chromosome in its nucleus. Thus, diploid cells are more resilient to DNA damage than haploid cells. For this reason if an $\mathbf{a}$ and α cell are close to each other they will almost always mate. Mating is an important feature of budding yeast. What makes budding yeast particularly interesting is that haploid cells can change sex, that is change from an $\mathbf{a}$ to an α cell or vice-versa to make mating possible, allowing them to mate and form the stronger diploid cell.

All three cell types can reproduce by mitosis, or budding, hence the name budding yeast. In this process a mother cell gives rise to a daughter cell which remains attached to the mother as it grows, only separating from the mother cell once it is mature. Initially the daughter cell is smaller than the mother cell and must grow independently before it can duplicate itself. For both the diploid and haploid cells this reproduction of the cell will continue as long as the cells are in a nutrient–rich environment, that is in an environment high in nitrogen and carbon. Haploid cells will temporarily stop budding if they are in the presence of another yeast cell with which they can mate, since in mating they form a strong diploid cell and then the diploid cell, which they form, will bud forming more diploid cells.

1.1.2 Yeast Cell's Developmental Network

Under various environmental conditions the diploid budding yeast cell will make various developmental decisions such as budding, pseudohyphal growth, and sporulation as seen in Figure 1.1. (Haploid cells have more limited options, they can only bud or mate).

Pseudohyphal Growth

When the diploid cell is starved for nitrogen it starts a process called pseudo-

hyphal growth. In this process cells undergo a transition that involves changes in cell shape and the pattern of cell division and results in invasive filamentous growth. Cells become long and thin and form pseudohyphal (long, branching filamentous structures) that grow away from the colony and attempt to find the nutrient rich environment. Pseudohyphal growth allows yeast cells to forage for nutrients (Gimeno et al. (1992)).

Sporulation

When the cell is starved for both nitrogen and carbon it will initiate meiosis and spore formation, collectively called sporulation. The single diploid cell will split into four haploid cells each of which is enclosed in a spore coat. All four haploid cells are wrapped together in a sac called the ascus. The cells will stay this way until the environment changes and is once again favorable to budding. When the spores are once again in a nutrient rich environment the sac will break and the spores will separate (Herskowitz (1988)).

The question that motivates our work is how do the budding yeast cells make these developmental decisions? A complex network of genes within the cell governs which response the cell takes to different environmental cues, proposed in Figure 1.2. This network is not entirely known, but is a proposed set of interactions thought to govern the cell's response. Rather than trying to model this entire network we focus on a key pathway within the larger network. We focus on understanding the cAMP-PKA network, which we will describe in detail in the next section. Many interactions between the genes in the cAMP-PKA network are already known. Our model focuses on proposing a few new interactions between genes to explain two specific sets of experimental data, described in Sections 1.3.1 and 1.3.2.

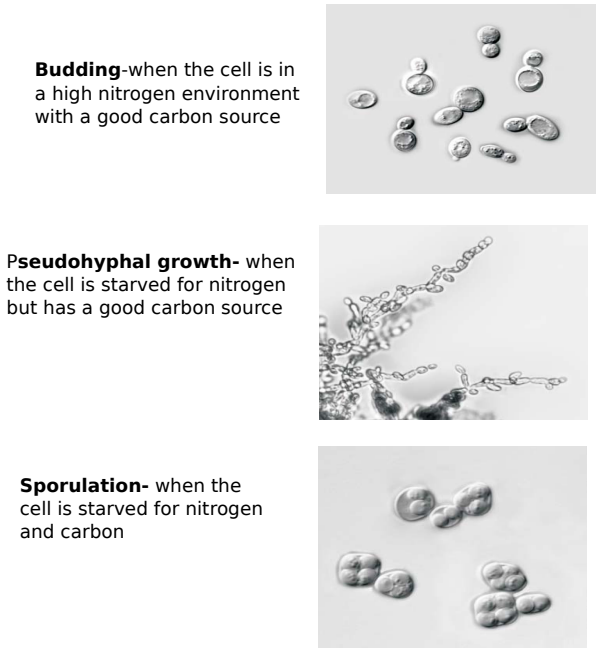

FIGURE 1.1: Nutrient dependent outcomes for a budding yeast *Saccharomyces cerevisiae* cell dependent on the nitrogen and carbon source.

1.2 cAMP-PKA Network

In this section we describe the reactions that govern the cAMP-PKA network, as seen in Figure 1.3. Note that in this figure the open arrows represent reactions in which proteins change form, for example become active or inactive; and closed arrows represents enzymatic reactions.

In our description of the cAMP-PKA network we start by describing the interactions that control the production of cAMP. We do this because our model focuses on understanding how the concentration of cAMP is affected by changes in external stimuli such as essential nutrients and fermentable carbon sources. We

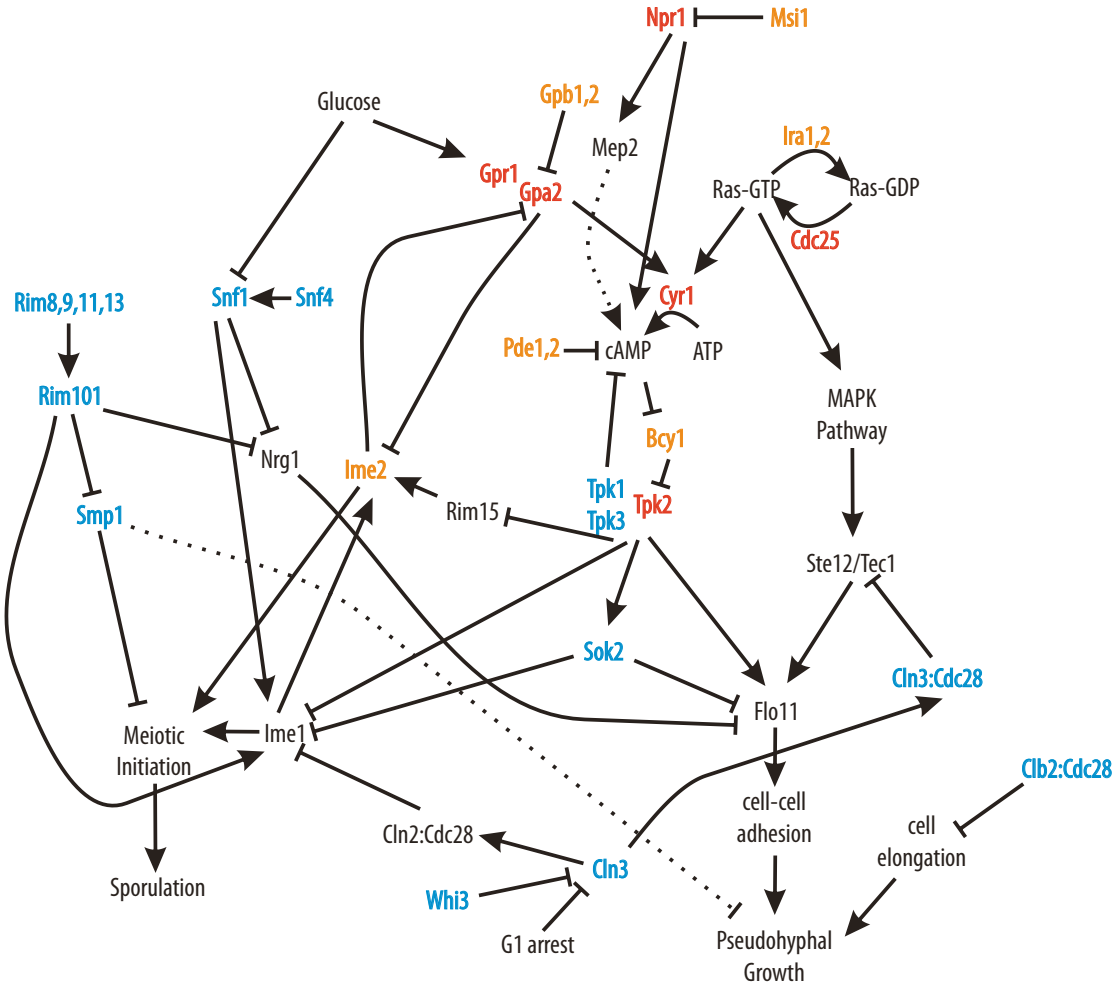

FIGURE 1.2: Yeast cell's developmental network (Magwene (unpublished data))

choose to focus on cAMP since the intracellular concentration of cAMP is an experimentally measurable variable in yeast cells.

Intracellular cAMP is synthesized from ATP in a reaction catalyzed by adenylate cyclase (Cyr1) (first part of reaction 3.9 in Fig. 1.3) (Rall and Sutherland (1958)). For our model we represent the concentration of cAMP by variable x and the concentration of adenylate cyclase by variable a. We assume that there is an unlimited amount of ATP and thus we do not model the intracellular levels of ATP. The ac-

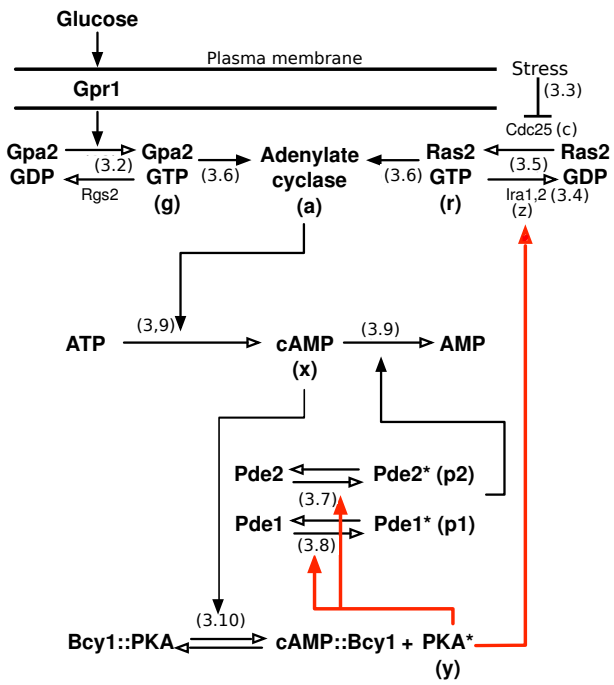

FIGURE 1.3: Key interactions of the cAMP-PKA network in yeast. See the main text and appendix for descriptions of each reaction. Arabic numerals refer to equations in Section 3 that describe each reaction. The key interactions in the model presented here are depicted with red lines.

tivity of adenylate cyclase is controlled by two different G-protein systems, Ras2 and Gpa2 (reaction 3.6) (Matsumoto et al. (1982); Toda et al. (1985)).

G-proteins (Guanine nucleotide binding proteins) act as molecular switches that transfer extracellular signals to intracellular signaling systems underlying various physiological responses (Malbon (2005); McCudden et al. (2005)). G-proteins take two forms, an active and inactive form. The G-protein is active when bound in GTP (Guanine tri-phosphate) form and inactive when bound in GDP (Guanine di-phosphate) form. Activation of a G-Protein is controlled by guanine nucleotide exchange factors (GEF) that replace GDP with GTP. Inactivation of a G-Protein is controlled by a GTPase activity that hydrolyze GTP to GDP (Malbon (2005); McCudden et al. (2005)).

In our model we represent the concentrations of Ras·GTP (active Ras2) and Gpa2·GTP (active Gpa2) (reaction 3.5) by variables r and g respectively. The total intracellular concentrations of both Ras2 and Gpa2, C_r and C_g respectively, remain constant. Thus, the concentrations of Ras·GDP (inactive Ras2) and Gpa2·GDP (inactive Gpa2) are represented by $(C_r - r)$ and $(C_g - g)$ respectively. Ras2 activity is positively regulated by the GEFs Cdc25 and Sdc25 as a function of intracellular glucose levels (Colombo et al. (2004); Thevelein et al. (2008)). That is, Cdc25 and Sdc25 activate Ras2 by transforming Ras2 from GDP to GTP form (reaction 3.3). Conversely, GTPase activating proteins, Ira1 and Ira2, down regulate Ras2 activity by stimulating the hydrolysis of GTP (reaction 3.4) (Tanaka et al. (1990)). That is, Ira1 and Ira2 inhibit the activity of Ras·GTP transforming Ras2 to GDP form. Since only the GTP form of Ras2 activates adenylate cyclase, Ira1 and Ira2 inhibit the production of cAMP. In our model we represent the concentration of both Ira1 and Ira2 with a single variable z. In parallel to Ras2, Gpa2 activity is positively regulated by the protein Gpr1 (reaction 3.2) (Thevelein et al. (2008); Rolland et al. (2000)). Gpr1 is a membrane bound G-protein coupled receptor that activates Gpa2 in response to extracellular glucose levels. That is, Gpr1 activates Gpa2 by transforming Gpa2 to GTP form. Conversely, the GTPase activating protein, Rgs2, down regulates Gpa2 activity (Versele et al. (1999); Kehrl and Sinnarajah (2002)). That is, Rgs2 transforms Gpa2 to GDP form. Gpa2 activation in response to glucose plays an important role in the experimental data we examine (see Section 1.3).

Moving from examining the production of cAMP to examining the effect of cAMP synthesis, we know that an increase in the concentration of cAMP activates PKA. PKA is made up of two subunits: a regulatory subunit (Bcy1) and a catalytic subunit (either Tpk1, Tpk2 or Tpk3) which we will refer to as the active form of PKA and model with variable y (Toda et al. (1987)). cAMP binding to Bcy1 leads

to the release of the active PKA subunits (reaction 3.10) which are then free to interact with downstream targets such as transcription factors and other kinases. In our model this activation of PKA plays a central role. Active PKA will be the catalyst in our three key reactions (shown as red arrows).

The concentration of cAMP is broken down to AMP by phosphodiesterases Pde1 and Pde2 (second half of reaction 3.9) which prevent cAMP accumulation in the cell (Mitsuzawa (1993); Ma et al. (1999)). In yeast cells there are two phosphodiesterases, the low-affinity (meaning low affinity for cAMP) phosphodiesterase Pde1 and the higher affinity Pde2. The affinity tells us how tightly bound Pde1 and Pde2 are to cAMP. Pde1 is more loosely bound to cAMP than Pde2 since Pde1 is low affinity. We propose that the active form of PKA, that is either Tpk1, Tpk2 or Tpk3 activates (phosphorylates) both Pde1 and Pde2 (reactions 3.7 and 3.8, shown as red arrows). These activated (phosphorylated) forms of Pde1 and Pde2 are more effective in their role of cAMP degradation. Thus, cAMP activation of PKA leads to activation of both Pde1 and Pde2, which increases the decay rate of cAMP, creating a negative feedback loop.

In our model we also propose that the active form of PKA activates (phosphorylates) Ira1 and Ira2 (reaction 3.4, shown as a red arrow) enhancing their effect on Ras·GTP. Again cAMP activates PKA, which activates Ira1 and Ira2, which in turn inhibit Ras·GTP. Reduced levels of Ras·GTP decrease the activity of adenylate cyclase inhibiting the production of cAMP, and creating a second negative feedback loop.

1.3 Motivating Experiments

There is a large body of experimental work that provides information on genetic and biochemical interactions relevant to the cAMP-PKA network. The strategy

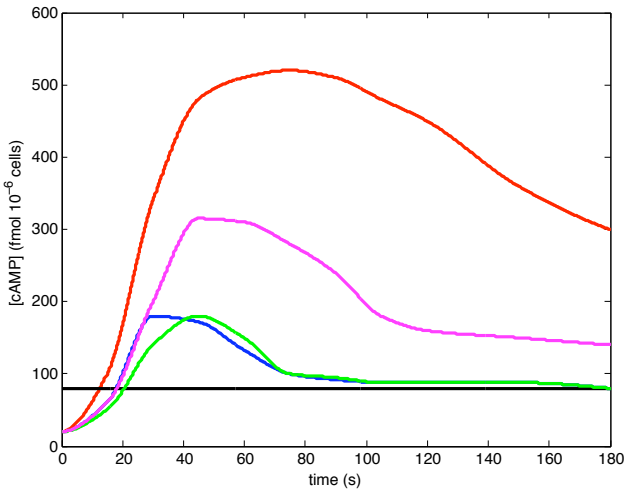

FIGURE 1.4: cAMP dynamics following glucose stimulus as described by Ma et al. (1999): wild type (blue), Δ*pde1*(red), Δ*pde2*(green), Δ*pde1*^{ala152} (pink), Δ*pde1*Δ*pde2*(black).

we adopt is to use this body of work as a basis for constraining interactions in our model. The model itself is developed to understand two specific experimental results: the short-term dynamics of cAMP following glucose stimulation reported by Ma et al. (1999) and the long-term dynamics of cAMP under various stress levels reported by Garmendia-Torres et al. (2007). In the development of our model we first considered only the Ma et al. (1999) data. After successfully developing a model that could explain these results we expanded our model to include the long-term dynamics proposed by Garmendia-Torres et al. (2007). In our work here we present the expanded model that incorporates both results.

1.3.1 Ma et al. (1999)

In their paper Ma et al. (1999) focused on the short-term dynamics of cAMP following glucose stimulation. In particular Ma et al. (1999) focused on PKA-mediated negative feedback involving the phosphodiesterases Pde1 and Pde2. Here we briefly summarize the key results that Ma et al. (1999) reported.

Ma et al. (1999) described cAMP dynamics following glucose stimulation for wild-type cells and various phosphodiesterase mutants. Figure 1.4 summarizes the five dynamic patterns we consider here (compare to Ma et al. (1999) Figs. 2a and 3a). These cases are:

Case 1: Wild-type (*wt*; blue line) – the concentration of cAMP in *wt* cells rapidly accumulates following glucose stimulation causing a transient response. After reaching a peak level, the concentration of cAMP decreases to a new steady state that is higher than its initial concentration.

Case 2: Pde1 knockout ($\Delta pde1$; red line) – the concentration of cAMP exhibits a much larger and longer transient response, about four times as large as the transient response exhibited by *wt*. The steady-state value is unclear in this case since the experimental data was taken for only three minutes. [1]

Case 3: Pde2 knockout ($\Delta pde2$; green line) – the concentration of cAMP exhibits similar dynamics to *wt*.

Case 4: Pde1 phosphorylation mutant ($\Delta pde1^{ala152}$; pink line) – the cAMP transient response is about twice as large as that exhibited by *wt*. The steady state appears to be greater than the *wt*.

Case 5: Double Pde knockout ($\Delta pde1\Delta pde2$; black line) – glucose stimulation has no effect on the concentration of cAMP present in the cytosol. The initial value in this case is much larger than the *wt* initial value.

These results are surprising in two ways: 1) in the double knockout case ($\Delta pde1\Delta pde2$) glucose stimulation has no effect on the concentration of cAMP, and 2) the dynamics observed in the Pde2 knockout case ($\Delta pde2$) are almost the same as those

[1] Our model predicts a higher steady–state value.

observed in the wild-type (*wt*). The double knockout case is surprising since both Pde1 and Pde2 are known to break cAMP apart but neither has a known direct effect on the production of cAMP. In knocking out both Pde1 and Pde2 we would expect that following the addition of glucose the concentration of cAMP would rapidly accumulate. If there were some basal decay of cAMP, independent of either form of Pde, then we would expect that at some point the concentration of cAMP would approach some high steady–state concentration. Instead, the concentration of cAMP no longer appears to be affected by glucose. We conclude that Pde1 and Pde2 must have a secondary effect on the cAMP–PKA network. We choose to model this secondary effect as competitive inhibition of PKA's activation of Ira1 and Ira2 by both Pde1 and Pde2. That is, in the absence of both Pde, PKA activation of Ira1 and Ira2 will be strong enough to force Ras2 almost completely to GDP form, inhibiting the production of cAMP.

The Pde2 knockout case is surprising since it appears from comparison to the wild type case that Pde2 has no effect on the system, yet the Pde1 knockout case (Δ*pde1*) and the double knockout case are very different. This implies that Pde2 must be effective only if Pde1 is eliminated. We conclude that Pde2 acts as a backup system to Pde1.

Ma et al. (1999) suggested that the likely explanation for the different Pde knockout cases was that elevated PKA activity in response to glucose stimulation causes increased feedback through Pde1 and Pde2 on the concentration of cAMP. PKA feedback on the phosphodiesterases is known to be important for efficient breakdown of cAMP. Ma et al. (1999) showed that mutants with decreased PKA activity show increased levels of cAMP. In particular they showed that destruction of a PKA phosphorylation site in Pde1 causes a dramatic increase in cAMP accumulation, that is not allowing PKA to activate Pde1 causes an increase in cAMP accumulation. There is less direct evidence for PKA interactions with Pde2 but

other class II phosphodiesterases are known to be targets of PKA.

In our model we assume that PKA binds to both Pde1 and Pde2 increasing their activity. We assume that PKA has a higher affinity for Pde1 than for Pde2, that is PKA is going to preferentially activate Pde1 over Pde2. This explains the Pde2 knockout case. Since PKA preferentially activates Pde1 over Pde2, the wild type and the Pde2 knockout cases are almost the same. We also assume that PKA has higher affinity for both Pde1 and Pde2 than for Ira1 and Ira2. This will explain the double knockout case. Whenever any form of Pde is present it inhibits PKA's activation of Ira1 and Ira2. In the absence of both forms of Pde, PKA is free to activate Ira1 and Ira2, restricting the activity of Ras·GTP, which then inhibits adenylate cyclase production of cAMP.

1.3.2 Garmendia–Torres et al. (2007)

In their paper Garmendia-Torres et al. (2007) predicted sustained oscillations in the concentration of cAMP at intermediate stress levels. However, they did not directly observe sustained oscillations in the concentration of cAMP. Rather, the prediction of sustained oscillations was motivated by oscillations observed in a downstream target of the cAMP-PKA network (Msn2) that is unable to oscillate independently. They concluded that only oscillations in the concentration of cAMP could cause this downstream target to oscillate.

To elaborate Garmendia-Torres et al. (2007) observed oscillations (nucleocytoplasmic shuttling) of the transcription factor Msn2 in budding yeast due to intermediate stress levels. Msn2 is negatively controlled by the cAMP-PKA network through Msn2 activation (phosphorylation) by the active form of PKA. Since Msn2 cannot oscillate independently, Garmendia-Torres et al. (2007) predicted that these oscillations should be driven by oscillations in the concentration of cAMP. Garmendia-Torres et al. (2007) created a differential equation model in

which negative PKA feedback on Ras·GTP induced this oscillation. This was similar to the model we had already started to develop; however, their model was not able to replicate the Ma et al. (1999) data. In addition, their model was analyzed only numerically, and for only a few parameter values.

The oscillations of Msn2 observed by Garmendia-Torres et al. (2007) only occur at intermediate stress levels. At high and low stress levels Msn2 did not oscillate. In their model Garmendia-Torres et al. (2007) predicted that at high stress levels the concentration of cAMP went to a low steady state, and at low stress levels the concentration of cAMP went to a high steady state.

In the Garmendia-Torres et al. (2007) model, the oscillations in the concentration of cAMP are a result of negative feedback on Ras·GTP via active PKA. One or more targets in the Ras2 network may be targets of PKA mediated feedback. For example, Ira1 and Ira2 both have predicted PKA phosphorylation sites. Similarly, PKA hyper-phosphorylates Cdc25, causing its dissociation from the adenylate cyclase/Ras2 complex. In the development of our model we could have chosen either Ira or Cdc25 as the target for PKA feedback. We chose to model PKA feedback through Ira.

In the development of our model we first looked exclusively at the Ma et al. (1999) experimental results. In this original model we predicted PKA feedback on Ras·GTP via Ira1 and Ira2. In the simplification of our original model we did not need to incorporate Ras·GTP dynamics. Rather the competitive inhibition of PKA's activation of Ira1 and Ira2 allowed us to treat the concentration of Ras·GTP as a constant whose value was case dependent. In considering the Garmendia-Torres et al. (2007) data we built upon the PKA feedback that was already part of our model, treating both Ira and Ras·GTP as dynamic variables. At intermediate stress levels our model is able to replicate the sustained oscillations predicted by Garmendia-Torres et al. (2007).

2

Introduction to the Model

In this section we introduce the mathematical background for our model of the cAMP-PKA network. First we introduce the key assumption that Pde1, Pde2, and Ira1/2 compete with each other for activation by PKA. This assumption sets our model apart from previous models of the cAMP-PKA network. We use this assumption to explain the surprising results reported by Ma et al. (1999) (see Section 1.3.1), particularly the Pde1 knockout case and double Pde knockout cases which the previous models of the cAMP-PKA network can not replicate. In this section we derive formulas describing the velocities of these three competitive reactions[1]. Then we look at other types of models for regulatory systems and explain why we chose not to use any of them to model the cAMP-PKA network. Finally we examine four previous models of the cAMP-PKA network.

2.1 Competitive Interactions in the cAMP-PKA Network

In our model, negative PKA feedback (red arrows in Figure 1.3) plays a central role. This feedback occurs in three ways: i) PKA activates (phosphorylates) Pde1 enhancing the Pde1 breakdown of cAMP; ii) PKA activates (phosphorylates) Pde2 enhancing the Pde2 breakdown of cAMP; and iii) PKA activates (phosphorylates) the Ras·GTPase Ira1 and Ira2. In Cases i and ii, PKA inhibits the concentration of cAMP by enhancing the breakdown of cAMP. In Case iii, PKA inhibits the production of cAMP by inactivating Ras·GTP.

We assume that there are much greater concentrations of Pde1, Pde2 and Ira (the combination of both Ira1 and Ira2) in the cytoplasm than of PKA. We also assume that Pde1, Pde2 and Ira compete with each other for activation by PKA. We assume that Ira1 and Ira2 can be simultaneously activated by PKA, thus we can treat Ira1 and Ira2 as a single variable Ira. These assumptions are taken in

[1] In the next section (Section 3) we will derive the full differential equation model for the cAMP-PKA network.

order to understand the Ma et al. (1999) cases.

Under these assumptions we propose to model the dynamics of Pde1, Pde2 and Ira by the following three differential equations:

$$\frac{d}{dt}[\text{Pde1}^*] = \frac{R_{p_1}[\text{Pde1}][\text{PKA}]}{\Gamma_1 + [\text{Pde1}] + \frac{\Gamma_1}{\Gamma_2}[\text{Pde2}] + \frac{\Gamma_1}{\Gamma_z}[\text{Ira}]} - D_{p_1}[\text{Pde1}^*] \tag{2.1}$$

$$\frac{d}{dt}[\text{Pde2}^*] = \frac{R_{p_2}[\text{Pde2}][\text{PKA}]}{\Gamma_2 + [\text{Pde2}] + \frac{\Gamma_2}{\Gamma_1}[\text{Pde1}] + \frac{\Gamma_2}{\Gamma_z}[\text{Ira}]} - D_{p_2}[\text{Pde2}^*] \tag{2.2}$$

$$\frac{d}{dt}[\text{Ira}^*] = \frac{R_z[\text{Ira}][PKA]}{\Gamma_z + [\text{Ira}] + \frac{\Gamma_z}{\Gamma_1}[Pde1] + \frac{\Gamma_z}{\Gamma_2}[Pde2]} - D_z[Ira^*] \tag{2.3}$$

where the asterisk (*) indicates the activated form of the enzyme. Each of these equations has an activation and inactivation term. We model the inactivation of Pde1, Pde2 and Ira with linear decay rates D_{p_1}, D_{p_2}, and D_z, respectively. The activation of each is modeled by an extension of Michaelis-Menten that incorporates the competition between the three substrates [Pde1], [Pde2] and [Ira] (Segel (1993)). The three competitive reactions are specified as follows:

$$[\text{Pde1}] + [\text{PKA}] \underset{k_{-1}}{\overset{k_1}{\rightleftharpoons}} [\text{Pde1} :: \text{PKA}] \xrightarrow{R_{p_1}} [\text{Pde1}^*] + [\text{PKA}]$$

$$[\text{Pde2}] + [\text{PKA}] \underset{k_{-2}}{\overset{k_2}{\rightleftharpoons}} [\text{Pde2} :: \text{PKA}] \xrightarrow{R_{p_2}} [\text{Pde2}^*] + [\text{PKA}]$$

$$[\text{Ira}] + [\text{PKA}] \underset{k_{-z}}{\overset{k_z}{\rightleftharpoons}} [\text{Ira} :: \text{PKA}] \xrightarrow{R_z} [\text{Ira}^*] + [\text{PKA}]$$

To fully model these three enzymatic reactions would require a system of 10 differential equations. To derive the activating piece of Equations (2.1)–(2.3) we

will first derive the Michaelis-Menten Equation for activation of a single substrate. Then we will derive an extension of the Michaelis-Menten Equation that accounts for competitive inhibition, and apply it to the three reactions given above.

Michaelis-Menten Kinetics

Michaelis-Mention kinetics are a standard way to model enzyme kinetics in biochemistry. The Michaelis-Menten Equation describes an irreversible enzymatic reaction in which an enzyme [E] activates a substrate [S]. In the development of the Michaelis-Menten Equation we must first introduce an underlying assumption, as in Segel (1980, 1984). We assume that there is a balance between the formation of the complex $[S :: E]$ by the union of the substrate $[S]$ and the enzyme $[E]$ and the breaking apart of this complex, either back to substrate and enzyme or to enzyme and product $[S^*]$. When the concentration of the substrate is large, this balance will be achieved before a full transformation of substrate to product $[S^*]$. Thus, we are assuming that even while this transformation is occurring the change in the complex $[S :: E]$ can be treated as at steady state:

$$\frac{d[S :: E]}{dt} \approx 0. \tag{2.4}$$

This is known as the quasi or pseudo-steady state assumption. We also assume the total intracellular concentration of the enzyme, both bound to the substrate and free, is a fixed constant $[E_0]$.

Claim 1. *Under the pseudo-steady state assumption* (2.4) *the enzymatic reaction:*

$$[S] + [E] \underset{k_i}{\overset{k_a}{\rightleftharpoons}} [S :: E] \xrightarrow{K} [S^*] + [E]$$

is described by the Michaelis-Mention Equation:

$$\frac{d[S^*]}{dt} = \frac{\kappa[S]}{\Gamma + [S]} \tag{2.5}$$

where $\kappa = K[E_0]$ *is the effective rate constant and* $\Gamma = \dfrac{(k_i + K)}{k_a}$ *is called the affinity of the enzyme [E] for the substrate [S].*

Note that the affinity $\Gamma = \dfrac{(k_i + K)}{k_a}$ is a deceptive name and really describes the inverse of the affinity. An enzyme with high affinity describes when the enzyme $[E]$ is likely to bind to the substrate $[S]$, and corresponds to small values of Γ, that is a fast binding rate k_a and slow unbinding rates k_i and K. Similarly low affinity corresponds to large values of Γ.

Proof. We can fully describe this enzymatic reaction with four differential equations.

$$\frac{d[S]}{dt} = -k_a[S][E] + k_i[S :: E] \tag{2.6}$$

$$\frac{d[E]}{dt} = -k_a[S][E] + (k_i + K)[S :: E] \tag{2.7}$$

$$\frac{d[S :: E]}{dt} = k_a[S][E] - (k_i + K)[S :: E] \tag{2.8}$$

$$\frac{d[S^*]}{dt} = K[S :: E] \tag{2.9}$$

The total concentration of the enzyme is conserved

$$\frac{d[E]}{dt} + \frac{d[S :: E]}{dt} = 0 \qquad \Rightarrow \qquad [E] + [E :: S] = [E_0].$$

We then apply the pseudo-steady state assumption (2.4) to Equation (2.8)

$$\frac{d[S :: E]}{dt} = k_a[S][E] - (k_i + K)[S :: E] = 0$$

which implies that

$$[S :: E] = \frac{k_a}{k_i + K}[S][E].$$

Then applying the conservation of the enzyme we get:

$$[S :: E] = \frac{k_a}{k_i + K}[S]([E_0] - [S :: E]),$$

which we can then solve in terms of the complex $[S :: E]$:

$$[S :: E](1 + \frac{k_a}{k_i + K}) = \frac{k_a}{k_i + K}[S][E_0].$$

Let $\kappa = K[E_0]$ and $\Gamma = \frac{(k_i + K)}{k_a}$. Then conservation of both the enzyme $[E]$ and the substrate $[S]$ along with the pseudo-steady-state assumption allows us to reduce Equations (2.6)–(2.9) to the single Michaelis-Menten Equation (2.5):

$$\frac{d[S^*]}{dt} = \frac{\kappa[S]}{\Gamma + [S]}.$$

□

Substrate Inhibition

When a single enzyme activates more than one substrate the different substrates can inhibit each other's activation in one of four different ways. The following descriptions were taken from Fersht (2002).

- **Noncompetitive Inhibition** The different substrates can be activated by the enzyme simultaneously. This occurs at the same rate at which each substrate is activated independently.

- **Mixed Inhibition** The different substrates can bind to the enzyme simultaneously, but the rate of activation when more than one substrate is bound to the enzyme is slower than when the substrate is independently activated.

- **Uncompetitive Inhibition** The enzyme can only bind to the combination of substrates. That is only when two or more substrates form a complex can they each be activated.

- **Competitive Inhibition** The different substrates cannot bind to the enzyme at the same time. This happens when the different substrates compete for the same binding site on the enzyme.

In our model we assume the last case, that Pde1, Pde2 and Ira competitively inhibit each other's activation by PKA. We also assume that Ira1 and Ira2 non-competitively inhibit each other's activation by PKA, thus we can treat them as a single variable Ira. To model this competitive inhibition requires an extension of the Michaelis-Menten Equation (Segel (1993)) derived in Claim 1. For ease in notation we develop a form for the Michaelis-Menten Equation that models three substrates $[S_1]$, $[S_2]$ and $[S_3]$ activated by a single enzyme $[E]$. Then we apply this to Pde1, Pde2 and Ira.

Claim 2. *Under the assumption that substrates* $[S_1]$, $[S_2]$, *and* $[S_3]$ *cannot bind to the enzyme* $[E]$ *simultaneously, and under the pseudo-steady state assumption* (2.4) *on each complex* $[S_1 :: E]$, $[S_2 :: E]$, *and* $[S_3 :: E]$ *the activation of substrates* $[S_1]$, $[S_2]$, *and* $[S_2]$ *is described by the following three differential equations modified from the Michaelis-Menten Equation:*

$$\frac{d[S_1^*]}{dt} = \frac{\kappa_1[S_1]}{\Gamma_1 + [S_1] + \frac{\Gamma_1}{\Gamma_2}[S_2] + \frac{\Gamma_1}{\Gamma_3}[S_3]} \tag{2.10}$$

$$\frac{d[S_2^*]}{dt} = \frac{\kappa_2[S_2]}{\Gamma_2 + [S_2] + \frac{\Gamma_2}{\Gamma_1}[S_1] + \frac{\Gamma_2}{\Gamma_3}[S_3]} \tag{2.11}$$

$$\frac{d[S_3^*]}{dt} = \frac{\kappa_3[S_3]}{\Gamma_3 + [S_3] + \frac{\Gamma_3}{\Gamma_1}[S_1] + \frac{\Gamma_3}{\Gamma_2}[S_2]} \tag{2.12}$$

where $[S_n^*]$ *is the active form of* $[S_n]$, $\kappa_n = K_n[E_0]$ *is the effective rate constant, and* $\Gamma_n = \dfrac{(k_{in} + K_n)}{k_{an}}$ *is the affinity of the enzyme* $[E]$ *for the substrate* $[S_n]$ *for* $n = 1, 2,$ *and* 3.

Proof. Let $[S_1]$, $[S_2]$ and $[S_3]$ be three separate substrates that are activated by a single enzyme $[E]$. These three reactions are written out in detail as follows.

$$[S_1] + [E] \underset{k_{i1}}{\overset{k_{a1}}{\rightleftharpoons}} [S_1 :: E] \xrightarrow{K_1} [S_1^*] + [E]$$

$$[S_2] + [E] \underset{k_{i2}}{\overset{k_{a2}}{\rightleftharpoons}} [S_2 :: E] \xrightarrow{K_2} [S_2^*] + [E]$$

$$[S_3] + [E] \underset{k_{i3}}{\overset{k_{a3}}{\rightleftharpoons}} [S_3 :: E] \xrightarrow{K_3} [S_3^*] + [E]$$

We can fully describe these three enzymatic reactions with ten differential equations. For $n = 1, 2$ and 3

$$\frac{d[S_n]}{dt} = -k_{an}[S_n][E] + k_{in}[S_n :: E] \qquad \text{for } n = 1, 2 \text{ and } 3 \tag{2.13}$$

$$\frac{d[S_n :: E]}{dt} = k_{an}[S_n][E] - (k_{in} + K_n)[S_n :: E] \qquad \text{for } n = 1, 2 \text{ and } 3 \tag{2.14}$$

$$\frac{d[S_n^*]}{dt} = K_n[S_n :: E] \qquad \text{for } n = 1, 2 \text{ and } 3 \tag{2.15}$$

$$\frac{d[E]}{dt} = \sum_{l=1}^{3}(k_{il} + K_l)[S_l :: E] - k_{al}[S_l][E]. \tag{2.16}$$

As with the general Michaelis-Menten Equation we observe that the total concentration of the enzyme is conserved:

$$\frac{d[E]}{dt} + \frac{d[S_1 :: E]}{dt} + \frac{d[S_2 :: E]}{dt} + \frac{d[S_3 :: E]}{dt} = 0.$$

Thus

$$[E] + [S_1 :: E] + [S_2 :: E] + [S_3 :: E] = [E_0]. \tag{2.17}$$

For $n = 1, 2$ and 3 we impose the pseudo-steady state assumption

$$\frac{d[S_n :: E]}{dt} = k_{an}[S_n][E] - (k_{in} + K_n)[S_n :: E] = 0,$$

which implies that

$$[S_n :: E] = \frac{k_{an}}{k_{in} + K_n}[S_n][E]. \tag{2.18}$$

We can rewrite Equation (2.18) using the fact that the total concentration of the enzyme is conserved as:

$$[S_n :: E] = \frac{k_{an}}{k_{in} + K_n}[S_n]\left([E_0] - \sum_{i=1}^{3}[S_i :: E]\right) \tag{2.19}$$

for $n = 1, 2$ and 3, giving us a system of three equations.

Recall that to make the pseudo-steady state assumption we assume that there is a balance between the formation of the complex $[S_n :: E]$ and the breaking apart of this complex. This balance can only be achieved when the concentration of the substrate $[S_n]$ is larger than the concentration of the enzyme $[E]$. Thus, we could not impose this condition if the total concentration of the enzyme was greater than the concentrations of the substrates.

Then define $\Gamma_n = \frac{k_{in}+K_n}{k_{in}}$ for $n = 1, 2$ and 3. We rewrite Equation (2.19) for $n = 1, 2$ and 3 using Γ_n:

$$[S_1 :: E] = \frac{S_1}{\Gamma_1}\left([E_0] - [S_1 :: E] - [S_2 :: E] - [S_3 :: E]\right)$$

$$[S_2 :: E] = \frac{S_2}{\Gamma_2}\left([E_0] - [S_1 :: E] - [S_2 :: E] - [S_3 :: E]\right)$$

$$[S_3 :: E] = \frac{S_3}{\Gamma_3}\left([E_0] - [S_1 :: E] - [S_2 :: E] - [S_3 :: E]\right)$$

If we add these three equations together we get:

$$[S_1 :: E]+[S_2 :: E]+[S_3 :: E] = \left(\frac{S_1}{\Gamma_1} + \frac{S_2}{\Gamma_2} + \frac{S_3}{\Gamma_3}\right)\left([E_0] - [S_1 :: E] - [S_2 :: E] - [S_3 :: E]\right). \tag{2.20}$$

We can solve Equation (2.20) in terms of the sum $[S_1 :: E] + [S_2 :: E] + [S_3 :: E]$ and get:

$$[S_1 :: E] + [S_2 :: E] + [S_3 :: E] = \frac{\frac{S_1}{\Gamma_1} + \frac{S_2}{\Gamma_2} + \frac{S_3}{\Gamma_3}}{1 + \frac{S_1}{\Gamma_1} + \frac{S_2}{\Gamma_2} + \frac{S_3}{\Gamma_3}}[E_0]. \tag{2.21}$$

Then plug the right hand side of Equation (2.21) into the the right hand side of (2.19) and rewrite:

$$[S_n :: E] = \frac{k_{an}}{k_{in} + K_n}[S_n]\left([E_0] - \frac{\frac{S_1}{\Gamma_1} + \frac{S_2}{\Gamma_2} + \frac{S_3}{\Gamma_3}}{1 + \frac{S_1}{\Gamma_1} + \frac{S_2}{\Gamma_2} + \frac{S_3}{\Gamma_3}}[E_0]\right)$$

for $n = 1, 2$, and 3. By finding a common denominator we can simplify this equation to:

$$[S_n :: E] = \left(\frac{[S_n]}{\Gamma_n}\right)\left(\frac{[E_0]}{1 + \frac{S_1}{\Gamma_1} + \frac{S_2}{\Gamma_2} + \frac{S_3}{\Gamma_3}}\right) \tag{2.22}$$

for $n = 1, 2$, and 3. Thus, by applying the conservation of the enzyme and applying the pseudo-steady-state assumption we reduce (2.13)–(2.16) to the following three differential equations, were $\kappa_n = K_n[E_0]$:

$$\frac{d[S_1^*]}{dt} = \frac{\kappa_1[S_1]}{\Gamma_1 + [S_1] + \frac{\Gamma_1}{\Gamma_2}[S_2] + \frac{\Gamma_1}{\Gamma_3}[S_3]}$$

$$\frac{d[S_2^*]}{dt} = \frac{\kappa_2[S_2]}{\Gamma_2 + [S_2] + \frac{\Gamma_2}{\Gamma_1}[S_1] + \frac{\Gamma_2}{\Gamma_3}[S_3]}$$

$$\frac{d[S_3^*]}{dt} = \frac{\kappa_3[S_3]}{\Gamma_3 + [S_3] + \frac{\Gamma_3}{\Gamma_1}[S_1] + \frac{\Gamma_3}{\Gamma_2}[S_2]}$$

□

By applying Claim 2 to the three enzymatic reactions describing PKA's activation of Pde1, Pde2 and Ira we obtain the activating piece of Equations (2.1)–(2.3) describing competitive inhibition of Pde1, Pde2 and Ira. Here PKA plays the role

of the activating enzyme $[E]$, and Pde1, Pde2, and Ira are the three competing substrates.

2.2 Alternate Models for Gene Regulatory Networks

We chose to model the cAMP-PKA network where the key interactions are modeled with Michaelis-Menten Kinetics, as described in Section 2.1. In this section we briefly describe alternate models for gene regulatory networks and why we did not choose to use them.

2.2.1 Discrete Models

Boolean Networks

A Boolean network, first proposed by Glass and Kauffman (1973) is a discrete description of a gene regulatory network in which each gene is described as a node x_i. The gene network (X) containing N distinct genes is described as:

$$X = \{x_i\}_{i=1}^{N}$$

Each node x_i takes a value of either one or zero. In determining when a gene is active or inactive a threshold parameter is defined. A gene is considered active when the activity of that gene is greater than the threshold, then the node describing that gene takes the value one ($x_i = 1$). Otherwise the gene is inactive and the node describing that gene equals zero ($x_i = 0$). A logic function F is imposed on this set of genes:

$$F = \{f_i(X)\}_{i=i}^{N}$$

Each function $f_i(X)$ describes the set of genes that interact with gene x_i. The logic function usually is visualized as a collection of nodes and edges, where a directed edge describes an interaction between the two genes, given as nodes, that the edge connects. The gene at the tail end of the edge either activates or inhibits the

gene that the edge points to. To understand the dynamics of this network we first impose some initial condition, stating which genes start active and inactive. Then the network is discretely updated:

$$X(t+1) = F(X(t)) \qquad \Rightarrow \qquad x_i(t+1) = f_i(x_1(t), x_2(t), ..., x_N(t)) \quad \forall \ \ 1 \leqslant i \leqslant N$$

Then the network is at steady-state if after some time T the network does not change when updated: $X(T+1) = X(T)$. The network oscillates if we can find an integer τ such that $X(t+\tau) = X(t)$ for all sufficiently large t.

Example 1 Let $X = \{x_1, x_2, x_3\}$ and logic on this three node network be defined as:

$$x_1 \qquad\qquad x_2 \underset{-}{\overset{+}{\rightleftharpoons}} x_3.$$

In this example gene x_1 is independent of the other two genes, x_2 and x_3. That is gene x_1 remains at its initial state, either one or zero; thus, gene x_1 is at steady state. Gene x_2 activates gene x_3 while x_3 inhibits x_2. Observe from Table 2.1 that this negative feedback loop causes oscillation with $\tau = 4$.

Table 2.1: Logic for the Boolean network $x_2 \underset{-}{\overset{+}{\rightleftharpoons}} x_3$.

$x_2(t)$	$x_3(t)$	$x_2(t+1)$	$x_3(t+1)$
0	0	1	0
1	0	1	1
1	1	0	1
1	0	0	0

Example 2 Let $X = \{x_1, x_2, x_3\}$ and logic on this three node network be defined as:

$$x_1 \overset{+}{\longrightarrow} x_2 \underset{-}{\overset{+}{\rightleftharpoons}} x_3.$$

Then gene x_1 is still independent of the other two genes and thus at steady state. Again gene x_2 activates gene x_3, while x_3 inhibits x_2. In this case if x_1 activates x_2

at the same time that x_3 is inhibiting x_2, we must decide what logic to use. One of three cases could happen: x_1 and x_3 affect x_2; x_1 or x_3 affect x_2; x_1 or x_3 but not both (XOR) affect x_2.

The Boolean model is useful in describing large gene networks, in particular in examining when a large gene network goes to steady state. It is also easy to write code for since the time is discretely iterated and each gene is binary. We do not choose to model the cAMP-PKA network with a Boolean model since the Ma et al. (1999) experimental results we are seeking to explain examine the continuous concentration of cAMP.

Multi-state Models

A problem with a Boolean model is that it treats the genes as either on or off. Rubinstein et al. (2007) attempted to fix this problem. In their model the network of genes is again treated as a set of nodes with corresponding directed edges:

$$X = \{x_i\}_{i=1}^{N},$$

where

$$x_i \in \{0, 1, , ..M\}.$$

Instead of each node being on or off, each node has a level of activity ranging from completely off ($x_i = 0$) to completely on ($x_i = M$). Once again a discrete time step is used. Define:

$$k_i(t_n) = \sum_{j}^{N} a_{ij} x_j(t_n)$$

where a_{ij} is the weight of the edge from node j to node i. Then $k_i(t_n)$ tells us if all the nodes affecting the node x_i at time t_n have a net positive effect on the node, or

a net negative effect on the node, or no net effect on the node. Then

$$x_i(t_n+1) = \begin{cases} \min(N, x_i(t_n)+1) & \text{if } k_i(t_n) > 0 \\ \max(0, x_i(t_n)-1) & \text{if } k_i(t_n) < 0 \\ x_i(t_n) & \text{if } k_i(t_n) = 0 \end{cases}$$

That is if the net effect of the other nodes on node i is positive at time t_n ($k_i(t_n) > 0$) then the activity of this node is increased, unless already at its maximum. Similarly, if the net effect is negative at time t_n then the activity of this node is decreased, unless already completely off. Although this helps to address the problem of the nodes being entirely on or off, the nodes are still discrete.

We did not choose to model the cAMP-PKA network with a multi-state model since this is a linear model and thus is not able to replicate the different Ma et al. (1999) Pde mutant cases.

Probabilistic Boolean Networks

Within a given network, there is biological uncertainty, for example at the molecular level it is uncertain when two molecules will bind with one another. The probabilistic Boolean model (Ching et al. (2007); Li et al. (2007); Shmulevich et al. (2002)) takes this uncertainty into account. The probabilistic Boolean model is an extension of the Boolean model. The genes within the network are still labeled as nodes:

$$X = \{x_i\}_{i=1}^n$$

Instead of one logic expression F that describes all the interactions in the network we have various expressions to choose from. In the probabilistic Boolean network:

$$F = \{F_i\}_{i=1}^n \qquad \text{where} \qquad F_i = \{f_k\}_{k=1}^{l(i)}$$

That is instead of one Boolean network we have $l(i)$ different possible sets of genes that affect gene i, and thus $\Pi_{i=1}^N l(i)$ different possible networks to choose

from. Since there are multiple update functions, we choose each function f_i^l with probability c_j^i where $\sum_j^{l(i)} c_j^i = 1$. Once we have a given network describing the interactions between the genes, we keep that network with probability λ; so that at each time step we have a probability of keeping our present network or randomly choosing a new one. Thus, the dynamics of a probabilistic Boolean network can be modeled by a Markov chain.

As with the Boolean model, we did not model the cAMP-PKA network with a probabilistic Boolean model since we are seeking to understand the continuous dynamics immediately following glucose stimulation, and this model is a discrete model.

2.2.2 Continuous Models

Stochastic Model

In a stochastic model (Li et al. (2007); Kim et al. (2004)), we must first define every state that the gene in the network can be in. For example, a gene can be by itself or bound together with another gene in the network. Then for a given network we can say that there are N states defined by S_1, S_2,...,S_N. Note that a state S_i that describes a gene by itself is different from a state S_j describing that same gene bound to another gene. These states can interact through M different chemical reactions given by R_1, R_2,...R_M. Let $X_i(t)$ be the number of molecules of a gene (or protein) in state S_i at time t. Then the network is defined as:

$$\mathbf{X}(t) = \{X_1(t), X_2(t), ..., X_N(t)\}$$

The network changes by giving a probability to each reaction. The network is updated discretely for a small time step τ:

$$\mathbf{X}(t+\tau) = \mathbf{X}(t) + \sum_{j=1}^{M} v_j P_j(a_j(\mathbf{X}), \tau)$$

Here $P_j(a_j(\mathbf{X}), \tau)$ is an independent sample of the Poisson random variable with mean and variance $a_j(\mathbf{X}) = h_j(\mathbf{X})c_j$ where $h_j(\mathbf{X})$ is the number of distinct reactant molecular combinations and c_j is the stochastic rate constant associated with reaction R_j. Finally v_j is a state change vector, where each element v_{ij} in this vector represents the change of state S_i due to reaction R_j.

We chose not to model the cAMP-PKA network with a stochastic model since this type of model requires us to model every reaction in the system. There is not an easy way to simplify the system in order to highlight the important interactions, or to analyze the model. Also we are required to have estimates on the number of molecules for every gene in the system, leading to many more parameters in the system.

Piecewise-Linear Models

A piecewise-linear model is the continuous analog to the Boolean network (Glass and Kauffman (1973); Casey et al. (2005, 2006); de Jong and Page (2008)). The variables in a piecewise-linear model are the genes in the network, while the differential equations describe regulatory interactions in the network as step functions. In piecewise linear models we define thresholds where the dynamics of the differential equations change when the concentrations of the proteins pass the threshold.

Example The dynamics of the two gene network

$$[A] \underset{\kappa_b}{\overset{\kappa_a}{\rightleftharpoons}} [B],$$

where gene A activates gene B and B activates A. The network can be described as a piecewise-linear model

$$\frac{d[A]}{dt} = \kappa_a S^+([B], \theta_b^1) - \gamma_a[A]$$

$$\frac{d[B]}{dt} = \kappa_b S^+([A], \theta_a^1) - \gamma_b[B]$$

Here:

$$S^+([i], \theta_i) = \begin{cases} 1 & \text{if } [i] > \theta_i \\ 0 & \text{if } [i] < \theta_i \end{cases}$$

Thus gene A is produced at rate k_a if the concentration of gene B is above the threshold θ_b^1. Similarly, gene B is expressed at a rate of k_b when the concentration of A is above the threshold θ_a^1. Using this model, we divide the domain into distinct regions based on the concentrations of A and B. In each domain the differential equation is a linear differential equation based on the concentrations of the genes.

Although a piecewise linear model is easy to understand, we chose not to model our system with a piecewise linear system since competitive reactions, needed in our model to explain the Ma et al. (1999) data, do not fit into a model of this form. Also this type of model requires many parameters, since we need to define all the threshold parameters.

Hill-Function Models

Instead of modeling reactions with piecewise linear equations, we can model with a continuous model using Hill functions (Alon (2007)).

Example The dynamics of the two gene network

$$[A] \underset{\kappa_b}{\overset{\kappa_a}{\rightleftharpoons}} [B],$$

where gene A activates gene B and B activates A. The network can be described as a Hill function model

$$\frac{d[A]}{dt} = \kappa_a \frac{[B]^n}{(\theta_b^1)^n + [B]^n} - \gamma_a[A]$$

$$\frac{d[B]}{dt} = \kappa_b \frac{[A]^n}{(\theta_a^1)^n + [A]^n} - \gamma_b[B]$$

Then the piecewise linear model is the case $n \to \infty$. We chose not to model the cAMP-PKA network with a Hill function model since we do not need a more complicated form ($n > 1$) to explain the experimental results.

2.3 Comparison to Previous Models of the cAMP-PKA Network

There have been a number of recent studies that have proposed mathematical models for the cAMP-PKA network (Cazzaniga et al. (2008); Gonze and Goldbeter (2008); Williamson et al. (2009)). We outline four models here, and explain why they can not adequately model both the short and long–term dynamics of the cAMP-PKA network that motivate our model. Competitive inhibition between Pde1, Pde2, and Ira, presented in Section 2.1, is the most important aspect of our model. This assumption sets our model apart from previous models of the cAMP-PKA network. We use this assumption to explain the surprising results reported by Ma et al. (1999), particularly the Pde1 knockout case and double Pde knockout out cases which the previous models of the cAMP-PKA network can not replicate.

We start by examining the model proposed by Garmendia-Torres et al. (2007) since we use their results to motivate our model. Garmendia-Torres et al. (2007) developed a system of seven differential equations, with Michaelis-Menten Equations. They account for only one form of Pde, thus their model can not replicate the dynamics of the cAMP-PKA network proposed by Ma et al. (1999).

Gonze and Goldbeter (2008) propose a stochastic model, which is a direct extension of the Garmendia-Torres et al. (2007) model, to explore the effects of the cAMP-PKA network on the transcription factor Msn2. This model only focuses on the long–term dynamics and can not be used to understand the Pde mutant

cases observed by Ma et al. (1999) that motivate our study.

Cazzaniga et al. (2008) employed a stochastic modeling approach to study the yeast cAMP-PKA network. For an outline of a stochastic model, see Section 2.2.2. Though they do explore the effects of different Pde activities, their model does not explicitly account for the mutant cases described by Ma et al. (1999) and again they can not replicate the double Pde knockout. Also they do not consider the long–term dynamics proposed by Garmendia-Torres et al. (2007).

The differential equation model of Williamson et al. (2009) is the closest in approach to ours. Their model is able to reproduce the relevant dynamics of the Pde1 and Pde2 single mutants but does not account for the behavior of the Pde double mutant. This is significant since the double Pde knockout case is the hardest to explain. In the double Pde knockout case their model would predict rapid accumulation of cAMP. Also their model only focuses on the short-term dynamics of cAMP and does not account for the longer-term dynamics of cAMP.

3

Model

To fully describe the reactions in the cAMP-PKA network, shown in Figure 1.3, a system of nine time-dependent differential equations is needed. In this section we examine this full nine-dimensional system. We then impose three conditions in order for our model to replicate the Ma et al. (1999) and Garmendia-Torres et al. (2007) data. We also impose four steady-state conditions to further simplify our model to a five-dimensional system. Treating both forms of Pde as a single variable allows us to reduce the model to a four-dimensional system. Once simplified to a four-dimensional system we rescale the model to eliminate as many parameters as possible. As a result we model the cAMP-PKA network with the following system of differential equations:

$$\frac{dr}{dt} = \frac{A(1-r)}{\Gamma_1 + 1 - r} - \frac{Bzr}{\Gamma_1 + r} \tag{3.1a}$$

$$\frac{dz}{dt} = N(x^2 - z) \tag{3.1b}$$

$$\frac{dp}{dt} = M(x^2 - p) \tag{3.1c}$$

$$\frac{dx}{dt} = C + Gr - D_0 x - \frac{Dpx}{\Gamma + x} \tag{3.1d}$$

In Equations (3.1a)–(3.1d) the concentration of Ras·GTP is represented by variable r; the concentration of Ras·GDP is represented by $(1 - r)$; the concentrations of Ira1 and Ira2 are represented by z; the variable p represents the concentration of Pde1 in Ma et al. (1999) Cases 1, 3, and 4 (*wt*, Δ*pde2*, and Δ*pde1*^{ala152}) and the concentration of Pde2 in Case 2; the concentration of cAMP is represented by x; x^2 represents the concentration of active PKA (Tpk1, 2 or 3); and time is given by variable t.

3.1 Full Model

The full model describing the reactions in Figure 1.3 is a system of nine time-dependent differential equations. This system models changes in the concentrations of: 1) Gpa2·GTP (active Gpa2); 2) Cdc25; 3) Ras·GTPase Ira1 and Ira2; 4) Ras·GTP (active Ras2); 5) adenylate cyclase activity; 6) activated Pde1; 7) activated Pde2; 8) cAMP; and 9) active PKA (free catalytic subunits). The concentrations have units of fmol/(10^6 cells) and time has a scale of minutes.

[Gpa2·GTP] $$\frac{dg}{dt} = P_g[Glu] - D_g g \tag{3.2}$$

[Cdc25*] $$\frac{dc}{dt} = P_c - D_c[Stress]c \tag{3.3}$$

[Ira*] $$\frac{dz}{dt} = \frac{R_z(C_z - z)y}{\Gamma_z \sum(z, p_1, p_2)} - D_z z \tag{3.4}$$

[Ras·GTP] $$\frac{dr}{dt} = \frac{R_r c(C_r - r)}{\Gamma_r + C_r - r} - \frac{\bar{R}_r z r}{\Gamma_r + r} \tag{3.5}$$

[Aden-cyc] $$\frac{da}{dt} = (P_a + \bar{P}_a g r) - D_a a \tag{3.6}$$

[Pde1*] $$\frac{dp_1}{dt} = \frac{R_{p_1}(C_{p_1} - p_1)y}{\Gamma_{p_1} \sum(z, p_1, p_2)} - D_{p_1} p_1 \tag{3.7}$$

[Pde2*] $$\frac{dp_2}{dt} = \frac{R_{p_2}(C_{p_2} - p_2)y}{\Gamma_{p_2} \sum(z, p_1, p_2)} - D_{p_2} p_2 \tag{3.8}$$

[cAMP] $$\begin{aligned}\frac{dx}{dt} = P_x a - \left(D_x x + \frac{R_{x1} p_1 x}{\Gamma_{x1} + x} + \frac{R_{x2} p_2 x}{\Gamma_{x2} + x} \right) \\ - 4\left(K_b x^4 (C_y - \frac{y}{2}) - K_f y^3 \right)\end{aligned} \tag{3.9}$$

[Tpk] $$\frac{dy}{dt} = 2\left(K_b x^4 (C_y - \frac{y}{2}) - K_f y^3 \right) \tag{3.10}$$

Here the asterisk (*) indicates the activated form of the enzyme. The notation for the parameters are as follows: P is a production term at a rate independent of

the concentration of the enzyme being produced; D is a linear decay rate; K is a reaction coefficient in a binary (or higher order) reaction; R is a reaction coefficient in a catalyzed reaction (that is the Michaelis-Menten rate); C is a total concentration of an enzyme; and Γ is a Michaelis-Menten affinity.

3.1.1 Derivation of Equations (3.2)–(3.10)

We modeled the reactions within the cAMP-PKA network with mass action kinetics and where possible applied the Michaelis-Menten Equation. We refer the reader to Claim 2 in Section 2.1 for the derivation of the Michaelis-Menten Equation modeling the activation of a substrate $[S]$ by an enzyme $[E]$. In this section we examine the derivation of each equation, highlighting the location of the variable in the cAMP-PKA network as seen in Figure 1.3.

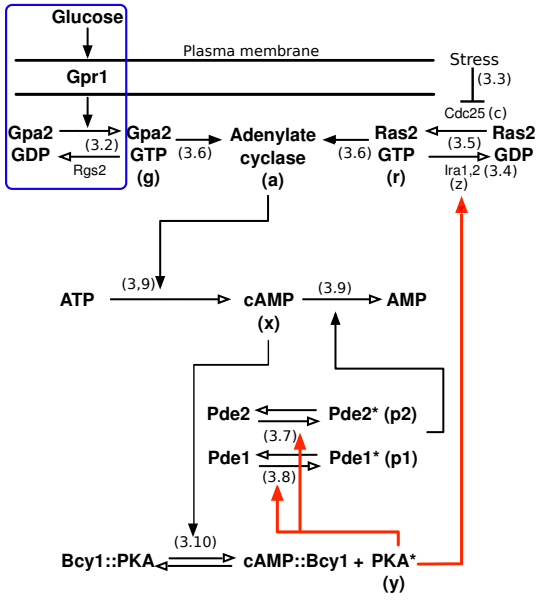

Equation (3.2)*:* We describe the activation of Gpa2 to GTP form with a Michaelis-Menten Equation in which the inactive form of Gpa2 (Gpa2·GDP) acts as the substrate and Gpr1 is the catalyzing enzyme. We describe the inactivation of Gpa2 to GDP form with a Michaelis-Menten Equation in which the active form of Gpa2 (Gpa2·GTP) acts as the substrate and Rgs2 is the catalyzing enzyme. We model the dynamics of Gpa2·GTP as the sum of these two Michaelis-Menten Equations. We then linearize to the form given by Equation (3.2). This linearization reduces the number of parameters in our system. We choose to linearize since in the simplifi-

cation of our model we assume that the concentration of Gpa2 is at steady state. We do not model the change in Gpr1, rather we assume that Gpr1 activity is proportional to the extracellular glucose levels ($[Glu]$).

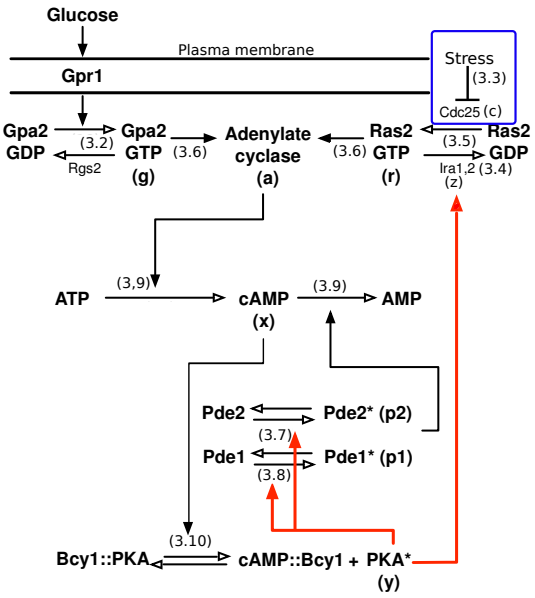

Equation (3.3)*:* We describe the activation of Cdc25 with a Michaelis-Menten Equation in which the inactive form of Cdc25 acts as the substrate and upstream targets, assumed to be constant in our model, act as catalyzing enzymes. We describe the inactivation of Cdc25 with a Michaelis-Menten Equation in which the active form of Cdc25 acts as the substrate and physiological stress levels catalyze this reaction. We model the dynamics of Cdc25 as the sum of these two Michaelis-Menten Equations. We then linearize this equation to the form given by Equation (3.3), again reducing the number of parameters in our model. We choose to linearize since in the simplification of the model we assume that the concentration of Cdc25 is at steady state. At steady state the activity of Cdc25 will be a function of the cell's stress levels.

Equations (3.4), (3.7), *and* (3.8)*:* We derive Equations (2.1)–(2.3) in Section 2.1 to describe the dynamics of Ira, Pde1 and Pde2 (shown in our figures as the three red arrows). In Equations (3.4), (3.7), and (3.8) the active concentrations of Ira ($[\text{Ira}^*]$ in (2.3)), Pde1 ($[\text{Pde1}^*]$ in (2.1)), and Pde2 ($[\text{Pde2}^*]$ in (2.2)) are represented by variables z, p_1, and p_2, respectively. To simplify the expression of these equations

we introduce the following notation,

$$\sum(c, p_1, p_2) = 1 + \frac{C_z - z}{\Gamma_z} + \frac{C_{p_1} - p_1}{\Gamma_{p_1}} + \frac{C_{p_2} - p_2}{\Gamma_{p_2}} \tag{3.11}$$

where $(C_z - z)$ is the inactive form of Ira ($[Ira]$ in (2.3)), $(C_{p_1} - p_1)$ is the inactive form of Pde1 ([Pde1] in (2.1)) and $(C_{p_2} - p_2)$ is the inactive form of Pde2 ([Pde2] in (2.2)).

Equation (3.5)*:* We describe the activation of Ras2 to GTP form with a Michaelis-Menten Equation in which the inactive form of Ras2 (Ras·GDP) acts as the substrate and Cdc25 is the catalyzing enzyme. We describe the inactivation of Ras2 to GDP form with a Michaelis-Menten Equation in which the active form of Ras2 (Ras·GTP) acts as the substrate and Ira1 and Ira2 (z) catalyze this reaction. Then the dynamics of Ras·GTP are modeled by the sum of these two Michaelis-Menten Equations in Equation (3.5). In order to model the sustained oscillations predicted by Garmendia-Torres et al. (2007) we need to model the dynamics of Ras·GTP, thus we choose not to simplify Equation (3.5) by linearizing.

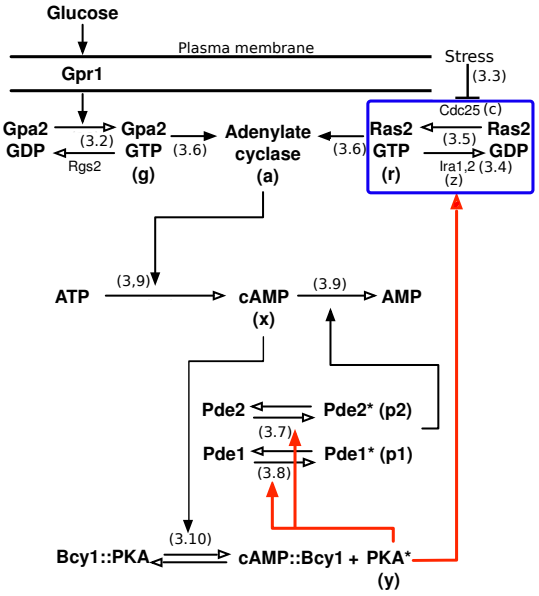

Equation (3.6)*:* The activity of adenylate cyclase is controlled simultaneously by both Gpa2·GTP and Ras·GTP, described using mass action kinetics in Equation (3.6) (pP_agr). The activity of adenylate cyclase also has a basal level independent of glucose levels (P_a), and a decay rate proportional to its own activity (D_a).

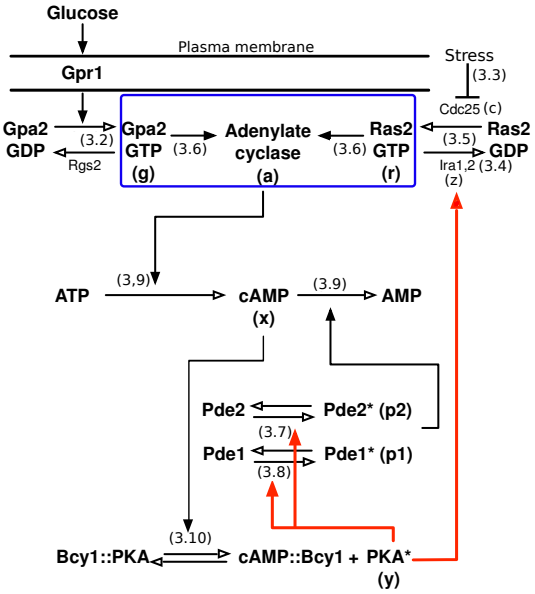

Equation (3.9)*:* We describe the production of cAMP by adenylate cyclase with mass action kinetics (P_xa). The decay of cAMP takes three forms, a small amount of basal decay (D_x), decay catalyzed by Pde1 modeled by a Michaelis-Menten Equation, and decay catalyzed by Pde2 also modeled by a Michaelis-Menten Equation. The basal decay is needed since in the absence of any Pde the concentration of cAMP remains bounded. Since Pde1 is low-affinity and Pde2 is high-affinity the Michaelis-Menten parameter Γ_{x1} has a value that is twice as large as Γ_{x2}.

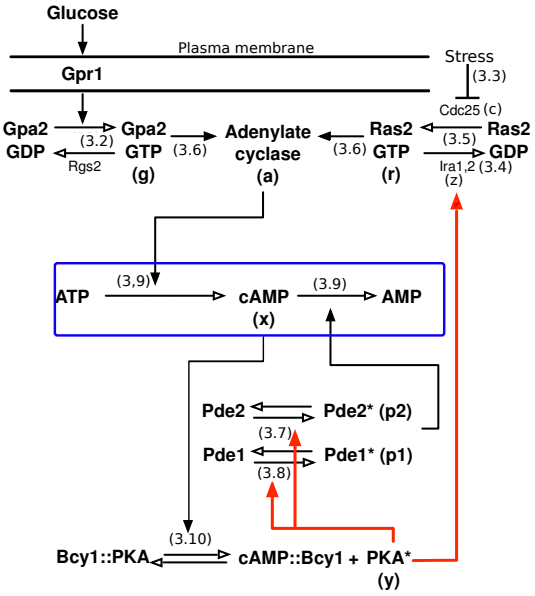

Equations (3.9) *and* (3.10)*:* We model cAMP binding to PKA and releasing the active form of PKA with mass action kinetics. In our model four cAMP bind to a single PKA unit, made up of two catalytic subunits (y) and two regulatory subunits ($C_y - \frac{y}{2}$). cAMP binds to the two regulatory subunits releasing the two catalytic subunits.

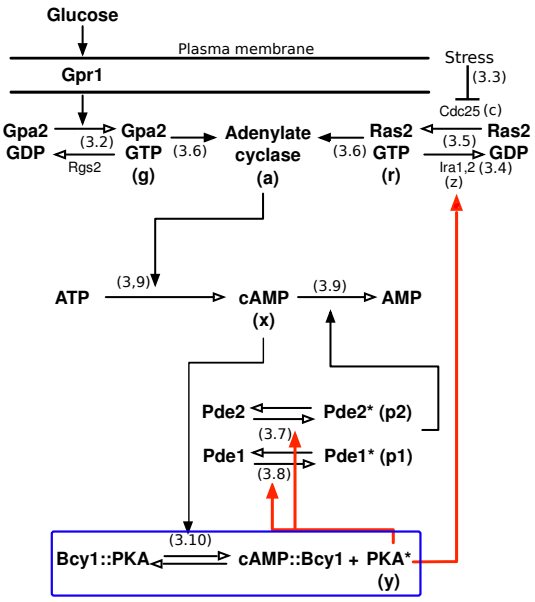

3.1.2 *Simplifying Assumption*

To simplify Equations (3.4), (3.7), and (3.8), we assume that the total concentrations of Ira, Pde1, and Pde2 (C_z, C_{p_1}, and C_{p_2}) are always much greater than the active concentrations of Ira, Pde1, and Pde2. Thus, we may approximate inactive Ira as C_z, inactive Pde1 as C_{p_1}, and inactive Pde2 as C_{p_2}. That is $C_z - z \approx C_z$, $C_{p_1} - p_1 \approx C_{p_1}$, and $C_{p_2} - p_2 \approx C_{p_2}$ in Equations (3.4), (3.7) and (3.8).

This assumption was only made for simplification of the model. It is not a necessary condition for the model to be able to replicate the experimental data of either Ma et al. (1999) or Garmendia-Torres et al. (2007) as we will see in Section 5. Lacking this simplification we would only be able to take a numerical approach to understanding the behavior of our system. Assuming that the inactive concentrations of Ira, Pde1 and Pde2 are much larger than the respective active concentrations, we can approximate Equation (3.11) as:

$$\sum(c, p_1, p_2) \approx 1 + \frac{C_z}{\Gamma_z} + \frac{C_{p_1}}{\Gamma_{p_1}} + \frac{C_{p_2}}{\Gamma_{p_2}}, \tag{3.12}$$

which is a constant. As a result, the activating terms in Equations (3.4), (3.7), and

(3.8) reduce to a constant multiplied by the concentration of active PKA (y):

$$\frac{dz}{dt} \approx \frac{R_z C_z}{\Gamma_z + C_z + \frac{\Gamma_z C_{p_1}}{\Gamma_{p_1}} + \frac{\Gamma_z C_{p_2}}{\Gamma_{p_2}}} y - D_z z \tag{3.13}$$

$$\frac{dp_1}{dt} \approx \frac{R_{p_1} C_{p_1}}{\Gamma_{p_1} + C_{p_1} + \frac{\Gamma_{p_1} C_z}{\Gamma_z} + \frac{\Gamma_{p_1} C_{p_2}}{\Gamma_{p_2}}} y - D_{p_1} p_1 \tag{3.14}$$

$$\frac{dp_2}{dt} \approx \frac{R_{p_2} C_{p_2}}{\Gamma_{p_2} + C_{p_2} + \frac{\Gamma_{p_2} C_z}{\Gamma_z} + \frac{\Gamma_{p_2} C_{p_1}}{\Gamma_{p_1}}} y - D_{p_2} p_2 \tag{3.15}$$

3.2 Imposed Conditions

In order for the model to replicate the dynamics observed by Ma et al. (1999) and Garmendia-Torres et al. (2007) we impose the following conditions:

Condition (a) The following inequalities must hold:

$$\frac{\Gamma_1[\text{Pde2}]}{\Gamma_2[\text{Pde1}]} << 1 \tag{3.16}$$

$$\frac{\Gamma_2[\text{Ira}]}{\Gamma_z[\text{Pde2}]} << 1 \tag{3.17}$$

Condition (b) In comparing analogous reactions of Pde1 and Pde2, the reactions of Pde2 are uniformly slower.

Condition (c) PKA rapidly activates Ira1 and Ira2.

3.2.1 Why Impose these Conditions

We impose Conditions (a) and (b) in order for our model, Equations (3.2)–(3.10), to be able to replicate the experimental dynamics observed by Ma et al. (1999). Condition (c) is imposed so that our model is able to replicate the dynamics proposed by Garmendia-Torres et al. (2007) while maintaining the Ma et al. (1999) results.

In this section we explain how these three conditions allow us to replicate the experimental dynamics. In the next section we look at other possible conditions that we could have imposed.

Condition (a) states that PKA's affinity for Pde1 is much greater than PKA's affinity for Pde2, which in turn is much greater than PKA's affinity for Ira. That is, PKA preferentially activates Pde1 over Pde2 and Pde2 over Ira1 and Ira2. Since PKA preferentially activates Pde1 over Pde2, when Pde1 is present Pde2's activity is minimal, and thus Pde2 has almost no effect on the concentration of cAMP. This explains the similarity in the Ma et al. (1999) wild type and the Pde2 knockout cases. Since PKA preferentially activates Pde1 and Pde2 over Ira1 and Ira2, whenever either form of Pde is present it inhibits PKA's activation of Ira1 and Ira2. In the absence of both forms of Pde, PKA is free to activate Ira1 and Ira2, strongly increasing their inhibition of Ras·GTP. This explains the Ma et al. (1999) double Pde knockout case. Since Ras·GTP is inhibited, and only the GTP form of Ras stimulates adenylate cyclase activity, adenylate cyclase is reduced to a basal level (P_a) independent of glucose.

Condition (b) states that the activation and inactivation of Pde2 is uniformly slow. This explains the Ma et al. (1999) Pde1 knockout case. Since Pde2 degrades the concentration of cAMP, slow accumulation of Pde2 results in a slow decay of cAMP. Thus, the slow activity of Pde2 will be responsible for the much larger and longer transient response to glucose observed by Ma et al. (1999). We assume that the activation and inactivation are uniformly slower simply for ease. This assumption allows us to model the activation of both Pde1 and Pde2 with a single variable that is case dependent.

Condition (c) states that when PKA activates Ira1 and Ira2 it does so rapidly. Negative feedback through PKA's activation of Ira1 and Ira2 is responsible for the sustained oscillations observed by Garmendia-Torres et al. (2007) at interme-

diate stress levels. When the cell experiences intermediate stress the inhibition of Ras·GTP by Ira1 and Ira2 will balance with the activity of Cdc25 which is reduced due to the stress. As a consequence, Ras will oscillate between GTP and GDP form. Since only Ras·GTP activates adenylate cyclase, this oscillation between GTP and GDP forms of Ras will drive the oscillations in the concentration of cAMP. Competitive inhibition between Pde1, Pde2, and Ira, presented in Section 2.1, is the most important aspect of our model. This assumption sets our model apart from previous models of the cAMP-PKA network. We choose to assume the particular form of Condition (c) so that we can replicate the sustained oscillations observed by Garmendia-Torres et al. (2007) while maintaining competitive inhibition between Ira, Pde1 and Pde2. Since Ira1 and Ira2 have low affinity for PKA (Condition (a)) if their activation by PKA was slow, Pde1 and Pde2 would almost completely inhibit PKA from interacting with Ira1 and Ira2 allowing us to neglect this interaction. However, due to the rapid activation of Ira1 and Ira2 by PKA, even when Pde1 and Pde2 inhibit PKA's interaction with Ira we cannot ignore this interaction.

3.2.2 Other Conditions We Could Have Imposed

We now examine other possible conditions that we could have imposed. In seeking to explain the Ma et al. (1999) data we need to find a reasonable explanation for both the Pde2 knockout case and the double Pde knockout case. The Pde2 knockout case could be explained by assuming that the decay of cAMP due to Pde1 is much more effective than the decay due to Pde2. However, this only explains the Pde2 knockout case, the real challenge is to explain the double Pde knockout case. In the absence of any Pde, cAMP is no longer affected by glucose, yet neither Pde1 or Pde2 are known to have a direct effect on the production of cAMP. Thus, Pde must have either a direct effect on cAMP that is not known, or indirect effect

on the activity of adenylate cyclase. A possible explanation for the double Pde knockout cases is that PKA inhibits Cdc25 or Gpr1 activity, or activates Rgs2. In order for any of these cases to replicate the Ma et al. (1999) dynamics we would again have to impose Condition (a) only with the new enzyme (Cdc25, Gpr1 or Rgs2) taking the place of Ira. Thus, these cases are not very different from our present assumption. We choose to model PKA activation of Ira over activation of Rgs2, or inactivation of Cdc25 and Gpr1, since there is the strongest biological support for PKA's interaction with Ira1 and Ira2 Kraakman et al. (1999); Lacal and McCormick (1993). We also could have assumed that both Pde1 and Pde2 act directly upstream of cAMP, so that in their absence the activity of adenylate cyclase would be reduced to a basal level. However, there is no biological evidence that this could be the case. Other types of models for the cAMP-PKA network, such as Boolean models or piecewise linear models presented in Section 2.2, can not incorperate competitive reactions needed to replicate the double Pde knockout case. In other model types we would need to impose some outside condition as an explanation for why glucose has no effect on the network in the absence of Pde.

Condition (b) is a stronger condition than is necessary. To replicate the Ma et al. (1999) data we only need the activation of Pde2 to be slower than the activation of Pde1. We assume the activation and inactivation of Pde2 are uniformly slower so that we can describe both Pde1 and Pde2 as a single variable. Another possible explanation for the longer transient response to glucose observed in the Pde1 knockout case is that the decay rate of cAMP due to Pde2 is much slower than the decay rate due to Pde1. However, this is not likely since Pde2 has much higher affinity for cAMP than Pde1 does.

Condition (c) is imposed so that our model is able to replicate the results predicted by Garmendia-Torres et al. (2007). We could also assume that PKA feed-

back on Cdc25 or on Gpa2 causes oscillations. However, the strongest biological evidence supports PKA feedback through Ira. Another possible assumption is that cAMP oscillations are not a result of negative feedback within the cAMP-PKA network; rather they are caused by negative feedback outside the cAMP-PKA network. This would require a much broader model, and thus be much harder to analyze. We also could have assumed that in the short term Ira's activation by PKA is inhibited by Pde1 and Pde2 but in the long term this inhibition no longer holds. With this condition we would effectively have two models to look at, a model for the short–term dynamics and a model for the long–term dynamics.

3.2.3 *Effect of Conditions (a), (b), and (c) on Equations* (3.13), (3.14), *and* (3.15)

Conditions (a), (b), and (c) simplify Equations (3.13), (3.14), and (3.15), with results for Ma et al. (1999) **Cases 1–5** as follows.

Equation (3.13)*:* In **Case 5**, both Pde1 and Pde2 are zero; therefore Equation (3.13) can be rewritten as:

$$\frac{dz}{dt} \approx N_z y - D_z z, \tag{3.18}$$

where

$$N_z = \frac{R_z C_z}{\Gamma_z + C_z}. \tag{3.19}$$

When either Pde1 or Pde2 is nonzero:

$$\frac{R_z C_z}{\Gamma_z + C_z + \frac{\Gamma_z}{\Gamma_{p_1}} C_{p_1} + \frac{\Gamma_z}{\Gamma_{p_2}} C_{p_2}} \approx \frac{R_z C_z}{\frac{\Gamma_{p_1}}{\Gamma_z} C_{p_1} + \frac{\Gamma_{p_2}}{\Gamma_z} C_{p_2}} = \tilde{N}_z. \tag{3.20}$$

We can make this approximation since the last two terms in the denominator are large, by Condition (a). By Condition (c) we know R_z is also large so we can not approximate this term by zero; therefore in **Cases 1–4** Equation (3.13) can be

rewritten as:

$$\frac{dz}{dt} \approx \tilde{N}_z y - D_z z \tag{3.21}$$

where $\tilde{N}_z << N_z$.

Equation (3.14)*:* To apply Condtion (a) examine the non-linear terms in the denominator of:

$$\frac{R_{p_1} y}{\frac{\Gamma_{p_1}}{C_{p_1}} + 1 + \frac{\Gamma_{p_1} C_{p_2}}{\Gamma_{p_2} C_{p_1}} + \frac{\Gamma_{p_1} C_c}{\Gamma_c C_{p_1}}}.$$

Inequalities (3.16) and (3.17) allow us to neglect the last two terms in the denominator. Thus in **Cases 1, 3, and 4** Equation (3.14) simplifies to:

$$\frac{dp_1}{dt} \approx N_1 y - D_{p_1} p_1, \tag{3.22}$$

where

$$N_1 = \frac{R_{p_1}}{\frac{\Gamma_{p_1}}{C_{p_1}} + 1}.$$

In **Case 2** Pde1 is eliminated, so Equation (3.14) is replaced by the trivial equation $p_1 \equiv 0$.

Equation (3.15)*:* In **Case 2**, Pde1 has been eliminated ($p_1 \equiv 0$), and as above Inequalities (3.16) and (3.17) allow us to neglect the last term in the denominator of Equation (3.15). Thus Equation (3.15) simplifies to:

$$\frac{dp_2}{dt} \approx N_2 y - D_{p_2} p_2, \tag{3.23}$$

where

$$N_2 = \frac{R_{p_2}}{\frac{\Gamma_{p_2}}{C_{p_2}} + 1}.$$

In all other cases Equation (3.15) is replaced by the trivial equation $p_2 \equiv 0$. In **Cases 1 and 4** this is because Pde1 is nonzero, so by Inequality (3.16) the denominator is

very large, and by Condition (b) the numerator is small, thus we can approximate the whole expression as zero. In **Cases 3 and 5** this is because Pde2 has been knocked out.

3.2.4 Effect of Condition (b) on Equation (3.23)

Condition (b) is imposed to fit **Cases 2 and 4** in the data reported by Ma et al. (1999). The slower activation of Pde2 is responsible for the larger transient response observed in these two cases (Figure 1.4). Applying this condition we can define a non-dimensional parameter

$$M = \frac{D_{p_2}}{D_{p_1}}, \tag{3.24}$$

such that the value of M must be much less than one ($M << 1$). Changing the units of Pde2 if necessary, we can arrange that

$$N_2 = MN_1. \tag{3.25}$$

Note that in every case at least one form of Pde has been eliminated. Since we have expressed the parameters in Equation (3.23) as a constant multiple of the parameters in Equation (3.22), we can express both as one equation:

$$\frac{dp}{dt} = M(N_1 y - D_1 p). \tag{3.26}$$

In **Cases 1 and 3** the variable p represents Pde1 and the parameter M takes the value 1. In **Case 2** the variable p represents Pde2 and the parameter M is given by Equation (3.24), which is much less than 1. In **Case 4** the variable p is again Pde1 but now parameter M is reduced to 0.2 since in this case the Pde1 mutant is slow activating. Of course in **Case 5**, the p-equation is not needed.

3.3 Steady-State Assumptions

The model may be further simplified by assuming that the following four reactions are fast and hence proceed to steady state.

I Gpa2·GDP $\rightleftharpoons$ Gpa2·GTP (reaction 3.2 in Figure 1.3).

II Activation/inactivation of Cdc25 (reaction 3.3 in Figure 1.3).

III Activation/inactivation of adenylate cyclase (reaction 3.6 in Figure 1.3).

IV cAMP+[Bcy1::PKA] $\rightleftharpoons$ [cAMP::Bcy1] +PKA* (reaction 3.10 in Figure 1.3).

Let us first discuss the steady-state assumptions for each of these four reactions, then we will explain why we made these steady–state assumptions.

Gpa2·GDP $\rightleftharpoons$ Gpa2·GTP at steady state

Gpa2·GTP is independent of all other variables, thus at steady state Gpa2·GTP is only a function of the glucose available to the cell:

$$g = \frac{P_g}{D_g}[\text{Glu}]. \tag{3.27}$$

Activation/inactivation of Cdc25 at steady state

Cdc25 is independent of all other variables, thus at steady state Cdc25 is only a function of the stress on the cell:

$$c = \frac{P_c}{D_c[Stress]}. \tag{3.28}$$

Thus, stress inhibits the activity of Cdc25.

Activation/inactivation of adenylate cyclase at steady state

Applying this steady-state assumption to Equation (3.6) we get that the steady-state value of adenylate cyclase is:

$$a = \frac{P_a}{D_a} + \frac{\bar{P}_a P_g}{D_a D_g}[\text{Glu}]r. \tag{3.29}$$

cAMP+[Bcy1::PKA] $\rightleftharpoons$ [cAMP::Bcy1] +PKA* at steady state

In Equation (3.10) we model this reaction with mass action kinetics as:

$$\frac{dy}{dt} = 2\left(K_b x^4 (C_y - \frac{y}{2}) - K_f y^3\right).$$

The reaction modeled here is: four cAMP molecules bind to a single PKA unit, which is made up of two catalytic subunits (either Tpk1, Tpk2 or Tpk3) and two regulatory subunits (Bcy1). cAMP binds to the regulatory subunits and releases the catalytic subunits creating the active form of PKA (PKA*). We can simplify this reaction in two ways, first by assuming that the concentration of Tpk does not approach its maximum ($C_y - \frac{y}{2} \approx C_y$), and second that we can approximate the 4 to 2 reaction by a 2 to 1 reaction. This simplifies Equation (3.10) to:

$$\frac{dy}{dt} = 2(K_b x^2 - K_f y).$$

Although we know from Garmendia-Torres et al. (2007) that this reaction (reaction 3.10 in Figure 1.3) is not faster than the other reactions in the system, we nevertheless make the simplest assumption consistent with the Ma et al. (1999) data. Thus, we assume that the activation/inactivation of PKA proceeds to steady state. We can then express the concentration of PKA (y) in terms of the concentration of cAMP (x):

$$y = \frac{K_b}{K_f} x^2.$$

Of course models in which the reaction cAMP+[Bcy1::PKA] $\rightleftharpoons$ [cAMP::Bcy1] +PKA* is not at steady state could fit the data of Ma et al. (1999) as well as our model or better. However, allowing this additional flexibility would lead to even more parameters needing to be chosen in the absence of sufficient data. Thus, this assumption is only taken for mathematical simplicity of the model, it is not a necessary condition to numerically replicate the dynamics observed by either Ma et al. (1999) or Garmendia-Torres et al. (2007).

3.3.1 Why Impose Steady-State Assumptions

To fully describe the reactions in Figure 1.3 requires a system of nine differential equations as described by Equations (3.2)–(3.10). This system has over 35 parameters, all of which need to be experimentally measured. Given a full list of parameters we could numerically solve this system and show that given Conditions (a), (b) and (c) we can numerically replicate the experimental and predicted results. We show this in Section 5. Our goal in building our model is to be able to both replicate the previously predicted dynamics and to make novel predictions about the cAMP-PKA network. We could make predictions based on numerical results alone; however, choosing which parameters to vary would just be a guessing game. In order to analyze our model we sought to simplify to only the key reactions. We model the concentration of cAMP since this is the experimentally measured variable. We model the dynamics of Pde since the Ma et al. (1999) data focus on Pde knockout cases. We simplify by modeling both forms of Pde as a single variable. We will show in Section 4.5 that for our system to experience sustained oscillations we need to model the dynamics of both Ira and Ras·GTP. Thus, the four dimensional model describing the dynamics of Ras·GTP, Ira, Pde, and cAMP is the simplest model that is capable of replicating the experimental data; thus, we assume the remaining variables are at steady state.

3.4 Simplified Model

Conditions (a), (b), and (c), along with the four steady-state assumptions and treating both forms of Pde as a single variable, allow us to reduce Equations (3.2)–(3.10) to the following system:

$$\frac{dr}{dt} = \frac{R_r \frac{P_c}{D_c[Stress]}(C_r - r)}{\Gamma_r + C_r - r} - \frac{\bar{R}_r z r}{\Gamma_r + r} \tag{3.30a}$$

$$\frac{dz}{dt} = N_z \frac{K_b}{K_f} x^2 - D_z z \tag{3.30b}$$

$$\frac{dp}{dt} = M(N_1 \frac{K_b}{K_f} x^2 - D_1 p) \tag{3.30c}$$

$$\frac{dx}{dt} = P_x \frac{P_a}{D_a} + \bar{P}_x \frac{\bar{P}_a P_g}{D_a D_g}[\text{Glu}]r - D_x x - \frac{R_x p x}{\Gamma_x + x} \tag{3.30d}$$

In Equations (3.30a)–(3.30d) the variable r is the concentration of Ras·GTP; z is the concentration of Ira1 and Ira2; p is the concentration of Pde1 in Cases 1, 3, and 4 (*wt*, Δ*pde2*, and Δ*pde1*^{ala152}) and the concentration of Pde2 in Case 2; in Cases 1–4 parameter N_z is defined by Equation (3.19), and in Case 5 parameter N_z is defined by Equation (3.20); x is the concentration of cAMP; and $\frac{K_b}{K_f}x^2$ is the concentration of active PKA.

For convenience, we rewrite these equations. The new parameters are now in bold.

$$\frac{dr}{dt} = \frac{\mathbf{R}_r(C_r - r)}{\Gamma_r + C_r - r} - \frac{\bar{R}_r z r}{\Gamma_r + r} \tag{3.31a}$$

$$\frac{dz}{dt} = \mathbf{P}_z x^2 - D_z z \tag{3.31b}$$

$$\frac{dp}{dt} = \mathbf{P}_p x^2 - D_p p \tag{3.31c}$$

$$\frac{dx}{dt} = \mathbf{P}_x + \bar{\mathbf{P}}_x G r - D_x x - \frac{R_x p x}{\Gamma_x + x} \tag{3.31d}$$

Parameter G is a nondimensional parameter that accounts for glucose, normalized so that $G = 1$ represents a glucose stimulus corresponding to the glucose stimulus applied in the Ma et al. (1999) experiment.

3.5 Scaled Model

To analyze Equations (3.31a)–(3.31d), we introduce the following non-dimensional variables:

First re-scale such that $\bar{r} = \dfrac{r}{R}$, $\bar{z} = \dfrac{z}{Z}$, $\bar{p} = \dfrac{p}{P}$, $\bar{x} = \dfrac{x}{X}$, and $\bar{t} = \dfrac{t}{T}$ with the following parameters:

$$R = C_r \qquad Z = \frac{C_r D_p \bar{\mathbf{P}}_x \mathbf{P}_z}{R_x D_z \mathbf{P}_p} \qquad P = \frac{C_r \bar{\mathbf{P}}_x}{R_x}$$

$$X = \sqrt{\frac{C_r D_p \bar{\mathbf{P}}_x}{R_x \mathbf{P}_p}} \qquad T = \sqrt{\frac{D_p}{R_x \mathbf{P}_p \bar{\mathbf{P}}_x C_r}}$$

This scaling of variables yields the following non-dimensional parameters:

$$A = \frac{\sqrt{D_p}\mathbf{R}_r}{C_r^{3/2}\sqrt{R_x \mathbf{P}_p \bar{\mathbf{P}}_x}} \qquad B = \frac{D_p^{3/2} \bar{R}_r \mathbf{P}_z \sqrt{\bar{\mathbf{P}}_x}}{\sqrt{C_r} R_x^{3/2} D_z \mathbf{P}_p^{3/2}} \qquad \Gamma_1 = \frac{\Gamma_r}{C_r}$$

$$N = D_z \sqrt{\frac{D_p}{C_r R_x \mathbf{P}_p \bar{\mathbf{P}}_x}} \qquad M = D_p \sqrt{\frac{D_p}{C_r R_x \mathbf{P}_p \bar{\mathbf{P}}_x}} \qquad C = \frac{\mathbf{P}_x}{C_r \bar{\mathbf{P}}_x}$$

$$D_0 = D_x \sqrt{\frac{D_p}{C_r R_x \mathbf{P}_p \bar{\mathbf{P}}_x}} \qquad \Gamma = \frac{\Gamma_x \sqrt{R_x \mathbf{P}_p}}{\sqrt{C_r D_p \bar{\mathbf{P}}_x}}$$

We rewrite Equations (3.31a)–(3.31d) in nondimensional form as:

$$\frac{dr}{dt} = \frac{A(1-r)}{\Gamma_1 + 1 - r} - \frac{Bzr}{\Gamma_1 + r} \tag{3.32a}$$

$$\frac{dz}{dt} = N(x^2 - z) \tag{3.32b}$$

$$\frac{dp}{dt} = M(x^2 - p) \tag{3.32c}$$

$$\frac{dx}{dt} = C + Gr - D_0 x - \frac{Dpx}{\Gamma + x} \tag{3.32d}$$

The reduced model, as described by Equations (3.32a)–(3.32d), is shown in Figure 3.1. In the Ma et al. (1999) wild type case parameter D is scaled to be one, and parameter G equals one after a glucose stimulus is applied.

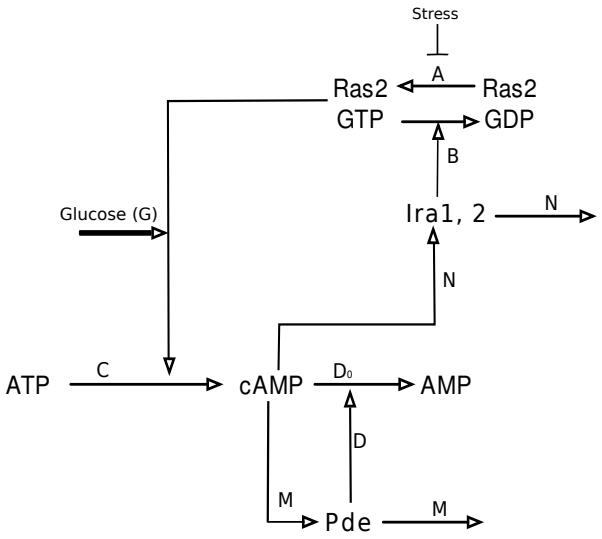

FIGURE 3.1: Simplified model of the cAMP-PKA network as described by Equations (3.32a)–(3.32d). Simplification from the full model described by Figure 1.3 to this model is done by Conditions (a), (b), and (c) given in Section 3.2 along with four steady-state assumptions given in Section 3.3.

4

Analysis

In this section we analyze the four-dimensional model, given by Equations (4.1a)–(4.1d), developed in Section 3 to describe the reactions in the cAMP-PKA network. First we show that Equations (4.1a)–(4.1d) have a unique positive equilibrium in the range $0 < r < 1$, that is the concentration of Ras is bounded between being totally active (in GTP form) and totally inactive (in GDP form). Next, we examine two extreme cases: when the steady-state value of variable r is approximately one ($r_{ss} \approx 1$) and when the steady-state value of r is approximately zero ($r_{ss} \approx 0$). In both of these extreme cases we can reduce the model to a two–by–two system modeling the dynamics of Pde (p) and cAMP (x). The equilibrium of this two-by-two system is always asymptotically stable. For a wide range of parameters, the solution of the two-by-two system will exhibit an oscillatory approach to its equilibrium. After examining these two extreme cases, we examine the four-dimensional model in general. The equilibrium of the four-dimensional model, given by Equations (4.1a)–(4.1d), may lose stability through a Hopf bifurcation. In the special case of $M = N$ we can find an explicit expression for when this occurs. Finally, we argue that the four–by–four system is the simplest model able to replicate both the Ma et al. (1999) and Garmendia-Torres et al. (2007) data by showing that when either Ras (r) or Ira (z) is fixed at steady state the reduced three-by-three system has an asymptotically stable equilibrium.

$$\frac{dr}{dt} = \frac{A(1-r)}{\Gamma_1 + 1 - r} - \frac{Bzr}{\Gamma_1 + r} \tag{4.1a}$$

$$\frac{dz}{dt} = N(x^2 - z) \tag{4.1b}$$

$$\frac{dp}{dt} = M(x^2 - p) \tag{4.1c}$$

$$\frac{dx}{dt} = C + Gr - D_0 x - \frac{Dpx}{\Gamma + x} \tag{4.1d}$$

4.1 Existence of Equilibrium

Claim 3. *Equations* (4.1a)–(4.1d) *have a unique positive equilibrium point in the range* $0 < r < 1$.

Proof. To prove this, we will set Equations (4.1a)–(4.1d) equal to zero and show that in the range $0 < r < 1$ there exists a unique positive solution (r_{ss}, z_{ss}, p_{ss}, x_{ss}). By setting Equations (4.1b) and (4.1c) equal to zero we can express variables p and z in terms of the x:

$$z = p = x^2.$$

Substituting $p = x^2$ into Equation (4.1d) and setting this equation equal to zero, we can solve for variable r in terms of x:

$$r = \frac{1}{G}\left(D_0 x + \frac{Dx^3}{\Gamma + x} - C\right). \tag{4.2}$$

Substituting this expression for r in terms of x, and $z = x^2$ into Equation (4.1a) and setting this equation equal to zero we reduce the four-by-four system to a single equation that we can solve for in terms of x. For convenience of notation define $f(x)$ as the right-hand side of Equation (4.2), then Equation (4.1a) set equal to zero becomes:

$$0 = \frac{A(1 - f(x))}{\Gamma_1 + 1 - f(x)} - \frac{Bx^2 f(x)}{\Gamma_1 + f(x)}. \tag{4.3}$$

Then, we need to show that there exists a unique solution to Equation (4.3). To do this first we will examine the behavior of $f(x)$. Observe that $f(x)$, given by Equation (4.2), is a continuous, monotonically increasing function for x greater than zero. Since

$$f(0) = -\frac{C}{G} \qquad \text{and} \qquad f(x) \to \infty \text{ as } x \to \infty,$$

there exists unique positive real points x_0 and x_1 such that $f(x_0) = 0$ and $f(x_1) = 1$.

Then to solve Equation (4.3) define

$$h(x) = \frac{A(1 - f(x))}{\Gamma_1 + 1 - f(x)} \qquad \text{and} \qquad g(x) = \frac{Bx^2 f(x)}{\Gamma_1 + f(x)}$$

and we will show that there is a unique solution to

$$h(x) = g(x)$$

for $x_0 < x < x_1$, that is $0 < r < 1$ by Equation (4.2).

Observe that

$$h(x_0) = \frac{A}{\Gamma_1 + 1} > 0, \qquad h(x_1) = 0,$$

and

$$h'(x) = \frac{-A\Gamma_1 f'(x)}{(\Gamma_1 + 1 - f(x))^2} < 0 \qquad \text{for } x_0 < x < x_1.$$

Thus, $h(x)$ is a continuous, monotonically decreasing function for $x_0 < x < x_1$.

Similarly, observe that

$$g(x_0) = 0, \qquad g(x_1) > 0,$$

and

$$g'(x) = \frac{\Gamma_1(2Bxf(x) + Bx^2 f'(x)) + 2Bx(f(x))^2}{(\Gamma_1 + f(x))^2} > 0 \qquad \text{for } x_0 < x < x_1.$$

Thus, $g(x)$ is a continuous, monotonically increasing function for $x_0 < x < x_1$.

Therefore, there exists a unique solution x_{ss} to $h(x) = g(x)$ such that $x_0 < x_{ss} < x_1$. Then the unique positive equilibrium point of Equations (4.1a)–(4.1d), implicitly defined in terms of x_{ss}, is $(f(x_{ss}), x_{ss}^2, x_{ss}^2, x_{ss})$. Since $0 < f(x_{ss}) < 1$ the equilibrium value of variable r is restricted to the range $0 < r < 1$.

□

This claim states that the cAMP-PKA network, as described by Equations (4.1a)–(4.1d), has a unique positive steady state. The restriction that $0 < r < 1$ in biological terms states that the concentration of Ras is bounded between being completely active (in GTP form) and completely inactive (in GDP form). There is also an implicit lower and upper bound on the steady-state concentration of cAMP (x), given by x_0 and x_1 respectively ($x_0 < x < x_1$), where x_0 satisfies:

$$C - D_0 x_0 - \frac{D x_0^3}{\Gamma + x_0} = 0 \tag{4.4}$$

and x_1 satisfies:

$$C + G - D_0 x_1 - \frac{D x_1^3}{\Gamma + x_1} = 0. \tag{4.5}$$

4.2 Reducing the Model in the Extreme Cases $r_{ss} \approx 1$ and $r_{ss} \approx 0$

In this section we divide the parameter space into the following three regions:

1. When $r_{ss} \approx 1$, that is in biological terms when the concentration of Ras is almost completely active (in GTP form).

2. When $r_{ss} \approx 0$, that is in biological terms when the concentration of Ras is almost completely inactive (in GDP form).

3. Parameters between regions 1 and 2, that is in biological terms when the concentration of Ras is partially active and partially inactive.

To understand what parameters cause $r_{ss} \approx 1$ or $r_{ss} \approx 0$ we will examine an approximation of these parameter regions when $\Gamma_1 \approx 0$. In the extreme cases of $r_{ss} \approx 1$ or $r_{ss} \approx 0$ we will show that we can reduce the four–by–four model, given by Equations (4.1a)–(4.1d), by assuming that both variables r and z are set at steady state, to a two–by–two system modeling the dynamics of variables p (Pde) and x (cAMP).

4.2.1 *Approximation of Parameter Ranges*

We now seek to characterize these three parameter ranges. To do so we will make the approximation that $\Gamma_1 \approx 0$. This is a good approximation since we know biologically that $\Gamma_1 = \dfrac{\Gamma_r}{C_r} << 1$. For example, in the fitting of our model to the Ma et al. (1999) data, $\Gamma_1 = \frac{.42}{1050} = 0.0004$. Our characterization is in terms of the following combination of parameters:

$$X = \frac{1}{G}\left(D_0\sqrt{\frac{A}{B}} + \frac{D\left(\frac{A}{B}\right)^{3/2}}{\Gamma + \sqrt{\frac{A}{B}}} - C \right). \tag{4.6}$$

Claim 4. *If* $\Gamma_1 \approx 0$ *then* $r_{ss} \approx 1$ *when* $X \geqslant 1$, $r_{ss} \approx X$ *when* $0 < X < 1$, *and* $r_{ss} \approx 0$ *when* $0 \geqslant X$.

Proof. If $\Gamma_1 \approx 0$ then Equation (4.1a) simplifies to:

$$\frac{dr}{dt} \approx A - Bz. \tag{4.7}$$

Under this approximation r may no longer be bounded by zero or one, thus this approximation may fail.

We will now set Equations (4.7) and (4.1b)–(4.1d) equal to zero and explicitly solve for the unique equilibrium. By setting Equation (4.7) equal to zero:

$$z_{ss} = \frac{A}{B}. \tag{4.8}$$

Then by setting Equations (4.1b) and (4.1c) equal to zero, with z defined by Equation (4.8),

$$x_{ss} = \sqrt{\frac{A}{B}} \qquad \text{and} \qquad p_{ss} = \frac{A}{B}. \tag{4.9}$$

Finally setting Equation (4.1d) equal to zero with x and p defined by Equation (4.9) and solving for r we get that:

$$r_{ss} = \frac{1}{G}\left(D_0\sqrt{\frac{A}{B}} + \frac{D\left(\frac{A}{B}\right)^{3/2}}{\Gamma + \sqrt{\frac{A}{B}}} - C\right) = X. \tag{4.10}$$

We proved in Claim 3 that the steady state value of r is bounded by zero and one, thus the approximation that $r_{ss} = X$ holds for $0 < X < 1$.

Note that $r_{ss} = X$ may no longer be bounded by one or zero. If $X \geqslant 1$ then X is not a good approximation for r_{ss}, and the approximation given by Equation (4.7) fails. Since $\Gamma_1 \approx 0$ the approximation given by Equation (4.7) only fails when r approaches one or zero. To see this we look at an expansion of Equation (4.1a) with respect to Γ_1:

$$\frac{dr}{dt} = A - Bx + (-\frac{A}{1-r} + \frac{Bz}{r})\Gamma_1 + O(\Gamma_1^2)$$

Thus when $X \geqslant 1$ we can make the approximation that $r_{ss} \approx 1$. Similarly if $X \leqslant 0$ then $r_{ss} \approx 0$.

□

A corollary to this claim is that when $\Gamma_1 \approx 0$ we can give the following approximations for the steady-state values of our system:

1. $r_{ss} \approx 1$, $p_{ss} = z_{ss} = x_{ss}^2$ and x_{ss} satisfies Equation (4.5).

2. $r_{ss} \approx X$, $z_{ss} = p_{ss} \approx \dfrac{A}{B}$ and $x_{ss} \approx \sqrt{\dfrac{A}{B}}$.

3. $r_{ss} \approx 0$, $p_{ss} = z_{ss} = x_{ss}^2$ and x_{ss} satisfies Equation (4.4).

We now seek to visualize the three parameter ranges: $r_{ss} \approx 1$, $r_{ss} \approx 0$, and in between using the approximations given in Claim 4. In the video given in Figure 4.1 we plot the approximation of these three regions.

FIGURE 4.1: Visualization of the parameter regions: $r_{ss} \approx 1$ when parameters lie on the right-hand side the shaded region, $0 < r_{ss} < 1$ when parameters lie in the shaded region, and $r_{ss} \approx 0$ when parameters lie on the left-hand side of the shaded region. Parameter D is plotted along the y-axis and the ratio A/B is plotted along the x-axis. The video shows how varying variables Γ, D_0, and G affect these regions.

For sufficiently large values of the ratio $\frac{A}{B}$, $r_{ss} \approx 1$, and for sufficiently small values of the ratio $\frac{A}{B}$, $r_{ss} \approx 0$. These values are dependent on the values of parameters D, D_0, G, and Γ. As the value of parameters D and D_0 decrease and/or as the value of Γ increases the range of the middle region increases. Thus, larger values of G, D and D_0 and/or smaller values of Γ are more likely to force r_{ss} to one or zero.

4.2.2 Reducing from a Four–by–Four System to a Two–by–Two System

When $r_{ss} \approx 1$ or $r_{ss} \approx 0$ we assume that variables r and z are set at steady state and reduce the four–by–by–four model to a a two–by–two system describing the dynamics of variables x (cAMP) and p (Pde), given by Equations (4.11a) and (4.11b)

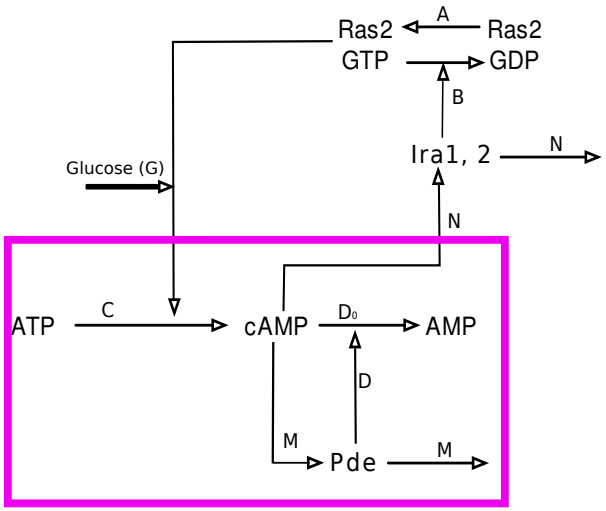

FIGURE 4.2: Reduced two–by–two system, highlighted in the box and given by Equations (4.11a) and (4.11b), modeling the dynamics of variables x (cAMP) and p (Pde). We may reduce the four–by–four system to the two–by–two system in the extreme cases of $r_{ss} \approx 1$ or $r_{ss} \approx 0$.

and shown in the box in Figure 4.2.

$$\frac{dp}{dt} = M(x^2 - p) \tag{4.11a}$$

$$\frac{dx}{dt} = C_0 - D_0 x - \frac{Dpx}{\Gamma + x}. \tag{4.11b}$$

Here $C_0 = C + G$ when $r_{ss} \approx 1$ and $C_0 = C$ when $r_{ss} \approx 0$.

To understand why this is a good assumption we examine the Jacobian matrix defined by Equations (4.1a)–(4.1d). The Jacobian matrix of Equations (4.1a)–(4.1d)

evaluated at the unique equilibrium point is:

$$\mathbf{J} = \begin{pmatrix} -\frac{A\Gamma_1}{(\Gamma_1+1-r_{ss})^2} - \frac{Bx_{ss}^2\Gamma_1}{(\Gamma_1+r_{ss})^2} & -\frac{Br_{ss}}{\Gamma_1+r_{ss}} & 0 & 0 \\ 0 & -N & 0 & 2Nx_{ss} \\ 0 & 0 & -M & 2Mx_{ss} \\ G & 0 & -\frac{Dx_{ss}}{\Gamma+x_{ss}} & -D_0 - \frac{D\Gamma x_{ss}^2}{(\Gamma+x_{ss})^2} \end{pmatrix}. \tag{4.12}$$

To understand the effect of $r_{ss} \approx 1$ or $r_{ss} \approx 0$ we need to focus on the first term in this matrix:

$$-\frac{A\Gamma_1}{(\Gamma_1+1-r_{ss})^2} - \frac{Bx_{ss}^2\Gamma_1}{(\Gamma_1+r_{ss})^2}. \tag{4.13}$$

The remaining terms in the Jacobian matrix will be order one or less. This is because in the scaling of our model, we scaled so that all the parameters in our system were order one or less in biologically relevant ranges, except nondimensional parameter Γ, in Equation (4.1d), which can be much greater than one.

1. **Case 1** If $r_{ss} \approx 1$, Equation (4.13) can be reduced to the approximation:

$$-\frac{A\Gamma_1}{(\Gamma_1+1-r_{ss})^2} - \frac{Bx_{ss}^2\Gamma_1}{(\Gamma_1+r_{ss})^2} \approx -\frac{A\Gamma_1}{(\Gamma_1+1-r_{ss})^2} \approx \frac{A}{\Gamma_1}.$$

We showed that $\Gamma_1 << 1$, thus we break into two cases: (**a**) when the value of parameter A is sufficiently large so that $\Gamma_1 << 1$ implies $\frac{A}{\Gamma_1} >> 1$ or (**b**) when A is not sufficiently large to cause $\frac{A}{\Gamma_1}$ to be much greater than one.

Case (a) When $\Gamma_1 << 1$ implies $\frac{A}{\Gamma_1} >> 1$ (for example in the Ma et al. (1999) wild type case $A = 1.45$ and $\Gamma_1 = .0004$ thus $\frac{A}{\Gamma_1} = 3625 >> 1$) the leading

order of the Jacobian matrix (4.12) is:

$$\begin{pmatrix} -\frac{A}{\Gamma_1} & 0 & 0 & 0 \\ 0 & 0 & 0 & 0 \\ 0 & 0 & 0 & 0 \\ 0 & 0 & 0 & 0 \end{pmatrix},$$

which has the single non-zero eigenvalue

$$\lambda = -\frac{A}{\Gamma_1},$$

and corresponding eigenvector

$$\vec{v} = (1, 0, 0, 0).$$

We are only concerned with the leading order eigenvalue and eigenvector because we want to show that variable r proceeds rapidly to steady state. Indeed from the leading order approximation we observe that when $r_{ss} \approx 1$ and $\frac{A}{\Gamma_1} >> 1$, variable r goes to steady state much faster than the remaining variables in the system. Thus, we assume that r is equal to one, reducing the four–by–four system to a three–by–three system. In this case $\frac{dz}{dt}$ is independent of the remaining equations, thus we may neglect this equation. Therefore, in Equation (4.1d) we replace variable r with its approximate steady-state value one, and reduce Equations (4.1a)–(4.1d) to the two–by–two system given by Equations (4.11a) and (4.11b).

Case (b) In cases when A is not sufficiently large enough to cause $\frac{A}{\Gamma_1}$ to be much greater than one, then $B << 1$ which may be seen as follows. If $\frac{A}{\Gamma_1}$ is order not much greater than $A < 1$, then $B << 1$ since $r_{ss} \approx 1$ when $\frac{A}{B} > 10$,

as seen in Section 4.2.1. Then in this case the Jacobian Matrix simplifies to:

$$\mathbf{J} = \begin{pmatrix} -\frac{A}{\Gamma_1} & 0 & 0 & 0 \\ 0 & -N & 0 & 2Nx_{ss} \\ 0 & 0 & -M & 2Mx_{ss} \\ G & 0 & -\frac{Dx_{ss}}{\Gamma+x_{ss}} & -D_0 - \frac{D\Gamma x_{ss}^2}{(\Gamma+x_{ss})^2} \end{pmatrix}. \tag{4.14}$$

We can immediately determine two of the four eigenvalues:

$$\lambda_1 = -\frac{A}{\Gamma_1} \qquad \lambda_2 = -N.$$

The remaining two eigenvalues are derived from the two–by–two sub-matrix that is determined by variables p and x:

$$\begin{pmatrix} -M & 2Mx_{ss} \\ -\frac{Dx_{ss}}{\Gamma+x_{ss}} & -D_0 - \frac{D\Gamma x_{ss}^2}{(\Gamma+x_{ss})^2} \end{pmatrix}. \tag{4.15}$$

Examining the eigenvectors of both the four–by–four matrix (4.14) and the two–by–two sub-matrix (4.15) we can find a linearized solution for both $x(t)$ and $p(t)$ in each case. These two solutions will differ by a term in the form $Ce^{-\frac{A}{\Gamma_1}t}$ where C is a constant. Although Ras does affect the dynamics of both p and x, the interesting dynamics (possible oscillations and possible loss of stability) are due to the two–by–two system determined by variables p and x. Thus, for ease of analysis we assume that variables r and z are set at steady state ($r_{ss} = 1$) and reduce to the two–by–two system given by Equations (4.11a) and (4.11b).

2. **Case 2** If $r_{ss} \approx 0$ then Equation (4.13) can be reduced to the approximation:

$$-\frac{A\Gamma_1}{(\Gamma_1 + 1 - r_{ss})^2} - \frac{Bx_{ss}^2\Gamma_1}{(\Gamma_1 + r_{ss})^2} \approx -\frac{Bx_{ss}^2\Gamma_1}{(\Gamma_1 + r_{ss})^2} \approx \frac{Bx_{ss}^2}{\Gamma_1}.$$

Then as in Case 1 we get two cases, either (**a**) the value of parameter B is large enough so that $\frac{Bx^2}{\Gamma_1} >> 1$ since $\Gamma_1 << 1$ and x is bounded below by x_0, given in Claim 3; or (**b**) we can reduce the Jacobian Matrix to the form given by (4.14). Case (b) is true even if A is not much less than one, since $r_{ss} \approx 0$ eliminates the second term in the Jacobian matrix (4.12). In both cases we can make a similar argument as Case 1 for why we can treat variables r and z as at steady state.

4.3 Analysis of the Simplified System in the Extreme Cases $r_{ss} \approx 1$ and $r_{ss} \approx 0$

We showed in Section 4.2.2 that when $r_{ss} \approx 1$ or $r_{ss} \approx 0$ we can reduce the four–by–four system to the following two–by–two system:

$$\frac{dp}{dt} = M(x^2 - p) \tag{4.16a}$$

$$\frac{dx}{dt} = C_0 - D_0 x - \frac{Dpx}{\Gamma + x} \tag{4.16b}$$

where $C_0 = C + G$ when $r_{ss} \approx 1$ (Ras is almost completely active) and $C_0 = C$ when $r_{ss} \approx 0$ (Ras is almost completely inactive).

4.3.1 Phase Plane of Equations (4.16a) *and* (4.16b)

To gain some intuition about the behavior of Equations (4.16a) and (4.16b) we plot the phase plane determined by these two equations, in Figure 4.3. The values of parameters M, Γ, D and D_0 change as the video plays, taking the values given at the end of the corresponding bars along the top of the figure. The black lines show the nullclines

$$\frac{dp}{dt} = 0 \qquad \Rightarrow \qquad p = x^2$$

and

$$\frac{dx}{dt} = 0 \qquad \Rightarrow \qquad p = \frac{(C_0 - D_0 x)(\Gamma + x)}{Dx}.$$

First we observe that the two nullclines have a unique intersection point, at the unique positive equilibrium of Equations (4.16a) and (4.16b). We also observe that for some parameters the system oscillates as it approaches its equilibrium; we will give an explicit formula for when this occurs in Claim 6.

FIGURE 4.3: Phase plane of Equations (4.16a) and (4.16b) where variable x is plotted along the x-axis and variable p along the y-axis. The black curves are the nullclines, and the red curve shows a solution to the system for initial conditions $x(0) = .5$ and $p(0) = 1$. The values of variables M, Γ, D and D_0 change as the video plays, taking the values given at the end of the corresponding bars along the top of the figure.

4.3.2 Stability of the Equilibrium of Equations (4.16a) *and* (4.16b)

Claim 5. *The unique positive equilibrium of Equations* (4.16a) *and* (4.16b) *is asymptotically stable.*

Proof. The Jacobian matrix of Equations (4.16a) and (4.16b) evaluated at the equilibrium point is:

$$\mathbf{J_1} = \begin{pmatrix} -M & 2Mx_{ss} \\ -\frac{Dx_{ss}}{\Gamma+x_{ss}} & -D_0 - \frac{\Gamma D x_{ss}^2}{(\Gamma+x_{ss})^2} \end{pmatrix}. \tag{4.17}$$

The trace and determinant of this matrix are:

$$\mathrm{Trace}(J_1) = -M - D_0 - \frac{\Gamma D x_{ss}^2}{(\Gamma + x_{ss})^2} < 0 \qquad \forall x_{ss} > 0 \tag{4.18}$$

$$\det(J_1) = M(D_0 + \frac{\Gamma D x_{ss}^2}{(\Gamma + x_{ss})^2} + \frac{2D x_{ss}^2}{\Gamma + x_{ss}}) > 0 \qquad \forall x_{ss} > 0 \tag{4.19}$$

Since the trace is negative and the determinant is positive, the eigenvalues of the Jacobian matrix (4.17) will have negative real part. Thus, the unique positive equilibrium is asymptotically stable. □

A corollary of this claim is that the two-by-two system defined by Equations (4.16a) and (4.16b) never experiences sustained oscillations. Thus, when the concentration of Ras is almost completely active ($r_{ss} \approx 1$) or inactive ($r_{ss} \approx 0$) the concentration of cAMP will not experience sustained oscillations. Since the value of parameter A is inversely proportional to the stress on the cell, this explains the prediction given by Garmendia-Torres et al. (2007) that at high or low stress levels the concentration of cAMP will eventually go to steady state. When stress levels are low the value of parameter A is larger and hence Ras is almost completely active ($r_{ss} \approx 1$). When stress levels are high the value of parameter A is very small, hence Ras is almost completely inactive ($r_{ss} \approx 0$). At intermediate stress levels Ras is free to alternate between active and inactive forms, and the concentration of cAMP can experience sustained oscillations as we will see in Section 4.4.

4.3.3 *When Equations* (4.16a) *and* (4.16b) *Experience Decaying Oscillations*

Claim 6. *Solutions of Equations* (4.16a) *and* (4.16b) *exhibit an oscillatory approach to equilibrium if and only if*

$$\left(M - D_0 - \frac{\Gamma D x_{ss}^2}{(\Gamma + x_{ss})^2}\right)^2 < 8M \frac{D x_{ss}^2}{\Gamma + x_{ss}}, \tag{4.20}$$

where x_{ss} *is the equilibrium solution of Equations* (4.16a) *and* (4.16b)*; i.e.,*

$$C_0 - D_0 x_{ss} - \frac{D x_{ss}^3}{\Gamma + x_{ss}} = 0. \tag{4.21}$$

Proof. To determine the parameter range for which Equations (4.16a) and (4.16b) exhibit decaying oscillations, examine the eigenvalues of the Jacobian matrix (4.17). When the Jacobian matrix (4.17) has complex eigenvalues with negative real part, the system will exhibit decaying oscillations as it approaches the equilibrium. From Claim 5, the trace of the Jacobian matrix (4.12) is given by Equation (4.18) and the determinant is given by Equation (4.19).

A two-by-two matrix has complex eigenvalues when

$$\mathrm{Trace}(J_1)^2 < 4 \det(J_1).$$

Thus using Equations (4.18) and (4.19), we can state that Equations (4.16a) and (4.16b) exhibit decaying oscillations when:

$$\left(M + D_0 + \frac{\Gamma D x_{ss}^2}{(\Gamma + x_{ss})^2}\right)^2 < 4M \left(D_0 + \frac{\Gamma D x_{ss}^2}{(\Gamma + x_{ss})^2} + 2\frac{D x_{ss}^2}{\Gamma + x_{ss}}\right). \tag{4.22}$$

We can simplify Equation (4.22) by subtracting $4M(D_0 + \frac{\Gamma D x_{ss}^2}{(\Gamma + x_{ss})^2})$ from both sides. The left hand side remains a complete square, and we can rewrite Equation

(4.22) as in Equation (4.20):

$$\left(M - D_0 - \frac{\Gamma D x_{ss}^2}{(\Gamma + x_{ss})^2}\right)^2 < 8M\frac{Dx_{ss}^2}{\Gamma + x_{ss}}.$$

□

Because of the implicit definition of x_{ss}, the inequality determined in Claim 6 is rather difficult to apply directly. Therefore, we refer to Figures 4.4α and 4.4β, in which the overlapping shaded regions show the ranges of D_0 and D for which the inequality (4.20) is satisfied, for several values of Γ and for M assumed equal to $.01$. Figure 4.4α shows the parameter range for a case when $r_{ss} \approx 1$ (that is when $C_0 = 1 + C = 1.044$), and Figure 4.4β shows the parameter range for a case when $r_{ss} \approx 0$ (that is when $C_0 = C = .044$).

Observe that the value of Γ has a large effect on when oscillations occur: when Γ is small, oscillations occur over a large parameter range, but as Γ increases, the parameter range decreases significantly. It is difficult to satisfy the inequality if M is very small, because of the factor of M on the right-hand side of Equation (4.20); thus decaying oscillations are less likely for the Δ*pde1* and Δ*pde1*^{ala152} mutants. We will examine the application of this claim in Section 6, looking at experimental evidence for decaying oscillations.

4.4 Stability of the Equilibrium of the Four–by–Four System

In this section we will examine the stability of the equilibrium point for the four–by–four system given by Equations (4.1a)–(4.1d). We will show that for a wide range of parameters the system loses stability by passing through a Hopf bifurcation, thus the system will experience sustained oscillations. In the special case of $M = N$ we can find an exact expression for when the Hopf bifurcation occurs. This expression is further simplified by the approximation that $\Gamma_1 \approx 0$. We will

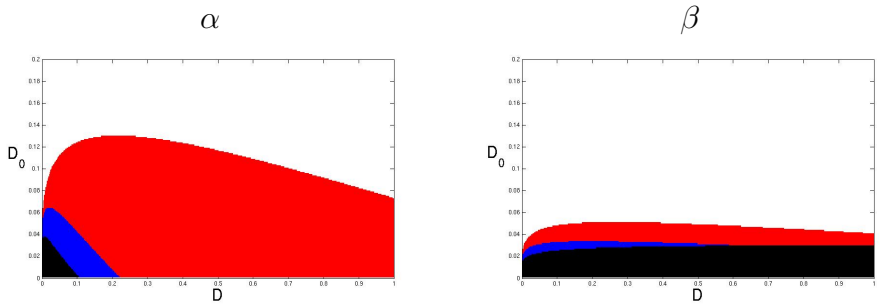

FIGURE 4.4: Solutions to the inequality given in Equation (4.20). The overlapping shaded regions of these figures illustrate the parameter ranges for D and D_0 where the model predicts the possibility of cAMP oscillations. The black region is $\Gamma = 33.6$, the Γ value for Ma et al. (1999) *wt*; the blue region is $\Gamma = 3.36$; and the red region is $\Gamma = .336$. In Figure α, $C_0 = 1.044$ and in Figure β, $C_0 = .044$. In all cases, $M = .01$.

then use these expressions to characterize the parameters that cause this system to experience sustained oscillations. Since when the system experiences sustained oscillations is the more interesting case we choose to examine this situation first. Then we will examine how the system approaches its equilibrium when the equilibrium is stable, and find a parameter range for which the system experiences decaying oscillations as it approaches its equilibrium. Finally we will compare the parameter ranges for which our system experiences sustained oscillations, decaying oscillations, or smooth approach to equilibrium.

4.4.1 Special Case of $M = N$

Claim 7. *In the special case of $M = N$ Equations* (4.1a)–(4.1d) *pass through a Hopf bifurcation when*

$$b = \frac{(a^2 + aTr + Det)Tr}{2x_{ss}MG} \tag{4.23}$$

where we make the following notation: r_{ss} and x_{ss} are the steady state values of Ras·GTP and cAMP,

$$a = \frac{\Gamma_1 A}{(\Gamma_1 + 1 - r_{ss})^2} + \frac{\Gamma_1 B x_{ss}^2}{(\Gamma_1 + r_{ss})^2} \qquad b = \frac{B r_{ss}}{\Gamma_1 + r_{ss}} \tag{4.24}$$

and $Tr = -\mathrm{Trace}(J_1)$ *as given by Equation* (4.18)*, that is* Tr *is the negative of the trace of the two–by–two matrix* (4.17) *determined by Pde and cAMP, and* $Det = \det(J_1)$ *as given by Equation* (4.19)*, the determinant of the two–by–two matrix* (4.17)*.*

Proof. Let a and b be defined by (4.24) and

$$d_1 = \frac{Dx_{ss}}{\Gamma + x_{ss}} \qquad d_2 = D_0 + \frac{\Gamma D x_{ss}^2}{(\Gamma + x_{ss})^2}.$$

Then at the unique positive equilibrium, the new parameters a, b, d_1 and d_2 are always positive. Using these new parameters we rewrite the Jacobian matrix (4.12) as:

$$\mathbf{J} = \begin{pmatrix} -a & -b & 0 & 0 \\ 0 & -M & 0 & 2Mx_{ss} \\ 0 & 0 & -M & 2Mx_{ss} \\ G & 0 & -d_1 & -d_2 \end{pmatrix}.$$

The characteristic polynomial of this matrix has the following form:

$$(\lambda + M)\left[(\lambda + a)(\lambda^2 + (M + d_2)\lambda + M(d_2 + 2x_{ss}d_1) + 2bx_{ss}MG)\right] = 0. \qquad (4.25)$$

From the characteristic polynomial we find that the first eigenvalue is $\lambda = -M$, which has corresponding eigenvector:

$$\vec{v} = \begin{pmatrix} 1 \\ -\frac{a-M}{b} \\ \frac{G}{d_1} \\ 0 \end{pmatrix}.$$

The remaining cubic can be rewritten in terms of the trace and determinant of the two–by–two matrix (4.17), accounting for only Pde and cAMP which we rewrite here in terms of d_1 and d_2 defined above:

$$Tr = -\mathrm{Trace}(J_1) = M + d_2$$

$$Det = \det(J_1) = Md_2 + 2Mx_{ss}d_1$$

To find the remaining three eigenvalues we need to solve the following cubic:

$$\big((\lambda + a)(\lambda^2 + Tr\lambda + Det) + 2bx_{ss}MG)\big) = 0. \tag{4.26}$$

Expand this cubic into the following form:

$$\lambda^3 + (Tr + a)\lambda^2 + (Det + aTr)\lambda + aDet + 2bx_{ss}MG = 0. \tag{4.27}$$

To find out when our system loses stability we apply the Routh-Hurwitz criterion (Engelberg (2005)). The Routh-Hurwitz criterion states that a cubic polynomial of the form:

$$\lambda^3 + c_1\lambda^2 + c_2\lambda + c_3 = 0$$

has roots all in the left half plane (that is, all having negative real part) if and only if

$$c_1 > 0 \qquad c_3 > 0 \qquad c_1c_2 - c_3 > 0.$$

We will focus only on when $c_1c_2 - c_3 > 0$ fails since the characteristic polynomial given by (4.27) has coefficients that are always positive. The cubic will have roots with non-negative real part when $c_1c_2 \leqslant c_3$. Applying this condition to the characteristic polynomial (4.27), we can state the our system loses stability when:

$$(Tr + a)(Det + aTr) = (aDet + 2bx_{ss}MG). \tag{4.28}$$

When Equation (4.28) is satisfied we can solve the cubic (4.27) explicitly by substituting the left hand side of Equation (4.28) into the characteristic polynomial (4.27):

$$\lambda^3 + (Tr + a)\lambda^2 + (Det + aTr)\lambda + (Tr + a)(Det + aTr) = 0. \tag{4.29}$$

Then we can factor this polynomial as

$$(\lambda + (Tr + a))(\lambda^2 + (Det + aTr) = 0,$$

with roots:

$$\lambda = -(Tr + a) \qquad \lambda = \pm\sqrt{-(Det + aTr)} = \pm i\sqrt{Det + aTr}.$$

As expected from Equation (4.28), our system loses stability through a Hopf bifurcation when Equation (4.28) is satisfied, which we can rewrite as Equation (4.23):

$$b = \frac{(a^2 + aTr + Det)Tr}{2x_{ss}MG}. \tag{4.30}$$

□

4.4.2 *Special Case of* $\Gamma_1 \approx 0$ *and* $M = N$

In the special case of $\Gamma_1 \approx 0$ we can simplify the expression for when Equations (4.1a)–(4.1d) pass through a Hopf bifurcation.

Claim 8. *In the special case of* $M = N$ *and* $\Gamma_1 \approx 0$ *Equations* (4.1a)–(4.1d) *pass through a Hopf bifurcation when:*

$$B = \frac{TrDet}{2x_{ss}^2 MG} \tag{4.31}$$

where

$$x_{ss} = \sqrt{\frac{A}{B}} \qquad Tr = -\text{Trace}(J_1) = M + D_0 + \frac{\Gamma D\frac{A}{B}}{(\Gamma + \sqrt{\frac{A}{B}})^2}$$

$$Det = \det(J_1) = M\left(D_0 + \frac{2D\frac{A}{B}}{\Gamma + \sqrt{\frac{A}{B}}} + \frac{\Gamma D\frac{A}{B}}{(\Gamma + \sqrt{\frac{A}{B}})^2}\right)$$

Proof. In Claim 4 we found that

$$x_{ss} = \sqrt{\frac{A}{B}}$$

as long as the steady-state approximation for r, given by Equation (4.6) in Claim 4, remains between one or zero. Then when $\Gamma_1 \approx 0$ the value of a, defined by

Equation (4.24), is approximately zero. Thus, in the case of $\Gamma_1 \approx 0$ we can simplify the expression for when the Hopf bifurcation occurs, given in Equation (4.23) to:

$$B = \frac{(Det)Tr}{2x_{ss}MG}.$$

Also from Claim 7 the complex conjugate pair of eigenvalues has positive real part when:

$$B > \frac{(Det)Tr}{2x_{ss}MG}.$$

□

4.4.3 Understanding the Parameters that Cause Sustained Oscillations

We now seek to understand the parameter values for which our system, given by Equations (4.1a)–(4.1d), experiences sustained oscillations. Because of the implicit definitions of x_{ss} and r_{ss}, the expression given by Equation (4.23) in Claim 7 is rather difficult to apply directly. Therefore, we refer to Figures 4.6α and 4.6β in which the shaded regions show ranges of parameters D and Γ_1 for which our system experiences sustained oscillations.

We characterize the parameter ranges for which sustained oscillations occur in terms of the ratio $\frac{A}{B}$. We choose to use this ratio since this ratio is used to determine when r_{ss} is either approximately one or zero, shown in Claim 4. This matters since in either extreme case the system is always asymptotically stable, shown in Section 4.3.2. Thus, we use the ratio $\frac{A}{B}$ to determine the middle region for which sustained oscillations are possible. Unfortunately we can not rewrite Equation (4.23) in terms of the ratio $\frac{A}{B}$, as we see from Figure 4.5. However, from Figure 4.5 observe that when A is sufficiency large (here $A > .5$) the region for sustained oscillations can be expressed in terms of $\frac{A}{B}$, to a good approximation. Thus, when

examining how the remaining parameters affect the region of sustained oscillations we will do so in terms of this ratio.

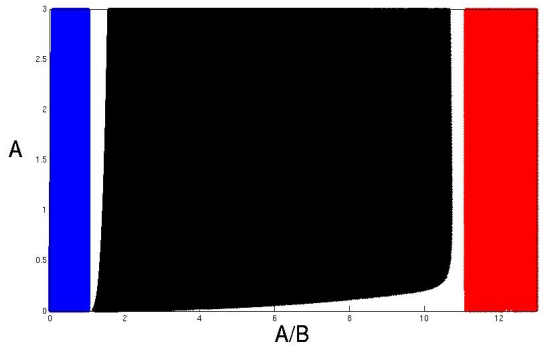

FIGURE 4.5: Illustration of why we choose to express the region of sustained oscillations in terms of the ratio $\frac{A}{B}$. In this figure the black region shows parameters for which our system, given by Equations (4.1a)–(4.1d), experiences sustained oscillations. The red region shows when $r_{ss} \approx 1$ and the blue region shows when $r_{ss} \approx 0$.

Sustained oscillations are suppressed by parameters that enhance the decay of cAMP (variable x). Specifically recalling that the dynamics of cAMP are represented by

$$\frac{dx}{dt} = C + Gr - D_0 x - \frac{Dpx}{\Gamma + x}$$

we see that the decay of cAMP is enhanced if either parameters D_0 or D are increased or parameter Γ is decreased. From Figure 4.6α observe that as parameter D increases the region of sustained oscillations decreases. We can also show that as we increase D_0 or decrease Γ the region of sustained oscillations decreases.

Finally from Figure 4.6β we observe that sustained oscillations only occur for sufficiently small values of parameter Γ_1.

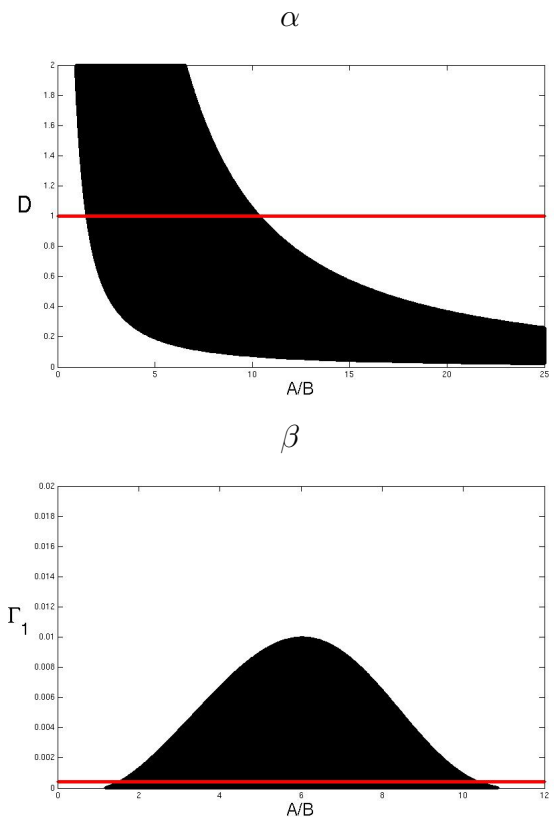

FIGURE 4.6: Parameters for when Equations (4.1a)–(4.1d) experience sustained oscillations. In each figure the shaded black regions show parameters for which Equations (4.1a)–(4.1d) experience sustained oscillations. In each figure we plot $\frac{A}{B}$ along the x-axis. In the top figure we plot D along the y-axis, compare with Figure 4.1; and in the bottom figure we plot Γ_1 along the y-axis. The red line in each figure shows the value of that parameter used in the other figure: $D = 1$ and $\Gamma_1 = .0004$, the values used to fit the Ma et al. (1999) data. Remaining parameters are the same as those used to fit the Ma et al. (1999) data and can be found in Tables 5.1 and 5.2. Note that in the Ma et al. (1999) fitting the ratio $\frac{A}{B}$ is very large.

4.4.4 When Equations (4.1a)–(4.1d) *Exhibit Decaying Oscillations*

For a wide range of parameters, when the equilibrium point of Equations (4.1a)–(4.1d) is stable this system experiences decaying oscillations as it approaches its unique equilibrium. To understand the parameters that cause decaying oscillations we break the parameter regions into two cases. **Case a**: parameters that

cause decaying oscillations in either extreme case of $r_{ss} \approx 1$ or $r_{ss} \approx 0$, shown as the green region in Figure 4.7α, characterized in Section 4.3.3. **Case b**: parameters that cause decaying oscillations when $0 < r_{ss} < 1$ shown as the blue regions in Figures 4.7α and 4.7β. Since we examined **Case a** in Section 4.3.3 we will only seek to understand **Case b** here.

In **Case b**, that is when r does not approach either extreme value of zero or one, we will show that our system almost always experiences some form of oscillation, either sustained or decaying. Intuitively this is because in **Case b** there are two forms of negative feedback that can cause the system to lose stability. To show this we will examine the special case of $\Gamma_1 \approx 0$ and $M = N$ and find an explicit expression for when all the eigenvalues of this matrix are real, given in Claim 9. We can find a similar expression for the case of $M = N$, however the form of this expression is long and not informative to the reader. Rather, when $M \neq N$ and/or $\Gamma_1 > 0$ we numerically examine when the Jacobian matrix (4.12) has all real eigenvalues.

Claim 9. *If $M = N$ and $\Gamma_1 \approx 0$ then the Jacobian Matrix determined by Equations* (4.1a)–(4.1d) *has all negative real eigenvalues only when:*

$$\frac{1}{54x_{ss}MG}\left(9DetTr - 2Tr^3 - 2\sqrt{(Tr^2 - 3Det)^3}\right) \leqslant B \leqslant \frac{1}{54x_{ss}MG}\left(9DetTr - 2Tr^3 + 2\sqrt{(Tr^2 - 3Det)^3}\right) \tag{4.32}$$

where x_{ss}, Tr and Det are as given in Claim 8.

Proof. To find when the Jacobian Matrix (4.12) determined by Equations (4.1a)–(4.1d) has all real eigenvalues we will examine the characteristic polynomial of this matrix. Simplifying the expression for the characteristic polynomial (4.25) found in Claim 7 by applying the condition $\Gamma_1 \approx 0$ we get the following polynomial:

$$(\lambda + M)\left[\lambda(\lambda^2 + Tr\lambda + Det) + 2Bx_{ss}MG\right] = 0. \tag{4.33}$$

The first eigenvalue is $\lambda = -M$ and to find the remaining eigenvalues examine the cubic:

$$\left[\lambda(\lambda^2 + Tr\lambda + Det) + 2Bx_{ss}MG\right] = 0. \tag{4.34}$$

Using Mathematica we find that the discriminant of polynomial (4.34) is

$$-27(2Bx_{ss}MG)^2 + Det^2(Tr^2 - 4Det) + 2Tr(2Bx_{ss}MG)(9Det - 2Tr^2). \tag{4.35}$$

When the discriminant is greater than or equal to zero, Equation (4.34) has three real roots since all the parameters are positive. First we observe that in both limits of $B \to \pm\infty$ the polynomial (4.35) goes to negative infinity. Thus, to find out when the discriminant is greater than or equal to zero we will set polynomial (4.35) equal to zero and solve in terms of B. Then the discriminant will only be positive in between these two roots. We find that polynomial (4.35) equals zero when:

$$B = \frac{1}{54x_{ss}MG}\left(9DetTr - 2Tr^3 \pm 2\sqrt{(Tr^2 - 3Det)^3}\right). \tag{4.36}$$

Note that when $Tr^2 < 3Det$ this expression is complex, thus polynomial (4.35) has no real roots and will always remain negative. Only when the condition $Tr^2 < 3Det$ fails does polynomial (4.35) have two real roots defined by Equation (4.36). Thus, polynomial (4.35) will be positive, and hence our system will have all real roots, only when Equation (4.32) is satisfied.

□

4.4.5 Comparison of Parameter Ranges

In order to understand how parameters affect when Equations (4.1a)–(4.1d) experience decaying oscillations we expand both Figures 4.6α and 4.6β to include regions of decaying oscillations shown as the shaded blue and green regions.

We conclude from Figure 4.7α that decaying oscillations are suppressed by increasing the decay of cAMP (variable x) as in the case of sustained oscillations,

shown in Figure 4.6α. By comparing this figure to Figure 4.1, which shows parameters for which r does not approach either extreme of zero or one, we note that for almost all parameters for which r is free to vary some form of oscillation is observed. We also observe from Figure 4.7β that although we require Γ_1 to be very small to observe sustained oscillations, as the value of Γ_1 increases our system is more likely to experience decaying oscillations. Again from this figure we note that for almost all parameters for which r is free to vary some form of oscillation is observed. In this figure $r_{ss} \approx 1$ when parameters lie to the right of the shaded blue region and $r_{ss} \approx 0$ when parameters lie to the left of the shaded blue region.

4.5 The Simplest Subsystem that Allows for Sustained Oscillations

In this section we argue that Equations (4.1a)–(4.1d) may not be simplified further and still be able to replicate both the Garmendia-Torres et al. (2007) and Ma et al. (1999) data. To replicate the Ma et al. (1999) data we must include the dynamics of both variables x (cAMP) and p (Pde) since cAMP is the experimentally measured variable, and the Ma et al. (1999) data examines Pde mutant cases. We showed in Section 4.3 that the two–by–two system describing Pde and cAMP could not experience sustained oscillations. Thus, we need to include the dynamics of variables r and z (the Ras pathway) to gain the sustained oscillations observed by Garmendia-Torres et al. (2007). We required the activation and inactivation of variable r to be modeled by Michaelis-Menten kinetics so that r would be bounded by one and zero, that is Ras bounded between being active and inactive. In Claims 10 and 11, given below, we will show that if we assume that either variable z (Ira) or r (Ras) proceeds rapidly to steady state the equilibrium point of the remaining three-by–three system is asymptotically stable. Hence we require

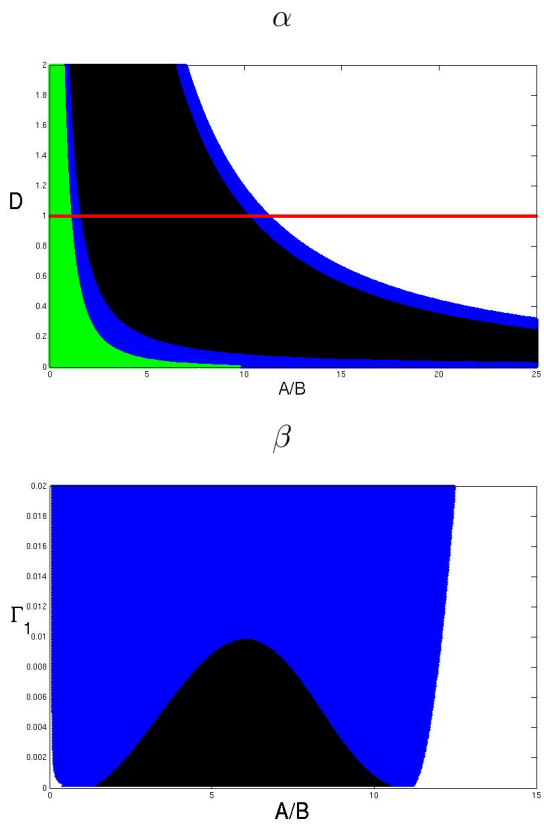

FIGURE 4.7: Expansion of Figures 4.6α and 4.6β to include regions of decaying oscillations. In each figure the shaded blue region shows parameters for which the system experiences decaying oscillations when $0 < r_{ss} < 1$ and the shaded green region shows parameters for which the system experiences decaying oscillations when $r_{ss} \approx 1$ or $r_{ss} \approx 0$. In each figure we plot $\frac{A}{B}$ along the x-axis. In Figure α we plot D along the y-axis, and in Figure β we plot Γ_1 along the y-axis. The red line in each figure shows the value of that parameter used in the other figure: $D = 1$ and $\Gamma_1 = .0004$, that is the values used to fit the Ma et al. data. Remaining parameters are the same as those used to fit the Ma et al. data and can be found in Tables 5.1 and 5.2.

the four–by–four system for sustained oscillations.

4.5.1 Ira at Steady State

Claim 10. *If variable z (Ira) is assumed to be at steady state, then the equilibrium of the reduced system is asymptotically stable.*

Proof. Assuming that variable z is at steady state reduces Equations (4.1a)–(4.1d) to the following three–by–three system:

$$\frac{dr}{dt} = \frac{A(1-r)}{\Gamma_1 + 1 - r} - \frac{Bx^2 r}{\Gamma_1 + r} \tag{4.37a}$$

$$\frac{dp}{dt} = M(x^2 - p) \tag{4.37b}$$

$$\frac{dx}{dt} = C + Gr - D_0 x - \frac{Dpx}{\Gamma + x} \tag{4.37c}$$

Of course this system has the same equilibrium point as the four–by–four system. The Jacobian matrix determined by Equations (4.37a)–(4.37c) is:

$$\mathbf{J_2} = \begin{pmatrix} -a & 0 & -b \\ 0 & -M & m \\ G & -d_1 & -d_2 \end{pmatrix}, \tag{4.38}$$

where

$$a = \frac{A\Gamma_1}{(\Gamma_1 + 1 - r_{ss})^2} + \frac{Bx_{ss}^2\Gamma_1}{(\Gamma_1 + r_{ss})^2} \qquad b = \frac{2Bx_{ss}r_{ss}}{\Gamma_1 + r_{ss}} \qquad m = 2Mx_{ss}$$

$$d_1 = \frac{Dx_{ss}}{\Gamma + x_{ss}} \qquad d_2 = D_0 + \frac{D\Gamma x_{ss}^2}{(\Gamma + x_{ss})^2}.$$

Then

$$\mathrm{Trace}(J_2) = -a - M - d_2 < 0$$

$$\det(J_2) = -a(Md_2 + md_1) - bMG < 0$$

and using Mathematica to expand we find that

$$\mathrm{Trace}(J_2^2) - (\mathrm{Trace}(J_2))^2 + 2\frac{\det(J_2)}{\mathrm{Trace}(J_2)} =$$

$$-\frac{2(bd_2G + a^2(d_2 + M) + (d_2 + M)(d_1m + d_2M) + a(bG + (d_2 + M)^2))}{a + d_2 + M} < 0.$$

Thus, the Jacobian matrix (4.38) has eigenvalues with negative real part. Therefore, the unique positive equilibrium is asymptotically stable. □

4.5.2 Ras·GTP at Steady State

Claim 11. *If variable r (Ras·GTP) is assumed to be at steady state, then the equilibrium of the reduced system is asymptotically stable.*

Proof. Assuming that variable r is at steady state reduces Equations (4.1a)–(4.1d) to the following three–by–three system:

$$\frac{dz}{dt} = N(x^2 - z) \tag{4.39a}$$

$$\frac{dp}{dt} = M(x^2 - p) \tag{4.39b}$$

$$\frac{dx}{dt} = C + Gr(z) - D_0 x - \frac{Dpx}{\Gamma + x} \tag{4.39c}$$

Of course this system has the same equilibrium point as the four–by–four system. The production term of cAMP ($r(z)$) is implicitly defined by setting Equation (4.1a) equal to zero and solving for r in terms of z. Then use the implicit derivative to solve for $r'(z) = \frac{dr}{dz}$:

$$\frac{-A\Gamma_1}{(\Gamma_1 + 1 - r)^2}dr - \frac{Bz\Gamma_1}{(\Gamma_1 + r)^2}dr - \frac{Br}{\Gamma_1 + r}dz = 0.$$

Thus

$$r'(z) = \frac{dr}{dz} = \frac{Br}{\Gamma_1 + r}\left(\frac{-1}{\frac{A\Gamma_1}{(\Gamma_1+1-r)^2} + \frac{Bz\Gamma_1}{(\Gamma_1+r)^2}}\right) < 0 \quad \forall \;\; 0 < r < 1 \;\text{ and } 0 < z$$

Then the Jacobian matrix determined by Equations (4.39a)–(4.39c) is:

$$\mathbf{J_3} = \begin{pmatrix} -N & 0 & -n \\ 0 & -M & m \\ -R & -d_1 & -d_2 \end{pmatrix}, \tag{4.40}$$

where

$$d_1 = \frac{Dx_{ss}}{\Gamma + x_{ss}} \qquad d_2 = D_0 + \frac{D\Gamma x_{ss}^2}{(\Gamma + x_{ss})^2}$$

$$n = 2Nx_{ss} \qquad R = G|r'(z)|$$

R is defined as the absolute value of $r'(z)$ since $r'(z)$ is negative for all positive values of z. Thus R is positive.

Then

$$\mathrm{Trace}(J_3) = -a - M - d_2 < 0$$

$$\det(J_3) = -a(Md_2 + md_1) - RM < 0$$

and using Mathematica to expand we find that

$$\mathrm{Trace}(J_3^2) - (\mathrm{Trace}(J_3))^2 + 2\frac{\det(J_3)}{\mathrm{Trace}(J_3)} =$$

$$-\frac{2(d_1 m(d_2 + M) + (d_2 + N)(M^2 + MN + d_2(M + N) + nR))}{d_2 + M + N} < 0.$$

Thus, the Jacobian matrix (4.40) has eigenvalues with negative real part. Therefore, the unique positive equilibrium is asymptotically stable. □

5

Numerics

In this section we will demonstrate that our model, given by Equations (5.1a)–(5.1d), can adequately replicate both the short-term dynamics of cAMP, reported by Ma et al. (1999), and the long-term dynamics of cAMP, replotted by Garmendia-Torres et al. (2007). We start with the Ma et al. (1999) experimental data since Ma et al. (1999) provide real data to fit. Then we will discuss in detail how we chose the parameters to fit the Ma et al. (1999) data. Next we will show that our model can also replicate the long-term dynamics of cAMP predicted by Garmendia-Torres et al. (2007), that is that stress can induce sustained oscillations in the concentration of cAMP. Finally we will discuss an experiment done by Williamson et al. (2009) and show that out model is able to replicate their reported results.

5.1 Short-Term Dynamics

In this section we will show that the model we developed in Section 3, given by Equations (5.1a)–(5.1d), is able to adequately replicate the short-term cAMP dynamics reported by Ma et al. (1999) by numerically solving the model for a given set of parameters.

$$\frac{dr}{dt} = \frac{A(1-r)}{\Gamma_1 + 1 - r} - \frac{Bzr}{\Gamma_1 + r} \tag{5.1a}$$

$$\frac{dz}{dt} = N(x^2 - z) \tag{5.1b}$$

$$\frac{dp}{dt} = M(x^2 - p) \tag{5.1c}$$

$$\frac{dx}{dt} = C + Gr - D_0 x - \frac{Dpx}{\Gamma + x} \tag{5.1d}$$

Then we will show that given this set of parameters, $r_{ss} \approx 1$ in Ma et al. (1999) Cases 1–4, and $r_{ss} \approx 0$ in Ma et al. (1999) Case 5. Thus, the two–by–two system,

given by Equations (5.2a) and (5.2b) is able to replicate the Ma et al. (1999) data.

$$\frac{dp}{dt} = M(x^2 - p) \tag{5.2a}$$

$$\frac{dx}{dt} = C_0 - D_0 x - \frac{Dpx}{\Gamma + x}. \tag{5.2b}$$

Finally we will discuss how we choose the parameters for fitting of the Ma et al. (1999) data.

5.1.1 Four–by–Four Model

Our first task is to demonstrate that Equations (5.1a)–(5.1d) can adequately replicate the cAMP dynamics reported by Ma et al. (1999). Indeed, Figure 5.1 shows a comparison between the experimental data given by Ma et al. (1999), shown in the top figure, and a numerical solution of Equations (5.1a)–(5.1d) shown in the bottom figure. We numerically solved our system using a fourth order Runge-Kutta method (for details see Appendix) for the parameter choices given in Tables 5.1 and 5.2. The dimensional concentrations in the figure were obtained by multiplying the concentration of cAMP, given by dimensionless variable x in Equations (5.1a)–(5.1d), by 24.95 fmol/(10^6 cells); and multiplying time, given by dimensionless variable t, by .038 minutes. These scale factors emerge from the scaling given in Section 3.5, for dimensional parameters given in Table 5.4 in Section 5.1.3. Initial conditions are the steady-state values that occur when $G = 0$, that is at glucose starvation. A glucose stimulus is applied at time zero, represented in our system as $G = 1$.

Note that the numbers in Columns *wt* and Δ*pde2* of Table 5.1 are identical. Because of Condition (a) (presented in Section 3.2), when Pde1 is present, the effect of Pde2 is negligible. Thus, the numbers in Columns *wt* and Δ*pde2* characterize properties of Pde1. Similarly, the numbers in Column Δ*pde1* characterize proper-

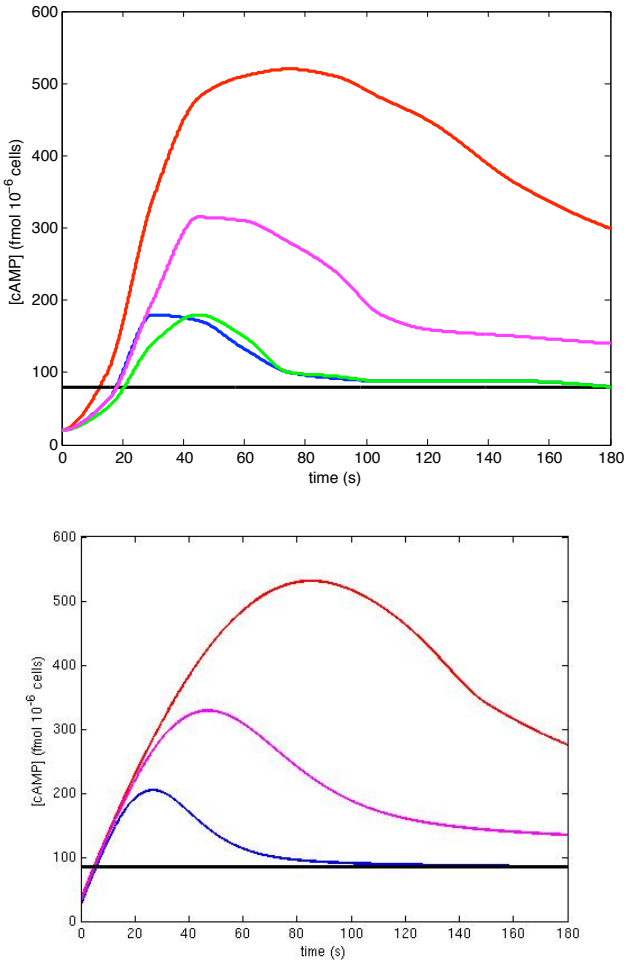

FIGURE 5.1: The top figure shows the cAMP dynamics following glucose stimulus as described by Ma et al. (1999). The bottom figure shows numerical simulations of our model, given by Equations (5.1a)–(5.1d), fit to the data of Ma et al. (1999). (Parameters as given in Tables 5.1 and 5.2). The corresponding genotypes in both figures are: wild type (blue), Δ*pde1*(red), Δ*pde2*(green), $\Delta pde1^{ala152}$(pink), Δ*pde1*Δ*pde2*(black). The *wt* and Δ*pde2* cases overlap each other in the bottom figure.

ties of Pde2. In Column $\Delta pde1^{ala152}$ the mutation of Pde1 causes both the activation and inactivation rate of Pde1 to decrease, but the affinity of Pde1 for cAMP (Γ) does not change. The value of B increases in Column Δ*pde1*Δ*pde2* because by Condition (a), when both forms of Pde are eliminated the effect of PKA on Ira1/2 is greatly enhanced.

Table 5.1: Parameter values that vary when fitting Equations (5.1a)–(5.1d) to the Ma et al. (1999) data. Here M is the quantitative expression of Condition (b) [see text]; D represents enhanced decay due to PKA feedback on Pde modified by Γ, the affinity of activated Pde for cAMP; B is the inactivation rate of Ras·GTP due to Ira1/2. Also see the text for a discussion of why Columns *wt* and Δ*pde2* have the same values.

Parameter	*wt*	Δ*pde1*	Δ*pde2*	Δ*pde1*^{ala152}	Δ*pde1*Δ*pde2*
M	0.01	0.0005	0.01	0.0025	–
D	1	0.26	1	0.54	–
Γ	33.6	16.8	33.6	33.6	–
B	.0051	.0051	.0051	.0051	.51

Table 5.2: Parameter values that are consistent when fitting Equations (5.1a)–(5.1d) to the Ma et al. (1999) data. Here A is the activation rate of Ras·GTP catalyzed by Cdc25; Γ_1 is the affinity of both Cdc25 and Ira1/2 for Ras·GTP; N is the reaction rate of Ira1/2; C is the production rate of cAMP due to the basal amount of adenylate cyclase; D_0 represents a "basal" decay rate of cAMP in the absence of activated Pde.

Parameter	Value
A	1.45
Γ_1	0.0004
N	0.032
C	0.044
D_0	0.013

5.1.2 Two–by–Two Model fitting Ma et al. (1999)

In Section 4.2.2 we showed that when either $r_{ss} \approx 1$ or $r_{ss} \approx 0$, we may reduce the four–by–four system, described by Equations (5.1a)–(5.1d) to a two–by–two system given by Equations (5.2a) and (5.2b). Given the parameters in Tables 5.1 and 5.2, $r_{ss} \approx 1$ in Cases 1–4 of the Ma et al. (1999) data, and $r_{ss} \approx 0$ in Case 5. Thus, we can use the two–by–two system described by Equations (5.2a) and (5.2b) to explain the Ma et al. (1999) data.

Indeed, Figure 5.2 shows a comparison between the experimental data given

by Ma et al. (1999), shown in the top figure, and a numerical solution of Equations (5.2a) and (5.2b) shown in the bottom figure. We numerically solved our system using a fourth order Runge-Kutta method (for details see Appendix) for the parameter choices given in Table 5.3. Note that the parameters in Table 5.3 are the same as the parameters found in the fitting of the four–by–four system given in Tables 5.1 and 5.2. This is because Equations (5.2a) and (5.2b) are a simplification of the four–by-four model with $r = 1$ in Cases 1–4 and $r = 0$ in Case 5. For the same reason the scaling also remains the same. Thus, the dimensional concentrations in Figure 5.2 were obtained by multiplying the concentration of cAMP, given by dimensionless variable x in Equations (5.2a) and (5.2b), by 24.95 fmol/(10^6 cells); and multiplying time, given by dimensionless variable t, by .037 minutes. Again, initial conditions are the steady-state values that occur when $G = 0$. A glucose stimulus is applied at time zero, given by $G = 1$.

Table 5.3: Parameter values that fit Equations (5.2a) and (5.2b) to the Ma et al. (1999) data. Here M is the quantitative expression of Condition (b) [see text]; D represents enhanced decay due to PKA feedback on Pde modified by Γ, the affinity of activated Pde for cAMP; C_0 is the production rate of cAMP due to adenylate cyclase; D_0 represents a "basal" decay rate of cAMP in the absence of activated Pde; and G accounts for glucose levels.

Parameter	*wt*	Δ*pde1*	Δ*pde2*	Δ*pde1*^{ala152}	Δ*pde1*Δ*pde2*
M	0.01	0.0005	0.01	0.0025	–
D	1	0.26	1	0.54	–
Γ	33.6	16.8	33.6	33.6	–
C_0	.044+G	.044 +G	.044+G	.044+G	.044
D_0	0.013	0.013	0.013	0.013	0.013

An intuitive biological explanation for the behavior of wild-type cells is that the overshoot in the transient concentration of cAMP is due to the delay between the increase of adenylate cyclase activity and PKA enhancement of Pde activity. Increased adenylate cyclase activity raises cAMP concentrations, leading to the

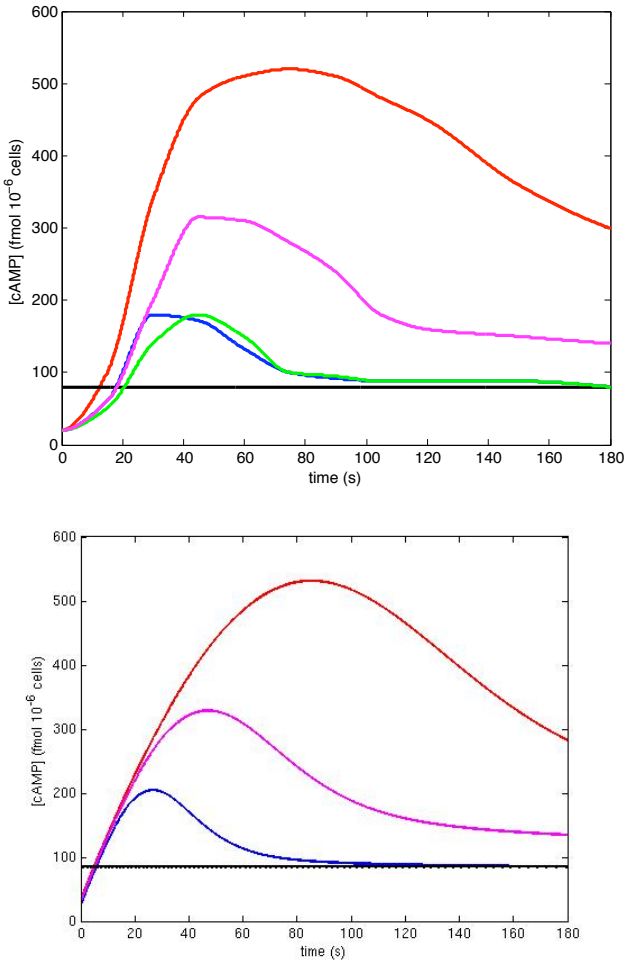

FIGURE 5.2: The top figure shows the cAMP dynamics following glucose stimulus as described by Ma et al. (1999). The bottom figure shows numerical simulations under the simplified model Equations (5.2a) and (5.2b), fit to the data of Ma et al. (1999). (Parameters as given in Table 5.3). The corresponding genotypes in both figures are: wild type (blue), $\Delta pde1$ (red), $\Delta pde2$ (green), $\Delta pde1^{ala152}$ (pink), $\Delta pde1\Delta pde2$ (black). The *wt* and $\Delta pde2$ cases overlap each other in the bottom figure.

activation of PKA by the release of PKAs catalytic subunits. PKA in turn activates both Pde1 and Pde2, which enhances the decay of cAMP and brings the concentration of cAMP down to its steady-state level. In wild type cells, Pde1 is the primary path of PKA feedback. In the $\Delta pde1$ and $\Delta pde1^{ala152}$ cases the slower activation of Pde accounts for the greater transient observed.

5.1.3 *Dimensional Parameters*

In this section we discuss how we choose the parameters to fit the Ma et al. (1999) data. The dimensionless parameters in Equations (5.1a)–(5.1d) are composites of dimensional parameters. Starting from a system of nine differential equations, given by Equations (3.2)–(3.10) in Section 3, we impose three conditions (Conditions (a), (b) and (c) given in Section 3.2) and four steady-state assumptions (given in Section 3.3) to simplify to the following dimensional model for the cAMP-PKA network.

$$\frac{dr}{dt} = \frac{R_r \frac{P_c}{D_c[Stress]}(C_r - r)}{\Gamma_r + C_r - r} - \frac{\bar{R}_r z r}{\Gamma_r + r} \tag{5.3a}$$

$$\frac{dz}{dt} = N_z \frac{K_b}{K_f} x^2 - D_z z \tag{5.3b}$$

$$\frac{dp_1}{dt} = N_1 \frac{K_b}{K_f} x^2 - D_1 p_1 \tag{5.3c}$$

$$\frac{dp_2}{dt} = M(N_1 \frac{K_b}{K_f} x^2 - D_1 p_2) \tag{5.3d}$$

$$\frac{dx}{dt} = P_x \frac{P_a}{D_a} + \bar{P}_x \frac{\bar{P}_a P_g}{D_a D_g}[\text{Glu}]r - D_x x - \frac{R_{x1} p_1 x}{\Gamma_{x1} + x} - \frac{R_{x2} p_2 x}{\Gamma_{x2} + x} \tag{5.3e}$$

To further simplify we treat variables p_1 and p_2 as the single variable p (See Section 3.2.3), however, in Equations (5.3a)–(5.3e) we write out equations for both p_1 and p_2 to highlight all the dimensional parameters that must be determined. We then scale these equations (with a scaling given in Section 3.5) yielding our non-dimensional model, Equations (5.1a)–(5.1d). To fit our model to the Ma et al. (1999) data with biologically relevant parameters, we must fit Equations (5.3a)–(5.3e) to the Ma et al. (1999) data then apply our scaling. The parameters used to fit the dimensional model are listed in Table 5.4.

In choosing dimensional parameters we use parameters given by Garmendia-Torres et al. (2007) when available. The units have been converted from μM to fmol/(10^6 cells) using the approximation that the volume of a cell is 42 fl (Jorgensen et al. (2002)).

$$\mu M = \frac{\mu mol}{l} = \frac{\mu mol}{l}\frac{42fl}{cell}\left(\frac{10^6 cells}{10^6 cells}\right) = \frac{42fmol}{10^6 cells}$$

The parameters not chosen from Garmendia-Torres et al. (2007) are: D_1, P_x, D_x, R_{x_1}, R_{x_2}, Γ_{x2}, and M. Since Pde2 has higher affinity for cAMP than Pde1, the value of Γ_{x2} is half the value of Γ_{x1}. Parameters D_1, P_x, R_{x_1}, R_{x_2}, and M were fit to the wild type and Pde1 knockout cases using a method of least squares, for details see Appendix. We chose to fit the two cases simultaneously since the values of P_x and D_1 affect both cases. The value of D_x was taken to be $P_x(1.25)/86.0$ in order to fit the steady-state value of cAMP in the double Pde knockout case.

To understand how tightly the parameters were fit we examine how the error changes when varying parameters in the range of $\pm 10\%$ of their fit value. Here the error is taken as the discrete L_1 norm between the numerical solution and the data given by Ma et al. (1999). In Figure 5.3 we plot the percent increase of error compared to the percent of change of parameters. Most of the error in our fitting can be attributed to the different production rates in the wild type and Pde1 case. Both cases will have the same production rate in our model; thus, varying P_x has the greatest effect on error. We also observe that parameters that affect the fit of the Pde1 knockout case, that is parameters R_{x_2} and M, are more tightly fit than parameters that only affect the wild type, that is R_{x_1} and D_1.

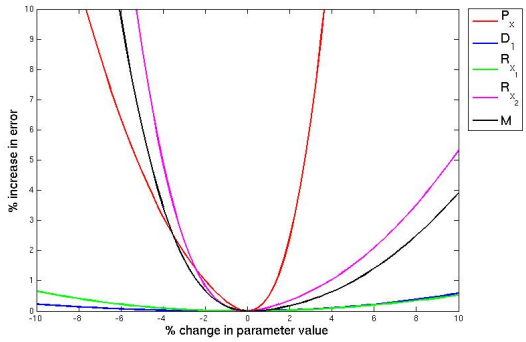

FIGURE 5.3: How varying parameters affects the error in the fitting of the numerical solution to the Ma et al. (1999) data. We plot the $\%$ change in parameter value along the x-axis and the corresponding $\%$ increase in the error along the y-axis.

5.2 Long-Term Dynamics

Our model predicts that the long-term concentration of cAMP may either go to a unique steady state or experience sustained oscillations. The Garmendia-Torres et al. (2007) paper predicts sustained oscillations in the concentration of cAMP at intermediate stress levels. Since stress affects our model through parameter A we choose parameter A as our bifurcation parameter. At intermediate stress levels, for example $A = .014$, the long-term concentration of cAMP experiences sustained oscillations, as seen by the red curve in Figure 5.4. When stress levels are low, for example $A = 1.4$, the long-term concentration of cAMP remains at a high steady-state value, as seen by the blue line in Figure 5.4. When stress levels are high, for example $A = .005$, the long-term concentration of cAMP remains at a low steady-state value, as seen by the black line in Figure 5.4.

An intuitive biological explanation of this behavior is that at intermediate stress levels the concentration of Ras (r) is free to alternate between being active (in GTP form, that is $r_{ss} \approx 1$) and inactive (in GDP form, that is $r_{ss} \approx 0$). This oscillation between Ras being active and inactive causes oscillations in the concentration of

Table 5.4: Parameter values used to fit Equations (5.3a)–(5.3e) to the Ma et al. (1999) data. Parameters in bold are parameters that are fit to the Ma et al. (1999) data using a method of least-squares. Parameters P_x, D_1, and R_{x_1} are fit to the wild-type, parameters R_{x_2} and M are fit to the Pde1 knockout case, and D_x is determined to fit the double Pde knockout case. The remaining parameters are taken from Garmendia-Torres et al. (2007).

Parameter	Value	Unit	Description
R_r	240	$(\text{min})^{-1}$	activation rate of Ras·GTP due to Cdc25
$\bar{R}_r$	120	$(\text{min})^{-1}$	inactivation rate of Ras·GTP due to Ira
C_r	1050	fmol/(10^6 cells)	total concentration of Ras
Γ_r	.42	fmol/(10^6 cells)	affinity of Cdc25 and Ira for Ras
P_c	168	fmol/(10^6 cells)$(\text{min})^{-1}$	activation rate of Cdc25
D_c	1	$(\text{min})^{-1}$	basal inactivation rate of Cdc25
P_z	.7	$(\text{min})^{-1}$	activation rate of Ira due to PKA
D_z	.86	$(\text{min})^{-1}$	inactivation rate of Ira
P_a	1.25	fmol/(10^6 cells) $(\text{min})^{-1}$	basal activation rate of AC
$\bar{P}_a$	.027	$(\text{min})^{-1}$	enhanced activation rate of AC
D_a	1	$(\text{min})^{-1}$	inactivation rate of AC
R_{p_1}	2	$(\text{min})^{-1}$	activation rate of Pde1 due to PKA
$\mathbf{D_{P_1}}$	.25	$(\text{min})^{-1}$	inactivation rate of Pde1
K_b	.007	(min fmol/(10^6 cells))$^{-1}$	rate at which cAMP binds to PKA
K_f	3	$(\text{min})^{-1}$	rate at which cAMP is released from PKA
$\mathbf{M}$	.047	–	ratio between the inactivation rates of Pde1 and Pde2
$\mathbf{P_x}$	23.3	$(\text{min})^{-1}$	production rate of cAMP due to AC
$\mathbf{D_x}$	.34	$(\text{min})^{-1}$	basal decay rate of cAMP
$\mathbf{R_{x_1}}$	56.8	$(\text{min})^{-1}$	decay rate of cAMP due to active Pde1
Γ_{x_1}	840	fmol/(10^6 cells)	affinity of Pde1 for cAMP
$\mathbf{R_{x_2}}$	14.7	$(\text{min})^{-1}$	decay rate of cAMP due to active Pde2
$\mathbf{\Gamma_{x_2}}$	420	fmol/(10^6 cells)	affinity of Pde2 for cAMP

cAMP since only the active form of Ras activates adenylate cyclase, increasing the concentration of cAMP. When stress levels are low the concentration of Ras is almost completely active, as in Ma et al. (1999) Cases 1–4, forcing the long-term concentration of cAMP to steady state. Similarly, when stress levels are high the concentration of Ras is almost completely inactive, as in Ma et al. (1999) Case 5,

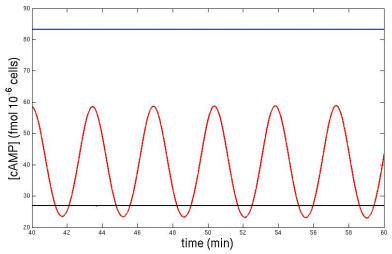

FIGURE 5.4: Long-term dynamics for the concentration of cAMP. The blue line shows the cAMP concentration at high nutrient levels and/or low stress levels (parameter $A = 1.4$). The black line shows the concentration of cAMP at low nutrient levels and/or high stress levels (parameter $A = .005$). The red curve shows the concentration of cAMP at intermediate nutrient levels and/or intermediate stress levels (parameter $A = .014$).

forcing the long-term concentration of cAMP to steady state.

5.2.1 How Oscillations are Dependent on Parameters

In this section we examine how sustained oscillations in the solution of Equations (5.1a)–(5.1d) depend on the parameters. First we will use the analysis from Section 4.4 to understand when sustained oscillations occur. Then we will examine how varying parameters affects the period and amplitude of oscillations.

In Section 4.4 we analyzed how the parameters in Equations (5.1a)–(5.1d) affect when the system experiences sustained oscillations by examining the stability of the unique equilibrium. We found that sustained oscillations are suppressed by parameters that enhance the decay of cAMP (variable x). That is as parameters D_0 and D increase or as parameter Γ decreases, the region of sustained oscillations decreases. From Section 4.4 we also observe that as the value of Γ_1 increases our system is less likely to experience sustained oscillations. Biologically this is saying that as Ira1/2 and Cdc25 affinity for Ras decreases the system becomes more stable. We do not show but can state that varying the values of M and N has very little effect on when the system experiences sustained oscillations.

We now seek to understand how the period of oscillation changes. To do so we first examine the complex pair of eigenvalues when Equation (4.31) in Claim 8 (given in Section 4.4) is satisfied, that is when the real part is zero. At the bifurcation point given in Claim 8 the complex conjugate pair of eigenvalues are:

$$\lambda = \pm i \sqrt{M \left(D_0 + \frac{\Gamma D \frac{A}{B}}{(\Gamma + \sqrt{\frac{A}{B}})^2} + 2 \frac{D \frac{A}{B}}{\Gamma + \sqrt{\frac{A}{B}}} \right)}. \tag{5.4}$$

Observe that the period of oscillation, at the bifurcation point, is lengthened as either: the activation/inactivation of Pde is decreased, that is as the value of parameter M decreases; and/or as the parameters that enhance the decay of cAMP are decreased, that is as parameters D_0 and D decrease or as parameter Γ increases. Examining the eigenvalues given in Claim 7 (given in Section 4.4) we can further state that the length of the period is increased by decreasing the value of Γ_1. Finally numerically examining the case when $M \neq N$ we observed that the length of the period is increased by decreasing the value of N.

When examining the amplitude of oscillations we focus on the amplitude of cAMP (x) oscillations. We do this since Ras (r) is bounded, thus the amplitude of Ras oscillations is bounded by one, and the amplitude of oscillations for both Ira (z) and Pde (p) will be the square of cAMP (x). The video in Figure 5.5 shows how varying the parameters in our system affects the cAMP oscillations. In this figure we plot the dynamics of cAMP ($x(t)$), for time varying for twenty minutes with initial conditions of all variables set to one half. The values of the parameters change as the video plays, taking the values given at the end of the corresponding bars along the top of the figure.

Sustained oscillations are the result of feedback through the Ras pathway (variables r and z). We conclude that negative feedback through Pde stabilizes our system. Thus, oscillations are more likely in systems where the effect of the Pde

FIGURE 5.5: Effect of changing parameters on the long-term dynamics of the concentration of cAMP. The values of the parameters change as the video plays, taking the values given at the end of the corresponding bars along the top of the figure.

is smaller. We observe that as both forms of feedback (through Ras and Pde) slow down, that is as the values of parameters N and M decrease, the length of the period of oscillation increases. Finally we conclude that as the parameters that enhance the decay of cAMP are decreased, that is as parameters D_0 and D are decreased and parameter Γ is increased, oscillations are more likely to have longer periods and larger amplitudes.

5.3 Multiple Glucose Pulses

In comparing our model to previous models of the cAMP-PKA network, the deterministic model presented by Williamson et al. (2009) is the closest in approach

to ours. Their model is able to recapitulate the relevant dynamics of the Pde1 and Pde2 single mutants but does not account for the behavior of the Pde double mutant. This is significant since the double knockout case is the most surprising case and the hardest case to explain. They also only examined the short–term dynamics of cAMP. However, Williamson et al. (2009) did account for one experiment which we will now examine. In their paper, Williamson et al. (2009) examine what happens when the glucose stimulus is applied in pulses instead of all at once. In their experiment, shown as the top figure in Figure 5.6, they start with a cAMP concentration when the cell is starved from glucose. Then they apply a partial stimulus (5 mM of glucose), allow the concentration of cAMP to come to steady state, and then apply a full stimulus (100 mM of glucose), the same as the Ma et al. (1999) stimulus. In their results they observe two smaller transients. After each transient the concentration of cAMP comes to a higher steady state. We show in the bottom figure of Figure 5.6 that we can numerically replicate the same results with our model, given by Equations (5.1a)–(5.1d), for parameter values taken from the fitting of the Ma et al. (1999) wild type. To do so we first allow cAMP to go to steady state when $G = 0$, that is glucose starvation. Then we apply a glucose stimulus of $G = .2$ and allow the concentration of cAMP to go to its higher steady state. Then when the concentration of cAMP is at steady state we apply a second glucose stimulus $G = 1$. Note that the glucose stimulus applied was $G = .2$ not $G = .05$. This value is generated from fitting only G to the Williamson et al. (2009) data, and leaving the remaining parameters the same. Biologically the most likely reason that this is not one-to-one is that glucose effect on the activity of Gpa2 is not linear, most likely it should be modeled with Michaelis Menten kinetics. However, in our model we assumed that it was linear for simplicity. Thus our model is able to replicate the results reported by Williamson et al. (2009).

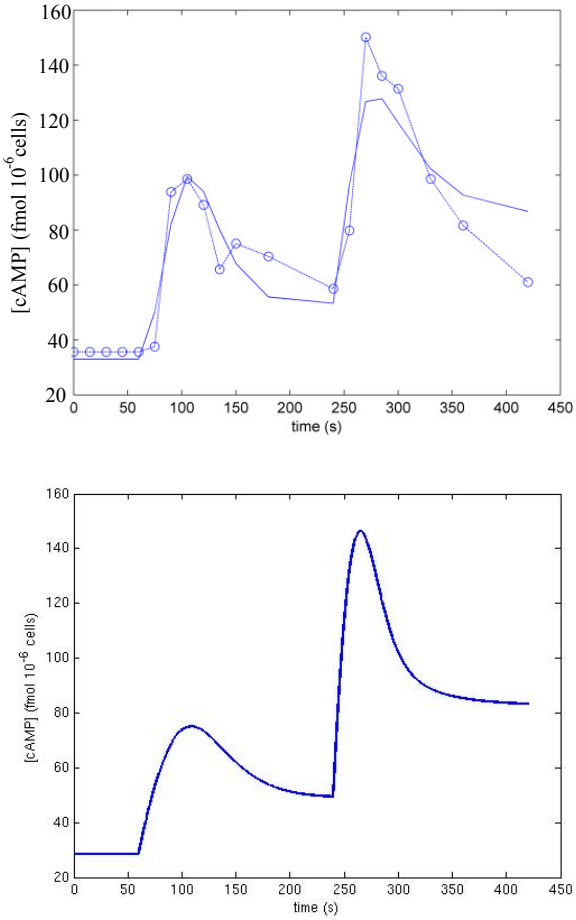

FIGURE 5.6: cAMP dynamics following a partial glucose stimulus followed by a full stimulus after four minutes. The top figure shows data described by Williamson et al. (2009), and the bottom figure shows numerical simulations under the simplified model Equations (5.1a)–(5.1d), fit to the Ma et al. (1999) wild type. In our numerical results a glucose stimulus of $G = .2$ is first applied, then at four minutes a full glucose stimulus of $G = 1$ is applied.

6

Experiments

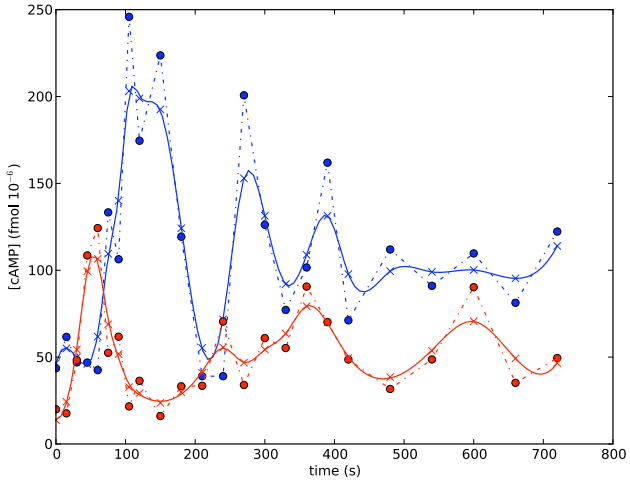

FIGURE 6.1: Experimental time series of cAMP concentration following glucose stimulus for S288c (red) and Σ1278b (blue). Circles indicate measured cAMP values, x's indicate smoothed values to which the curves were fit.

In this section we will show experimental evidence that validates our model. We will show evidence for decaying and sustained cAMP oscillations.

Our model makes the novel prediction that for many choices of parameter values, cAMP levels should exhibit decaying oscillations towards a steady state following glucose stimulus. In order to test this hypothesis Dr. Magwene's Lab measured the dynamics of the cAMP response in diploid cells of two strains of budding yeast, *S. cerevisiae*, S288c and Σ1278b. S288c is considered the standard "reference" genome for yeast studies while Σ1278b is commonly used for studies of developmental pathways in yeast (Gimeno et al. (1992)). Their genomes differ by approximately 30,000 SNPs (Magwene, in prep.). SNP is short for single-nucleotide polymorphism and is a DNA sequence variation occurring when a single nucleotide in the genome differs between members of the same biological species, here two different strains of budding yeast (Campbell (2008)).

For each strain Dr. Magwene's Lab monitored cAMP levels for eight to twelve minutes following a glucose stimulus. Two typical experimental time series are

illustrated in Figure 6.1. They found evidence for cAMP oscillations in both genetic backgrounds but the quantitative features of the oscillations appear to be strain dependent. Σ1278b exhibits a classical form of decaying oscillations characterized by a large cAMP peak immediately after the stimulus, and dampening oscillations towards a new steady state. In the S288c strain, by contrast, the oscillations appear to be delayed, occur with a lower amplitude and do not decay as rapidly. The Σ1278b strain has a cAMP peak approximately twice as large as that of S288c.

There are various ways in which we could fit the dynamics reported here. We could assume that Ras·GTP is saturated, as in Ma et al. (1999) Cases 1–4 and seek to fit only the two–by–two system, given by Equations (5.2a) and (5.2b), to this data. Alternatively we could fit all four equations, (5.1a)–(5.1d), to this data. Since this experiment was done in a similar way to the Ma et al. (1999) experiment, we seek to fit the data to parameters relating to only Pde feedback, that is parameters D, Γ, and M. The data is taken in increments of fifteen seconds for the first two minutes, thirty seconds for the next five minutes and every minute for the last five minutes. Since we are using a method of least squares the fitting will more closely resemble the initial data. We could correct this by either fitting the data at minute intervals or by increasing the number of data points. Fitting at minute intervals is not that useful since we are losing a lot of detail in our experimental data. Arbitrarily increasing the number of data points undervalues the true experimental data. Thus we will only show the fitting for the unaltered data.

We can approximate the dynamics observed for both Σ1278b and S288c using the model described by Equations (5.1a)–(5.1d) (Figure 6.2). Table 6.1 shows the parameter values used to fit the oscillations in Σ1278b and S288c compared to the parameter values used to fit the Ma et al. (1999) wild type. For both cases the

$S288c$

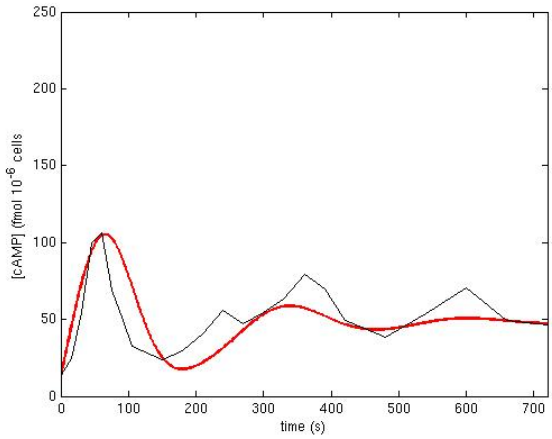

$\Sigma 1278b$

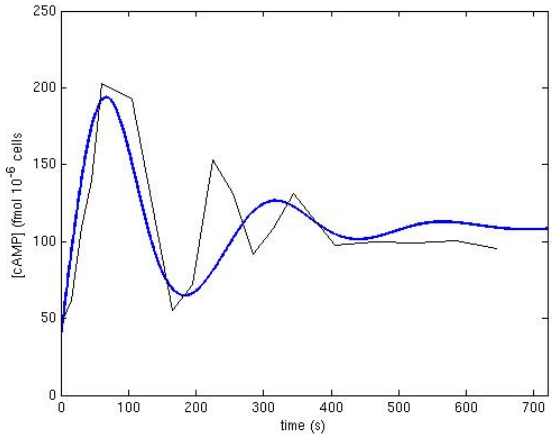

FIGURE 6.2: Numerical simulations under the non-dimensional model to fit Σ1278b (blue) and S288c (red), compared to the experimental data shown as the black curve in each case.

model requires Pde's affinity for cAMP, $\frac{1}{\Gamma}$, to be much greater than Pde's affinity for cAMP in the Ma et al. (1999) case. In our fitting we note that the most significant difference between the two strains is in the decay of cAMP with respect to Pde (parameter D).

Table 6.1: Parameter values used to replicate cAMP dynamics for strains Σ1278b and S288c (both wild types) compared to parameter values used to fit the wild type data reported in Ma et al. (1999).

Parameter	Interpretation	Ma ·	Σ1278b	S288c
M	activation/inactivation of rate Pde	.042	.06	.07
D	decay rate of cAMP due to active Pde1	1	0.06	.3
Γ	Pde1 affinity for cAMP	33.6	0.3	0.2
T	Time scale	.0377	.11	.19

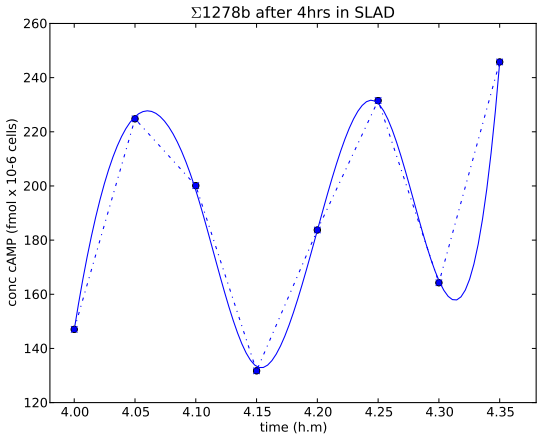

FIGURE 6.3: Experimental time series of cAMP concentration showing the possibility of sustained oscillations.

6.1 Sustained Oscillations

In their paper Garmendia-Torres et al. (2007) predicted the possibility of sustained oscillations. However, this was only a prediction, they never experimentally observed sustained oscillations in the concentration of cAMP. Since the model we developed also predicts the possibility of sustained oscillations we sought to experimentally verify the existence of sustained oscillations at intermediate stress levels. In Figure 6.3 we show initial experimental evidence showing sustained oscillations.

This is only an initial experiment, thus we do not seek to fit the data yet. However, we note that the period and amplitude of oscillations are much larger and longer than the period and amplitude of oscillations given in Figure 5.4 which shows sustained oscillations for parameter choices consistent with the Ma et al. (1999) wild type. The most likely reason for this is that our experiment was done on a Σ1278b stain, whereas the Ma et al. (1999) experiment was done for a S288c strain. From both this initial data and the decaying oscillations data, seen in Figure 6.1, we suspect that the production of cAMP is more efficient in the Σ1278b strain compared to the S288c strain.

7

Further Work

In this section we give an overview of three possible future extensions to our model:

1. Understand the role that proteins Krh1 and Krh2 have within the cAMP-PKA network.

2. Examine how predicted oscillations in the concentration of cAMP would affect the yeast cell's developmental network.

3. Explore how adding spatial dimensions to our variables would affect the dynamics of this system.

We will give a detailed description of this first extension, but only give an overview of the second two ideas.

7.1 Understanding the Role of Proteins Krh1 and Krh2

A natural extension to our model is to seek to understand the role of Kelch Repeat Proteins Krh1 and Krh2 within the cAMP-PKA network. There are a variety of previous papers that have proposed different ways that Krh1 and Krh2 could affect this network: Harashima and Heitman (2002, 2005); Peeters et al. (2006, 2007); Williamson et al. (2009); and Phan et al. (2010). We will start by examining an experimental result published by Harashima and Heitman (2002). In this paper, the authors experimentally examine how Krh1 and Krh2 affect the dynamics of cAMP by comparing the results of glucose stimulation (similar to the Ma et al. (1999) experiment) on cAMP in the wild type with Krh1 and Krh2 single knockouts and a double Krh1–Krh2 knockout. Figure 7.1 summarizes the four dynamic patterns that we consider here. These cases are:

Case 1: Wild-type (*wt*)–as in the Ma et al. wild type the concentration of cAMP experiences a transient following glucose stimulation, after which the con-

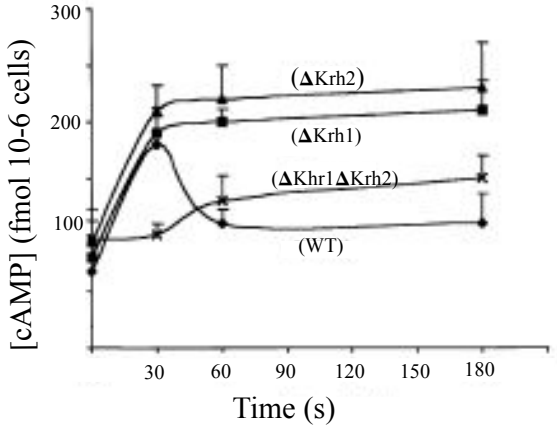

FIGURE 7.1: Effect of glucose stimulation on Krh knockout cases reported by Harashima and Heitman (2002).

centration of cAMP smoothly comes to a steady-state concentration that is slightly greater than the initial concentration.

Case 2: Krh1 knockout ($\Delta Krh1$)–following glucose stimulation the concentration of cAMP increases at a rate similar to the wild type; however, in this case no overshoot is observed, instead the concentration of cAMP remains at the peak level.

Case 3: Krh2 knockout ($\Delta Krh2$)–this case is almost the same as the Krh1 knockout case, but ends at a slightly higher steady-state value.

Case 4: Double Krh1 Krh2 knockout ($\Delta Krh1\Delta Krh2$)–the response to glucose stimulation is much slower and weaker than the wild type. No overshoot is observed in this case, thus the concentration of cAMP ends at a higher steady state than the wild type.

When any form of Krh is present (in the *wt*, $\Delta Krh1$, and $\Delta Krh2$ cases) the production of cAMP immediately following glucose stimulation is almost the same.

When both forms of Krh are knocked out the rate of cAMP production is radically decreased. This suggests that Krh1 and Krh2 must independently promote the production of cAMP.

When any form of Krh is knocked out (in the $\Delta Krh1$, $\Delta Krh2$, and $\Delta Krh1\Delta Krh2$ cases) the concentration of cAMP does not experience a transient, thus the steady-state concentration is greater than in the wild-type case. This suggests that Krh1 and Krh2 must jointly enhance the decay of cAMP.

The double knockout case is the most surprising case, as was the double–Pde–knockout case in the Ma et al. (1999) data (presented in Section 1.3). Both of the single knockout cases have a similar effect on the concentration of cAMP; however, the double knockout case is not the sum of these results, rather the double knockout case has an entirely different dynamic form. In our present model we required a secondary role for Pde in order to explain the double–Pde–knockout case (Ma et al. (1999) Case 5). This role was subtle, it was that Pde1 and Pde2 competitively inhibit PKA from activating Ira. The surprising results given here suggest that Krh1 and Krh2 must also have a secondary role, however determining this role can be challenging, as it was to determine the secondary role that Pde played.

It is not presently known how Krh1 and Krh2 affect the developmental network. In response to their experimental results Harashima and Heitman (2002) propose two possible ways that Krh1 and Krh2 could interact with the yeast's developmental network, either Krh1 and Krh2 could act directly on the cAMP-PKA network, or Krh1 and Krh2 could act away from the cAMP-PKA network. For our initial extension to the model we are only interested in the possibility of the first case since we desire to keep our model as simple as possible while still being able to explain the results. Thus, in our future work we desire to see if it is possible to explain the results given by Harashima and Heitman (2002) while Krh1 and Krh2

only interact within the cAMP-PKA network.

As noted above, from the Harashima and Heitman (2002) data we conclude that both Krh1 and Krh2 must together enhance the decay of cAMP and independently promote the production of cAMP. Since there is strong evidence to support the fact that Krh1 and Krh2 can not directly interact with either Pde1 or Pde2 they must affect the decay of cAMP in a more indirect way, most likely by affecting the activity of PKA, which activates Pde. Similarly there is no evidence to suggest that Krh1 and Krh2 directly affect the activity of adenylate cyclase, which produces cAMP. Again Krh1 and Krh2 must affect the production of cAMP indirectly by interacting with either Ras or Gpa2.

7.1.1 Possible Krh Interactions

In this section we introduce five different possible interactions, stated below and shown in Figure 7.2, that Krh1 and Krh2 could have within the cAMP-PKA network. We present two possible interactions that set the level of Krh1 and Krh2, either (A) or (B); and three possible ways that Krh1 and Krh2 could affect the cAMP-PKA network, (C), (D), or (E). Note that any model would probably have to make a choice between (A) or (B), but Krh1 and Krh2 could affect the network in more than one way.

(A) Gpa2·GDP inhibits Krh1 and Krh2, proposed by Harashima and Heitman (2005).

(B) Gpa2·GTP inhibits Krh1 and Krh2, proposed by Peeters et al. (2006) and Williamson et al. (2009).

(C) Krh1 and Krh2 inhibit Gpa2 from activating by inhibiting Gpa2·GDP from binding to Gpr1, proposed by Harashima and Heitman (2005) and Peeters et al. (2007).

(D) Krh1 and Krh2 increase the association between the regulatory and catalytic subunits of PKA (Tpk and Bcy1), proposed by Peeters et al. (2006, 2007) and Williamson et al. (2009).

(E) Krh1 inhibits Ira2, and possibly Krh2 inhibits Ira1, proposed by Phan et al. (2010).

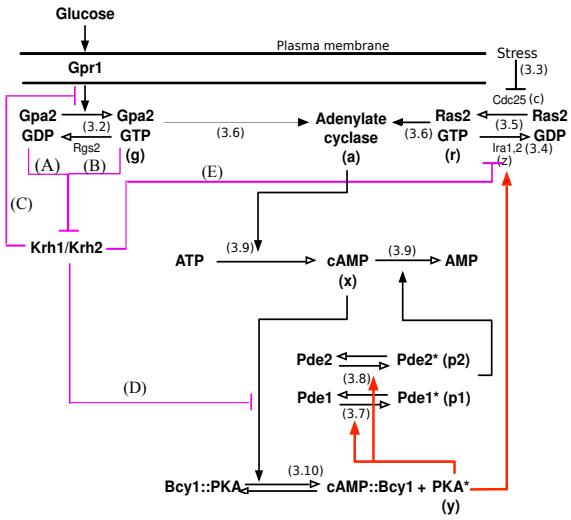

FIGURE 7.2: Five possible ways that Krh1 and Krh2 could interact within the cAMP-PKA network, shown as the purple lines. (A) Gpa2·GDP inhibits Krh activation, (B) Gpa2·GTP inhibits Krh activation, (C) Krh1 and Krh2 inhibit Gpa2 from activating by inhibiting Gpa2·GDP from binding to Gpr1, (D) Krh1 and Krh2 increase the association between the regulatory and catalytic subunits of PKA (Tpk and Bcy1), and (E) Krh1 inhibits Ira2, and possibly Krh2 inhibits Ira1.

7.2 How cAMP Oscillations Affect the Yeast Cell's Developmental Network

Another possible extension to our model would be to consider the effect of cAMP oscillations on the larger developmental network within yeast, shown in Figure 7.3. Presently our model only examines the cAMP-PKA network. We chose to examine this network due to the key role that it plays in determining the cell's developmental outcome, see Section 1.2 for more details. A natural extension to our model would be to start incorporating downstream targets of PKA. In particular we would like to examine how the predicted oscillations in the concentration of cAMP would affect these downstream targets, and possibly predict how oscillations in the concentration would affect the overall developmental decisions the cell makes. The really interesting question is does the cell oscillate between sporulation and pseudohyphal growth? Or if there are pronounced cAMP oscillations is there some threshold under which or over which the downstream targets ignore the oscillation? Any extension to our model would be done as a linear differential equation to start with to see if we could make any predictions, and to keep the model simple as we add many more variables. The hope would be to highlight the important downstream targets of cAMP and then we could model these targets with more detail.

7.3 Spatial Dimensions

Presently we assume the concentrations of our variables are spatially uniform. It would be interesting to examine how the dynamics of our system would be affected by adding spatial dimensions to our model and letting concentrations depend on spatial coordinates. A natural preliminary step would be to allow enzymes to move between the cell's cytoplasm and the cell's nucleus. Presently

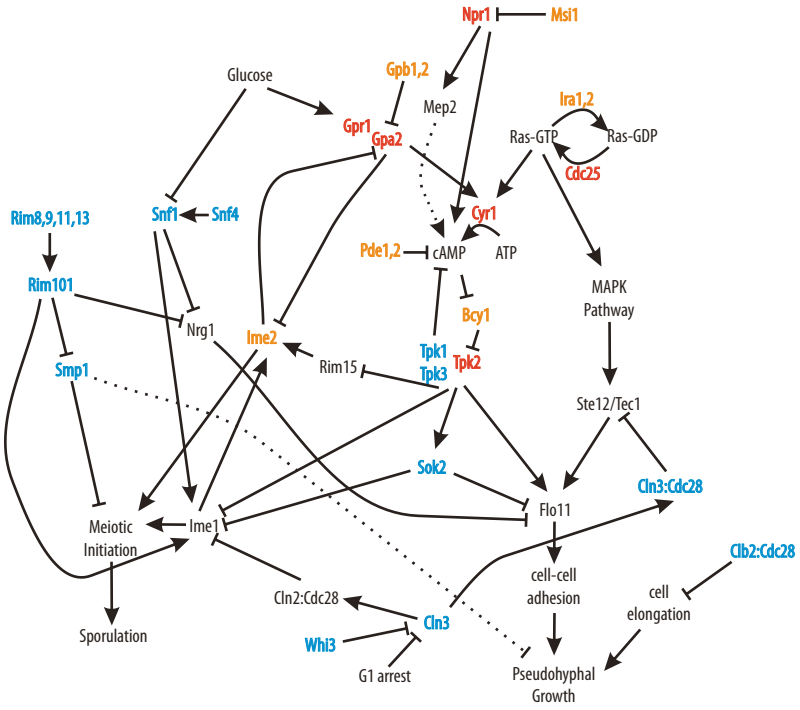

FIGURE 7.3: Yeast cell's developmental network (Magwene (unpublished data))

we treat all variables as in the cell's cytoplasm. In a compartment model, we would suppose that the variables are homogeneous in the cell's cytoplasm and nucleus.

Appendix A

Code Used

In this section we outline the code used to numerically solve our system, fit the data, and analyze our model. We do not include the code directly since it is more informative to the reader to include the methods used to code rather than the actual code.

A.1 Code for Numerically Solving Equations

In this section we outline the code written to numerically solve our system. We used a fourth order Runga-Kutta method to solve the system of differential equations, written in C. We wrote three separate programs, one to solve the two–by–two system, given by Equations (5.2a) and (5.2b); one to solve the four–by-four system, given by Equations (5.1a)–(5.1d); and one to solve the dimensional model, given by Equations (5.3a)–(5.3e). First we describe the fourth order Runga-Kutta method (Heath (2002); Moore (1995)), and then we explain how we used it to solve our systems.

Fourth order Runga-Kutta method

Given a set of ordinary differential equations:

$$\frac{d\vec{y}(t)}{dt} = F(\vec{y}(t), t)$$

and given a time step Δt we numerically increment the system as:

$$\vec{y}_{n+1} = \vec{y}_n + \frac{\Delta t}{6}(k_1 + 2k_2 + 2k_3 + k_4) \qquad \text{and} \qquad t_{n+1} = t_n + \Delta t$$

where

$$k_1 = F(\vec{y}_n, t_n)$$

$$k_2 = F(\vec{y}_n + \frac{\Delta t}{2}k_1, t_n + \frac{\Delta t}{2})$$

$$k_3 = F(\vec{y}_n + \frac{\Delta t}{2}k_2, t_n + \frac{\Delta t}{2})$$

$$k_4 = F(\vec{y}_n + \Delta t k_3, t_n + \Delta t)$$

In our code the function F is defined by the set of differential equations that govern the model. In the two–by–two case $\vec{y} = \{p, x\}$ and F is defined by Equations (5.2a) and (5.2b). In the four–by–four case $\vec{y} = \{r, z, p, x\}$ and F is defined by Equations (5.1a)–(5.1d). In the dimensional model $\vec{y} = \{r, z, p_1, p_2, x\}$ and F is defined by Equations (5.3a)–(5.3e). In each case we wrote a subroutine that applies the fourth order Runga-Kutta method on the corresponding function F.

In all three cases we started at glucose starvation $G = 0$ and allowed the system to come to steady state. Then we applied a glucose pulse at $G = 1$ and reset time to zero ($t_0 = 0$).

We output the value of the variables at each time step, $\vec{y}(t_n)$, into a data file. We then used Matlab to plot this data file to form our plots. We plotted only the concentration of cAMP with respect to time, however we could plot any of the variables.

A.2 Code for Fitting the Data

To fit the Ma et al. (1999) data we used a method of least squares. A good method of least squares (Heath (2002); Trefethen (1997)) subroutine is open access that is written in FORTRAN. This code is called $lmdif1.f$. Here we will give a brief outline of how this code determines the best fit for parameters.

This algorithm seeks to minimize the sum of squares:

$$S = \sum_i (y_i - f(x_i, \beta))^2$$

where y is a vector of data points, and $f(x, \beta)$ is the approximation function evaluated given the vector of parameters β that we are seeking to fit. The dimension of vector β should be less than the dimension of vectors y and x. We start with an

initial guess as to the value of β. This subroutine uses the Levenberg-Marquardt algorithm to find the value of β that minimizes S, defined above. The function $f(x, \beta)$ and the data set y are provided by the user.

The Levenberg-Marquardt algorithm (Heath (2002); Levenberg (1944)) is an iterative algorithm that seeks to improve the estimate, given by S, at each step. The next step in the process is determined by finding the value of δ so that

$$S = \sum_i (y_i - f(x_i, \beta + \delta))^2$$

is minimized. To find the value of δ we use the fact the

$$f(\beta + \delta) \approx f(\beta) + \mathbf{J}\delta,$$

where

$$\mathbf{J} = \frac{\partial f}{\partial \beta}.$$

That is **J** is the Jacobian matrix with respect to the parameters β, computed in this subroutine by a forward difference approximation (Heath (2002); Moore (1995)). Then the following system is solved in order to determine the value of δ:

$$(\mathbf{J^T J} + \lambda diag(J^T J))\delta = \mathbf{J^T}(y - f(\beta))$$

This is a modified version of steepest descent, modified with a damping term λ that can change after each iteration. If the result in the updated parameter vector $\beta + \delta$ leads to a reduction in the sum of squares (S) the update is accepted and the damping parameter is decreased and we repeat the process. Otherwise the damping parameter is increased and we resolve this equation increasing the damping parameter until the sum of squares is decreased. This process is repeated until either the error drops below a predetermined threshold, the magnitude of δ drops below some threshold, or a maximum number of iterations is reached.

To use the subroutine $lmdif.f$ the user must write a linked subroutine that provides the values of the function $f(x, \beta)$ at each step. In our code the vector y is the data provided by Ma et al. (1999) and $f(x, \beta)$ is the concentration of cAMP (variable x) found by solving our system of equations using a fourth order Runga-Kutta method. Given the Ma et al. (1999) data, we needed to fit parameters D_1,P_x, R_{x_1}, R_{x_2}, and M. Parameters D_1, P_x, and R_{x_1} were fit to the Ma et al. (1999) wild type data, and parameters R_{x_2} and M were fit to the Pde1 knockout case.

A.3 Code for Parameter Ranges

Parameter Range Motivated by Claim 6

We showed in Section 4.3 that when $r_{ss} \approx 1$ or $r_{ss} \approx 0$ we can find an exact expression for when the reduced two–by–two system, given by Equations (5.2a) and (5.2b), experiences decaying oscillations, given in Claim 6. Since this expression is implicitly defined in terms of x_{ss} we chose to examine this inequality numerically. To do so we first solved for the equilibrium point. Taking advantage of the fact that the equilibrium is unique, we used the method of bisection (Heath (2002); Moore (1995)) on the function:

$$f(x) = C_0 - D_0 x - \frac{D x^3}{\Gamma + x},$$

to solve for this equilibrium point. By choosing $x_l = 0$ and $x_r = \frac{C_0}{D_0}$ we applied the method of bisection and solved for the unique equilibrium since $f(x_l) < 0$ and $f(x_r) > 0$. We then varied parameters D, D_0 and Γ and for each parameter choice we first solved for the equilibrium, then checked to see if the inequality, given in Claim 6, was satisfied. If the inequality was satisfied we output the parameters into a data file and then used Matlab to plot the data.

Parameter Range Motivated by Claim 7

We showed in Section 4.4 that the four–by–four system, given by Equations (5.1a)–(5.1d), can experience sustained oscillations. In the special case of $M = N$ we found an exact expression for when the system experiences sustained oscillations, given in Claim 7. This expression is implicitly defined in terms of r_{ss} and x_{ss}. To see if a given set of parameters satisfies this expression we first solved for the equilibrium values x_{ss} and r_{ss}. To do so we used Claim 3 as an outline. First we used bisection to solve for the values of x such that $r = 0$ and $r = 1$ given

$$r = f(x) = \frac{1}{G}\left(D_0 x + \frac{Dx^3}{\Gamma + x} - C\right).$$

Using these two x values as end points, we solved for the equilibrium x_{ss} using bisection on:

$$\frac{A(1 - f(x))}{\Gamma_1 + 1 - f(x)} - \frac{Bx^2 f(x)}{\Gamma_1 + f(x)}.$$

This gave us the unique equilibrium point for a given set of parameters. Then we tested the inequality found in Claim 7 and when satisfied we output this into a data file which we plotted in Matlab.

A.4 Code for Eigenvalues in General

In general to find the eigenvalues we used a code that was written in la-pack: the subroutine $dgeev$ (Barker et al. (2001)). This subroutine finds the eigenvalues of a matrix that has been passed to it. We wrote a code that varies parameters A, B, Γ_1 and N, and for each parameter set we first solved for the equilibrium, then used this subroutine $dgeev$ to find the corresponding eigenvalues. We examined when the eigenvalues are complex with positive real part, and created an output file for parameters that satisfy this condition. Then we examined when the eigenvalues are complex with negative real part and output a separate file for when this occurs. Again we used Matlab to plot these data files.

A.5 Code to Generate Figure 4.1

Using Mathematica we wrote the following code for the approximation of the parameter regions: $r_{ss} \approx 1$, $r_{ss} \approx 0$, and in between. To do so we solved Equation (4.6) in terms of $\frac{A}{B}$, then plotted with respect to parameter D. To shade the middle region we allowed C to vary from $0.0440 \leqslant C \leqslant G + 0.044$. The output of this code is a video in avi format that we run in Figure 4.1 showing how varying parameters D_0, Γ and G changes the approximation of the regions when $r_{ss} \approx 1$, $r_{ss} \approx 0$, and in between.

```
Export["./Thesis/figures/approx.avi",
Manipulate[
  Module[{bound = 1, bound2 = .5, bound3 = 25},
   Show[ParametricPlot[{x, -(((R + Sqrt[x]) (-c + d0 Sqrt[x]))/x^(
       3/2))}, {x, 0.00001, bound3}, {c, 0.044, G + .044},
     Mesh -> False, PlotStyle -> {Thick, Red}],
    PlotRange -> {{0.0, bound3}, {0.0, bound}},
    AspectRatio -> 1/1]], {{R, 33.6, "Parameter Gamma"}, 0, 50,
   Appearance -> "Labeled"}, {{d0, .013, "Parameter D0"}, 0, .1,
   Appearance -> "Labeled"}, {{G, 1, "Parameter G"}, 0.1, 1,
   Appearance -> "Labeled"}, FrameLabel -> {"A/B", "D"},
  TrackedSymbols -> True]]
```

A.6 Code to Generate Figure 4.3

We wrote the following code in Mathematica to determine the phase plane of Equations (4.16a) and (4.16b). The output is a video that shows how the phase plane varies as parameters M, D, D_0 and Γ vary, shown in Figure 4.3.

```
Export["./Thesis/figures/phaseplane.avi",Manipulate[Module[{p, x, Dp, Dx, bound = 20, bound2 = 12, T = 100},
   Dp[p_, x_] := m*(x^2 - p);
   Dx[p_, x_] := 1.044 - d0*x - d*x*p/(R + x);
   Show[VectorPlot[
     Normalize@{Evaluate@Dx[x, p], Evaluate@Dp[x, p]}, {p, 0,
      bound2}, {x, 0, bound}, VectorScale -> 0.025],
    ParametricPlot[
```

```
     Evaluate[
      First[{x[t], p[t]} /.
        NDSolve[{x'[t] == 1.044 - d0*x[t] - d*x[t]*p[t]/(R + x[t]),
          p'[t] == m*(x[t]^2 - p[t]),
          Thread[{x[0], p[0]} == point]}, {x[t], p[t]}, {t, 0,
          T}]]], {t, 0, T}, PlotStyle -> {Thick, Red}],
    ParametricPlot[{t, t^2}, {t, 0.00001, bound},
     PlotStyle -> {Thick, Black}],
    ParametricPlot[{t, (1.04 - d0*t)*(R + t)/(d*t)}, {t, 0.00001,
      bound}, PlotStyle -> {Thick, Black}],
    PlotRange -> {{0, bound2}, {0, bound}}, ImageSize -> {450, 450},
    ImagePadding -> {{55, 20}, {25, 10}}]], {{m, .001, "Parameter M"},
    0, .1, Appearance -> "Labeled"}, {{R, 33.6, "Parameter Gamma"}, 0,
    50, Appearance -> "Labeled"}, {{d0, .013, "Parameter D0"}, 0, .5,
   Appearance -> "Labeled"}, {{d, 1, "Parameter D"}, 0.1, 1,
   Appearance -> "Labeled"}, {point, {.5, 1}, Locator},
  FrameLabel -> {"X", "P"}, TrackedSymbols -> True]]
```

A.7 Code to Generate Figure 5.5

We wrote the following code in Mathematica to solve Equations (4.1a)–(4.1d). The output is a video that shows how the solution $x(t)$, that is cAMP, varies as all the parameters in this system vary, shown in Figure 5.5.

```
Export["./Thesis/figures/susosc.avi",
 Manipulate[
  Module[{r, x, p, z, bound = 200, bound1 = 20, bound2 = 40,
    T1 = 1000, point = {.5, .1, .1, .1}},
   Show[ParametricPlot[
     Evaluate[
      First[{t*0.05, x[t]*30.9} /.
        NDSolve[{r'[t] ==
           A*(1.0 - r[t])/(R1 + 1.0 - r[t]) - B*z[t]*r[t]/(R1 + r[t]),
          z'[t] == n*(x[t]^2 - z[t]), p'[t] == m*(x[t]^2 - p[t]),
         x'[t] == 0.044 + r[t] - 0.015*x[t] - d*x[t]*p[t]/(R + x[t]),
          Thread[{r[0], z[0], p[0], x[0]} == point]}, {r[t], z[t],
         p[t], x[t]}, {t, 0, T1}]]], {t, 0, T1},
     PlotStyle -> {Thick, Red}], PlotRange -> {{0, 20}, {0, bound}},
    ImageSize -> {450, 450}, ImagePadding -> {{55, 20}, {25, 10}},
    AspectRatio -> 1/1]], {{A, .19, "Parameter A"}, 0, .5,
```

```
 Appearance -> "Labeled"}, {{B, .05, "Parameter B"}, 0, .1,
 Appearance -> "Labeled"}, {{R1, .0004, "Parameter Gamma1"},
 0, .0004, Appearance -> "Labeled"}, {{m, .025, "Parameter M"},
 0, .05, Appearance -> "Labeled"}, {{n, .043, "Parameter N"},
 0, .05, Appearance -> "Labeled"}, {{R, 27, "Parameter Gamma"}, 0,
 50, Appearance -> "Labeled"}, {{d, 1, "Parameter D"}, 0.1, 1,
 Appearance -> "Labeled"}, FrameLabel -> {"Min", "cAMP"},
TrackedSymbols -> True]]
```

Bibliography

Alberts, B., Bray, D., Johnson, A., Lewis, J., and Raff, M. (1998), *Essential cell biology: an introduction to the molecular biology of the cell*, Garland Publishers.

Alon, U. (2007), *An Introduction to Systems Biology - Design Principles of Biological Circuits*, Chapman and Hall.

Barker, V. A., Blackford, L. S., Dongarra, J. J., Croz, J. D., Hammarling, S., Marinova, M., Wasniewski, J., and Yalamov, P. (2001), *LAPACK95 Users' Guide*, Society for Industrial and Applied Mathematics.

Campbell, N. A. (2008), *Biology*, Parson, Benjamin Cummings.

Casey, R., de Jong, H., and Gouze, J. (2005), "Stability of Equilibria for Piecewise-linear Models of Genetic Regulatory Networks," *Proceedings of the 44th IEEE Conference on Decisions and Control, and the Europena Control Conference*, pp. 3693–3698.

Casey, R., de Jong, H., and Gouze, J. L. (2006), "Piecewise-linear Models of Genetic Regulatory Networks: Equilibria and their Stability," *J Math Biol.*, 52, 27–56.

Cazzaniga, P., Pescini, D., Besozzi, D., Mauri, G., Colombo, S., and Martegani, E. (2008), "Modeling and stochastic simulation of the Ras/cAMP/PKA pathway in the yeast *Saccharomyces cerevisiae* evidences a key regulatory function for intracellular guanine nucleotides pools." *J Biotechnol*, 133, 377–385.

Ching, W.-K., Zhang, S., Ng, M. K., and Akutsu, T. (2007), "An approximation method for solving the steady-state probability distribution of probabilistic Boolean networks," *Bioinformatics*, 23, 1511–1518.

Colombo, S., Ronchetti, D., Thevelein, J. M., Winderickx, J., and Martegani, E. (2004), "Activation state of the Ras2 protein and glucose-induced signaling in *Saccharomyces cerevisiae*." *J Biol Chem*, 279, 46715–46722.

de Jong, H. and Page, M. (2008), "Search for Steady State of Piecewise-Linear Differential Equation Models of Genetic Regulatory Networks," *IEEE/ACM Transactions on Computational Biology and Bioinformatics*, 5.

Engelberg, S. (2005), *A Mathematical Introduction to Control Theory*, Imperial College Press.

Fersht, A. (2002), *Structure and Mechanism in Protein Science*, W.H. Freeman and Company.

Garmendia-Torres, C., Goldbeter, A., and Jacquet, M. (2007), "Nucleocytoplasmic Oscillations of the Yeast Transcription Factor Msn2: Evidence for Periodic PKA Activation," *Current Biology*, 17, 1044–1049.

Gimeno, C. J., Ljungdahl, P. O., Styles, C. A., and Fink, G. R. (1992), "Unipolar cell divisions in the yeast *S. cerevisiae* lead to filamentous growth: regulation by starvation and RAS." *Cell*, 68, 1077–1090.

Glass, L. and Kauffman, S. (1973), "The Logical Analysis of Continuous Nonlinear Biochemical Control Networks," *J Theor Biol*, 39, 103–129.

Gonze, D. and Goldbeter, M. J. A. (2008), "Stochastic modelling of nucleocytoplasmic oscillations of the transcription factor Msn2 in yeast." *J R Soc Interface*, 5 Suppl 1, S95–109.

Harashima, T. and Heitman, J. (2002), "The Galpha Protein Gpa2 Controls Yeast Differentiation by Interacting with the Kelch Repeat Proteins that Mimic Gbeta Subunits," *Mol Cell*, 10, 163–173.

Harashima, T. and Heitman, J. (2005), "Galpha Subunit Gpa2 Recruits Kelch Repeat Subunits That Inhibit Receptor-G Protein Coupling during cAMP-induced Dimorphic Transitions in *Saccharomyces cerevisiae*," *Mol Biol of the Cell*, 16, 4557–4575.

Heath, M. T. (2002), *Scientific Computing An Introductory Survey*, The McGraw-Hill Companies Inc.

Herskowitz, I. (1988), "Life Cycle of the Budding Yeast *Saccharomyces cerevisiae*," *Microbiological Reviews*, 52, 536–553.

Jorgensen, P., Nishikawa, J. L., Breitkreutz, B. J., and Tyers, M. (2002), "Systematic identification of pathways that couple cell growth and division in yeast." *Science*, 297, 395–400.

Kehrl, J. and Sinnarajah, S. (2002), "RGS2: a multifunctional regulator of G-protein signaling." *Int J Biochem Cell Biol*, 34, 432–438.

Kim, S., Imooto, S., and Miyano, S. (2004), "Dynamic Bayesian network and nonparametric regression for nonlinear modeling of gene networks from time series gene expression data," *Biosystems*, 75, 57–65.

Kraakman, L., Lemaire, K., Ma, P., Teunissen, A. W., Donaton, M. C., Dijck, P. V., Winderickx, J., de Winde, J. H., and Thevelein, J. M. (1999), "A *Saccharomyces cerevisiae* G-protein coupled receptor, Gpr1, is specifically required for glucose activation of the cAMP pathway during the transition to growth on glucose." *Mol Microbiol*, 32, 1002–1012.

Lacal, J. C. and McCormick, F. (1993), *The Ras superfamily of GTPases*, CRC Press.

Levenberg, K. (1944), "A method for the solution of certain non-linear problems in least squares." *Quarterly Journal of Applied Mathematics II*, 2, 164–168.

Li, P., Zhang, C., Perkins, E., Gong, P., and Deng, Y. (2007), "Comparison of probabilistic Boolean network and dynamic Bayesian network approaches for inferring gene regulatory networks," *BMC Bioinformatics*, 8.

Ma, P., Wera, S., Dijck, P. V., and Thevelein, J. M. (1999), "The PDE1-encoded low-affinity phosphodiesterase in the yeast *Saccharomyces cerevisiae* has a specific function in controlling agonist-induced cAMP signaling." *Mol Biol Cell*, 10, 91–104.

Malbon, C. C. (2005), "G proteins in development," *Nature Reviews Molecular Cell Biology*, 6, 689–701.

Matsumoto, K., Uno, I., Oshima, Y., and Ishikawa, T. (1982), "Isolation and characterization of yeast mutants deficient in adenylate cyclase and cAMP-dependent protein kinase." *Proc Natl Acad Sci U S A*, 79, 2355–2359.

McCudden, C. R., Hains, M. D., Kimple, R. J., Siderovski, D. P., and Willard, F. S. (2005), "G-protein signaling: back to the future," *CMLS Cell. Mol. Life Sci*, 62, 551–577.

Mitsuzawa, H. (1993), "Responsiveness to exogenous cAMP of a *Saccharomyces cerevisiae* strain conferred by naturally occurring alleles of PDE1 and PDE2." *Genetics*, 135, 321–326.

Moore, R. E. (1995), *Mathematical Elements of Scientific Computing*, Holt and Rinehart and Winston Inc.

Peeters, T., Louwet, W., Gelad, R., Nauwelaers, D., Thevelein, J. M., and Versele, M. (2006), "Kelch-repeat proteins interacting with the Galpha protein Gpa2 bypass adenylate cyclase for direct regulation of protein kinase A in yeast." *Proc Natl Acad Sci U S A*, 103, 13034–13039.

Peeters, T., Versele, M., and Thevelein, J. M. (2007), "Directly from Galpha to protein kinase A: the kelch repeat protein bypass of adenylate cyclase," *Trends in Biochem Sci.*, 32, 547–547.

Phan, V., Ding, V., Li, F., Chalkley, R., Burlingame, A., and McCormick, F. (2010), "The RasGAP proteins Ira2 and neurofibromin are negatively regulated by Gpb1 in yeast and ETEA in humans." *Mol Cell Biol*, 30, 2264–2279.

Rall, T. W. and Sutherland, E. W. (1958), "Formation of a cyclic adenine ribonucleotide by tissue particles." *J Biol Chem*, 232, 1065–1076.

Rolland, F., Winde, J. H. D., Lemaire, K., Boles, E., Thevelein, J. M., and Winderickx, J. (2000), "Glucose-induced cAMP signalling in yeast requires both a G-protein coupled receptor system for extracellular glucose detection and a separable hexose kinase-dependent sensing process." *Mol Microbiol*, 38, 348–358.

Rubinstein, A., Gurevich, V., Kasulin-Boneh, Z., Pnueli, L., Kassir, Y., and Pinter, R. (2007), "Faithful modeling of transient expression and its applications to elucidating negative feedback regulation," *Proc Natl Acad Sci U S A*, 104, 6241–6246.

Segel, I. H. (1993), *Enzyme Kinetics: Behavior and Analysis of Rapid Equilibrium and Steady-State Enzyme Systems*, John Wiley and Sons Inc.

Segel, L. A. (ed.) (1980), *Mathematical Models in Molecular and Cellular Biology*, Cambridge University Press.

Segel, L. A. (1984), *Modeling Dynamic Phenomena in Molecular and Cellular Biology*, Cambridge University Press.

Shmulevich, I., Dougherty, E. R., and Zhang, W. (2002), "From Boolean to Probabilistic Boolean Networks as Models of Genetic Regulatory Networks," *Proceedings of the IEEE*, 90.

Tanaka, K., Nakafuku, M., Tamanoi, F., Kaziro, Y., Matsumoto, K., and Toh-e, A. (1990), "IRA2, a second gene of *Saccharomyces cerevisiae* that encodes a protein with a domain homologous to mammalian Ras GTPase-activating protein." *Mol Cell Biol*, 10, 4303–4313.

Thevelein, J. M., Bonini, B., C., D., Haesendonckx, S., K., J., Louwet, W., Thayumanavan, P., Popova, Y., Rubio-Texeira, M., Schepers, W., Vandormael, P., Zeebroeck, G. V., Verhaert, P., Versele, M., and Voordeckers, K. (2008), "Novel mechanisms in nutrient activation of the yeast protein kinase A pathway." *Acta Microbiol Immunol Hung*, 55, 75–89.

Toda, T., Uno, I., Ishikawa, T., Powers, S., Kataoka, T., Broek, D., Cameron, S., Broach, J., Matsumoto, K., and Wigler, M. (1985), "In yeast, RAS proteins are controlling elements of adenylate cyclase." *Cell*, 40, 27–36.

Toda, T., Cameron, S., Sass, P., Zoller, M., Scott, J. D., McMullen, B., Hurwitz, M., Krebs, E. G., and Wigler, M. (1987), "Cloning and characterization of BCY1, a locus encoding a regulatory subunit of the cyclic AMP-dependent protein kinase in *Saccharomyces cerevisiae*." *Mol Cell Biol*, 7, 1371–1377.

Trefethen, L. N. (1997), *Numerical Linear Algebra*, Society for Industrial and Applied Mathematics.

Versele, M., de Winde, J. H., and Thevelein, J. M. (1999), "A novel regulator of G protein signalling in yeast, Rgs2, downregulates glucose-activation of the cAMP pathway through direct inhibition of Gpa2." *EMBO J*, 18, 5577–5591.

Williamson, T., Schwartz, J., Kell, D. B., and Stateva, L. (2009), "Deterministic mathematical models of the cAMP pathway in *Saccharomyces cerevisiae*." *BMC Syst Biol*, 3, 70.

Biography

NAME

Kevin E. Gonzales

BORN

December 28, 1982, Long Beach, California

EDUCATION

Duke University, Department of Mathematics

Ph.D. in Mathematics *May 2011*

M.S. in Mathematics *May 2007*

Rochester Institute of Technology, Department of Mathematics

M.S. in Applied Mathematics *May 2005*

B.S. in Mathematics *May 2005*